Electronic Thesis and Dissertation Repository

10-7-2019 1:00 PM

Characterization of Wilms' Tumour 1 (Wt1) as a Biomarker for Fibrosis in Duchenne Muscular Dystrophy

Patrick Murphy, *The University of Western Ontario*

Supervisor: Hoffman, Lisa, *The University of Western Ontario*
A thesis submitted in partial fulfillment of the requirements for the Master of Science degree in Anatomy and Cell Biology
© Patrick Murphy 2019

Recommended Citation

ABSTRACT

Duchenne muscular dystrophy (DMD) is the most common inherited pediatric muscle dystrophy. It is characterized by muscle degeneration, resulting in fibrosis that is a significant impediment to both endogenous muscle repair and any potential regenerative strategy. At present, there are few therapies that specifically address fibrosis and microenvironment improvement, but one possibility rests in targeting the Wilms' tumour 1 (Wt1) protein. Wt1 is a zinc finger transcription factor, recently shown to be expressed in fibrotic conditions such as Dupuytren's disease and pulmonary fibrosis. This thesis examines the expression pattern of Wt1 in several mouse models of DMD, through both histological quantification of Wt1 protein, and quantification of *Wt1* isoform mRNA. Additionally, fibrosis is quantified through Masson's trichrome staining of collagen. An increased proportion of Wt1 immunoreactive nuclei was found in the diaphragm and gastrocnemius of DMD disease models prior to and during early fibrosis, but returned to basal levels during late fibrosis. These results suggest that nuclear Wt1 immunoreactivity may precede college deposition, and that it should be investigated further in the future.

KEYWORDS

Duchenne Muscular Dystrophy, Wilms' Tumour 1, Fibrosis, Immunohistochemistry, qPCR, *Mdx*

SUMMARY FOR LAY AUDIENCE

Duchenne muscular dystrophy (DMD) is a severe muscle disorder affecting children. DMD has no cure, and most patients with the disease are expected to only live to their mid-twenties. The most recognizable symptoms of DMD are muscle weakness and muscle loss. DMD is a genetic condition, caused by a mutation in the gene that normally produces dystrophin protein. Genes make proteins by first making RNA, which can then be read by cells to assemble the protein. Dystrophin is an important protein for maintaining the structure of muscle cells. Mutations in the gene which produces dystrophin can make the dystrophin it produces not function properly. When the function of dystrophin is reduced, muscle cells become more likely to die. Over time, this increased muscle cell death causes scarring inside of muscles, preventing muscles from functioning properly. This scarring acts as a barrier, preventing both normal muscle repair and treatments to increase muscle function. Presently, there are few treatments that specifically target this scarring, but one possibility rests in targeting the Wilms Tumor 1 (Wt1) protein. Wt1 is a protein which can alter the production of other proteins. It was originally found in cancer, but it has recently been shown to be expressed in some diseases where scarring occurs, such as Dupuytren's disease. This indicates its production might occur when scarring occurs. This thesis examines the patterns of Wt1 production in several mouse models of DMD. This is done by, in these models, staining Wt1 protein and looking at it under a microscope, and also examining how much RNA of Wt1 is made. Additionally, scarring is examined by staining the scar tissue and examining it under a microscope. The percent of cell nuclei which had Wt1 inside of them was found to be increased prior to, and during, scarring, but decreased back down to normal levels after scarring had taken place. These results suggest that an increased presence of Wt1 in the nucleus may take place before scarring, and that it should be investigated further.

CO-AUTHORSHIP STATEMENT

William Tom Hrinivich wrote the Matlab^{TM} code to analyze Masson's trichrome images. Vytas Bindokas wrote the original white balance macro, which was modified by Patrice Mascalchi, for ImageJ.

Andrew McClennan performed a portion of the mouse care and handling.

ACKNOWLEDGEMENTS

work, and Brenda Strutt for her assistance in my RNA work and teaching me microscopy. I must also thank Caroline O'Neil at Robarts Research Institute for conducting our tissue embedding and sectioning.

Finally, I must extend great thanks to my parents, Elizabeth and Brian Murphy, as well as my sister, Theresa Murphy, who have been with me throughout this entire journey, for better and for worse. It would not be possible for me to have accomplished this work without their help.

TABLE OF CONTENTS

LIST OF TABLES

LIST OF FIGURES

LIST OF ABBREVIATIONS

⁰C	Degrees Centigrade
ACE1	Angiotensin-converting Enzyme 1
ANOVA	Analysis of Variance
α-SMA	Alpha Smooth Muscle Actin
AT1/2	Angiotensin II Receptors
BMD	Becker's Muscular Dystrophy
Bmp7	Bone Morphogenetic Protein 7
BSA	Bovine Serum Albumin
CACC	Canadian Council on Animal Care
Cas9	Clustered Regularly Interspaced Short Palindromic Repeats associated protein 9
cDNA	Complementary Deoxyribonucleic Acid
CK	Creatine Kinase
Col4	Collagen 4
CRISPR	Clustered Regularly Interspaced Short Palindromic Repeats
DAB	3,3'-diaminobenzidine
DD	Dupuytren's Disease
DMD	Duchenne Muscular Dystrophy
DNA	Deoxyribonucleic Acid
EGR1	Early Growth Response-1
EDTA	Ethylenediaminetetraacetic Acid
EX5	Exon 5
FAP	Fibro/adipogenic Progenitor
FAM	Fluorescein
GAPDH	Glyceraldehyde 3-phosphate dehydrogenase
HIF1	Hypoxia-inducible Factor 1
IGF1	Insulin-like Growth Factor 1
IGF2	Insulin-like Growth Factor 2
Itg2	Integrin beta 2
Itg7	Integrin beta 7

KTS	Lysine Threonine Serine
MAPK	Mitogen-activated Protein Kinase
Mdx	X Chromosome-linked Muscular Dystrophy
MMP9	Matrix Metalloproteinase 9
MRI	Magnetic Resonance Imaging
mRNA	Messenger Ribonucleic Acid
NF-κB	Nuclear Factor Kappa-Light-Chain-Enhancer of Activated B Cells
nNOS	Neuronal Nitric Oxide Synthase
PAX2	Paired Box Gene 2
PBS	Phosphate Buffered Saline
PCR	Polymerase Chain Reaction
PDGF-A	Platelet Derived Growth Factor Subunit A
PET-CT	Positron Emission Tomography – Computed Tomography
qPCR	Quantitative Polymerase Chain Reaction
RNA	Ribonucleic Acid
Sal1	Spalt Like Transcription Factor 1
shRNA	Short Hairpin Ribonucleic Acid
SJHC	St. Joseph's Health Care
SRY	Sex-determining region Y
TAE	Tris-Acetate- Ethylenediaminetetraacetic Acid
TAMRA	5-Carboxytetramethylrhodamine
TGF-α	Transforming Growth Factor Alpha
TGF-β	Transforming Growth Factor Beta
TNF	Tumour Necrosis Factor
TSP4	Thrombospondin 4
US	United States
Utrn	Utrophin
Wt1	Wilms' Tumour 1

LIST OF APPENDICIES

1   LITERATURE REVIEW

1.1   Duchenne Muscular Dystrophy (DMD)

1.1.1 Overview

Duchenne muscular dystrophy (DMD) is a progressive neuromuscular disorder and the most common inherited pediatric muscle dystrophy. It is characterized by muscle wasting and muscle weakness, which worsens throughout development. Initial presentation in children takes place at three to five years of age[1–3]. DMD follows an X-linked recessive pattern of inheritance, producing pathology at a far higher rate in males rather than females. It arises due to spontaneous or inherited mutations in the dystrophin gene[4]. In most cases, the muscle degeneration present in DMD ultimately results in cardiac and respiratory complications that reduce life expectancy to the mid-twenties[5–8] .

1.1.2 Clinical Features

In DMD patients, muscle degeneration is most severe in skeletal and cardiac muscle. Newborns exhibit no symptoms of pathology, but slowly become more affected over time, occasionally with mild delays in gross motor development as early as age two[2,3]. Weakness begins centrally in the proximal lower limbs and trunk, and progresses to eventually include the upper limbs and distal muscles[9–11]. Calf hypertrophy, waddling gait, and increased lumbar lordosis become more common by six years of age. Gowers' sign may also become visible at this time[2,3,11]. This disorder often culminates in orthopedic complications, such as scoliosis, and frequent joint contractures in the lower limbs[11–13]. By the onset of puberty, both extensive postural distortion and substantial loss of motor function have taken place, forcing use of orthopedic aids to maintain mobility[2,11].

As muscles throughout the body weaken, the heart and lungs begin to fail[7]. Loss of musculature needed for respiration produces several secondary conditions, such as obstructive sleep apnea and hypoventilation[14]. Pulmonary infection affecting the respiratory tract can further complicate this. Heart failure can occasionally remain masked until late into the disease course due to inactivity[2]. Early pre-clinical cardiac involvement is present in 25% of patients under six years of age. This transitions into full cardiac involvement over time, affecting all patients over eighteen years of age[15].

Females which possess only a single mutant allele often have a much milder form of DMD, and act as carriers for the condition. Generally, symptoms in females are limited to mild muscle weakness, and elevated creatine kinase (CK) levels, with a small chance of cardiac involvement[16,17].

1.1.3 Diagnosis

Diagnosis of DMD involves several strategies. Serum CK levels are often used as an initial criterion, and are usually ten or twenty fold the norm in children with the condition[2,11,18]. Genetic testing is the standard method to confirm a diagnosis of DMD, though it still struggles with cost and availability issues, and does not account for other factors influencing dystrophin function or expression[2,19,20]. In the case that genetic testing is not conclusive, muscle biopsy must be utilized. Immunostaining[21] and western blot analysis[22] can be used to evaluate dystrophin size, expression level, and expression location. Unfortunately, this technique also has marked downsides[2,7,11,22]. DMD patients already experience reduced ability to replenish dying muscle tissue, and the process of the biopsy may exacerbate issues associated with this.

1.1.4 Pathology

The pathology in DMD results from minimal dystrophin function, or decreased synthesis of functional dystrophin[23–25]. The gene coding for dystrophin is over 2000 kb in length, and is the largest in the human body. It is expressed as early as nine weeks during human fetal development[26]. Dystrophin has multiple isoforms, and is expressed in various organ systems. Some isoforms are expressed near-ubiquitously, while others are restricted to particular organ systems. Nonetheless, the major burden of the DMD pathology is linked to muscle decline, and dystrophin's function therein[27]. The most common mutations which produce cases of DMD are deletions of one or more exons, usually those which cause disruption of the reading frame. This produces dystrophin transcripts which are vulnerable to nonsense mediated decay[28–31]. This contrasts with Becker's muscular dystrophy (BMD), another condition produced by mutations in the dystrophin gene, where in-frame mutations are the cause of the condition. This results in production of still partially functional dystrophin. Individuals with BMD usually experience milder symptoms, and may live 50-60 years before serious complications develop[23,31,32].

Normally, dystrophin expressed in muscle cells localizes to the cytoplasmic face of the sarcolemma, where it can form the dystrophin-associated protein complex[33] (Fig. 1). This complex spans the sarcolemma, and its components can be divided into three categories of protein dependent on their location. In the intracellular compartment, neuronal nitric oxide synthase (nNOS), dystrobrevin, syntrophins, and dystrophin can be found. Dystrobrevin and the syntrophins mediate binding of nNOS to dystrophin, and dystrophin itself acts as the key protein connecting these intracellular proteins to the other components of the dystrophin-associated protein complex. The transmembrane proteins forming part of this complex are β-dystroglycan, sarcoglycans and sarcospan. β-dystroglycan links these proteins to dystrophin, and to the

extracellular components of the dystrophin-associated protein complex[31,34]. Sarcoglycans and sarcospan play additional roles in stabilizing the complex through interactions with dystrobrevin, and securing the complex to the sarcolemma[35,36].
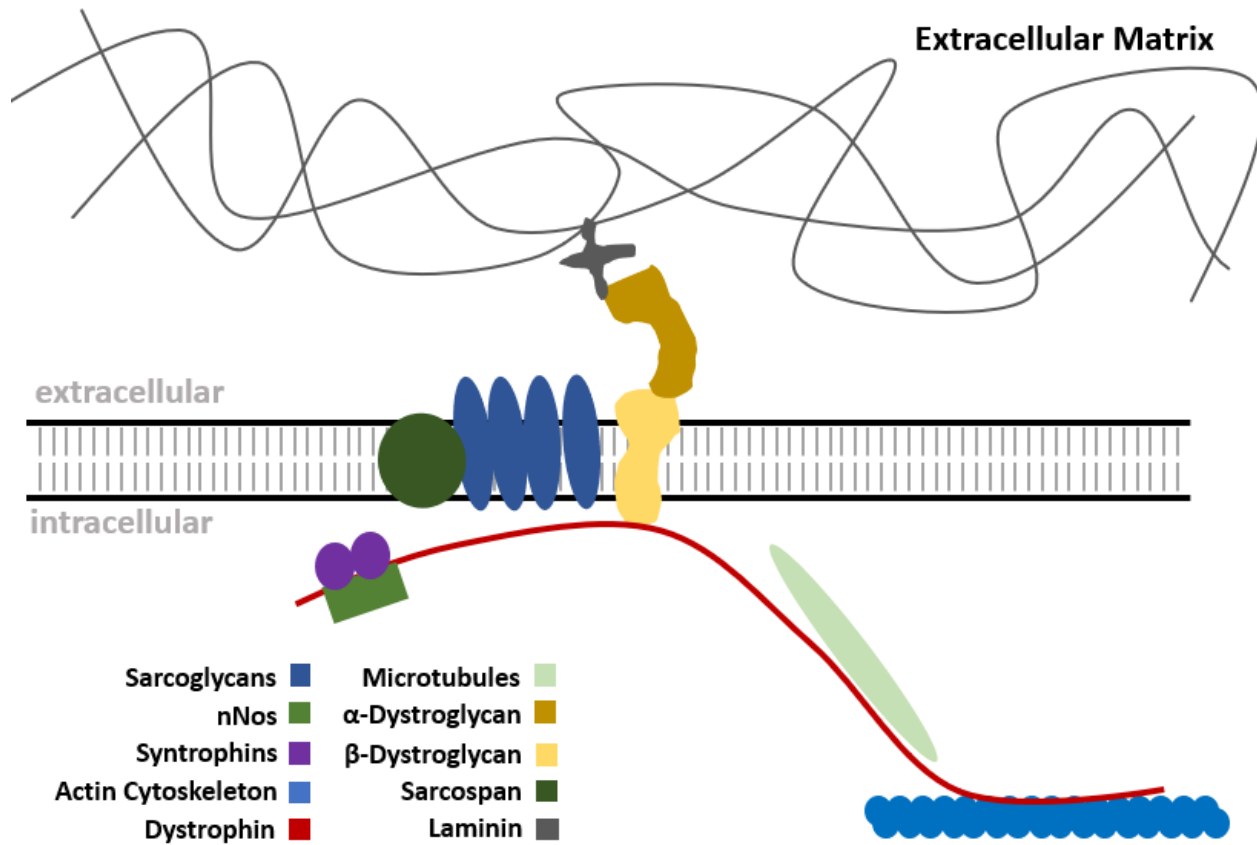
Figure 1. Dystrophin-associated protein complex

Dystrophin's amino-terminus interacts with the actin cytoskeleton, while its carboxyl-terminus forms the dystrophin-associated protein complex alongside several other proteins, including dystroglycans and sarcoglycans. This complex can then interact with the extracellular matrix, through mediators such as laminin. This provides integrity to the muscle cell sarcolemma. This complex, additionally, allows localization of other proteins to the plasma membrane, such as neuronal nitroc oxide synthase (nNOS).

The major extracellular component is α-dystroglycan, which binds to β-dystroglycan, and enables the connection of the complex to components of the extracellular matrix, such as laminin[34]. Few mutations in dystroglycans are identified, though this appears to be as a result of these mutations being embryonically lethal, as opposed to any protective mechanism[33,37,38]. Dystrophin itself mediates the connection of these components to microtubules and the actin cytoskeleton. Its absence can lead to a disorganization of the microtubule network[31,39,40]. The dystrophin-associated protein complex interacts with several other proteins to form rib-like lattices around the cell, termed costameres[41,42]. These structures distribute contractile forces laterally throughout the sarcolemma to the basal lamina[43]. The dystrophin-associated protein complex additionally enables transduction of mechanical signals between the intracellular and extracellular environments[44]. The absence of dystrophin increases the permeability of muscle cells, as confirmed by dye incorporation rates[45,46].

There are several theories linking dystrophin loss to the dystrophic phenotype present in DMD. The first, and most widely accepted theory, is that with the loss of the dystrophin-associated protein complex, cells lose the ability to cope with mechanical stress. During contraction, the sarcolemma tears, allowing accumulation of extracellular protein inside the muscle cell, ultimately triggering cell death[42,45,47]. In X chromosome-linked muscular dystrophy (*Mdx*) mice, a dystrophin knockout model which experiences muscle degeneration and thus a higher proportion of centrally-nucleated myofibers, immobilization has been shown to reduce the proportion of centrally-nucleated myofibres[48]. Beyond the mechanical implications of dystrophin loss, other cell functions also become dysregulated, indirectly bringing about cell death. Stretching of the sarcolemma inappropriately opens calcium channels, and compounded with Ca^{2+} influx through microlesions, it becomes impossible to maintain cytosolic Ca^{2+}

concentration. Consistent high Ca^{2+} levels prompt a positive feedback loop, as calpain proteases become active and cleave proteins in the plasma membrane, eventually causing apoptosis[45,49]. Neuronal nitric oxide synthase (nNOS) is normally sequestered to the sarcolemma by dystrophin-associated proteins. It is delocalized into the cytoplasm in cases of DMD[50]. This impedes adequate vasodilation, reducing the ability for muscle to regulate oxygen exchange, and can thus cause muscle ischemia. However, studies using nNOS knockout mice show different phenotypes than those observed in dystrophin knockout mice, suggesting that the loss of nNOS localization regulation does not alone account for the pathophysiology of DMD[45,51,52]. Nonetheless, experimental models have shown that boosting NO signaling may ameliorate some of the skeletal muscle pathology in DMD[53]. A portion of muscle cell mechanotransduction is lost when the dystrophin-associated protein complex fails to form, leading to dysregulation of multiple genes. Unfortunately, little research has so far been conducted on this topic, and there is a poor understanding in the literature of how this interacts with DMD pathology[44,45]. It is likely a combination of these pathways which results in the DMD dystrophic phenotype. As muscle cells die, the tissue becomes chronically inflamed, and is remodeled into fatty and fibrous connective tissue through fibrosis[47].

1.1.5 Initiation of Fibrosis in DMD

Fibrosis is a pathological deposition of extracellular matrix, resulting in damage to the architecture of the tissue in which the fibrosis is occurring. Tissue injury is the initial cause of fibrosis[54,55]. This can be through external means, such as chemical or physical insult, or internally, such as in the case of genetic conditions. Some extracellular matrix deposition occurs normally in the process of tissue repair, but when this lasts too long, or is too severe, clearance becomes difficult, and permanent scarring takes place[54,55]. Conditions where fibrosis is a major

component of pathology affect a wide range of organ systems: chronic renal disease[56], fibrotic

pulmonary diseases[57], alcoholic liver disease[58], and DMD[59], are all examples. Estimates place the

number of United States (US) adults with chronic renal disease alone at several million cases[60].

DMD itself makes up a comparatively smaller proportion of fibrotic conditions in the US, but the

disease course and outcomes are much more severe, with muscle loss and ensuing fibrosis

causing death. For some fibrotic conditions, addressing the underlying causes of fibrosis

initiation may be difficult or impossible. It is therefore pertinent that research is conducted on

methods to predict, halt, and even reverse fibrosis, in order to reduce disease burden in the

future.

The fibrogenic response, in broad terms, consists of four phases. The first phase is

initiation, where the structure to become fibrotic is injured. In the case of DMD, this is through

the uncontrolled death of muscle cells. This triggers release of inflammatory mediators such as

cytokines and chemokines, recruiting inflammatory cells[55,61]. There are several types of

inflammatory cells, but some of the most common are lymphocytes and macrophages[55,62]. The

macrophage population at the site of damaged muscle is heterogenous, with some portion being

M1 and another portion being M2[63,64]. Once they arrive at the site of cell death, macrophages and

lymphocytes can induce the second and third phases of fibrosis. These are, respectively, effector

cell activation, and extracellular matrix production[55]. The activated effector cells can engage in

signaling feedback with the inflammatory cell population, potentially modifying their behavior

further[65–67]. The initial M1 macrophage population can furthermore prompt myogenic precursor

cell growth[68]. Some of the key effector cell types are fibroblasts and myofibroblasts, which both

synthesize extracellular matrix proteins[69]. This new matrix consists primarily of type I and III

collagen, basement-membrane proteins, and fibronectins[55,70], but also has several other elements,

such as proteoglycans, and fibrinogen[71–73]. Myofibroblasts also function to contract this matrix

and surrounding tissue structure together[55,63]. There are numerous pathways used by

inflammatory cells in this process, such as the transforming growth factor beta (TGF-β) pathway.

TGF-β is not only secreted by inflammatory cells, but is also secreted by effector cells to sustain

the fibrogenic response once it is active[55,62]. TGF-β may act through a canonical pathway in

which its binding to one of the TGF-β receptors mediates SMAD signaling, or through non-

canonical mitogen-activated protein kinases (MAPKs) and c-abl pathways that upregulate the

transcription of other fibrotic signals[73–75]. Under normal circumstances, these effects can be

beneficial, allowing repair of damaged structures[55,63,69]. The initial matrix scaffold set down in

the inflammatory response is gradually replaced by new cells. The M1 macrophages give way to

their M2 counterparts. In muscle, they prompt differentiation of myogenic precursor cells into

myofibers, and the tissue is repaired[63,68]. In chronically inflamed tissue, this process is

unbalanced. There can be persistence of the M1 macrophage population, or an unbalanced

activation of M2 macrophage population subsets. This leads into the fourth phase of the

fibrogenic response, where there is excessive deposition and insufficient resorption of

extracellular matrix, ultimately resulting in pathogenesis[55,63].

The fibrosis experienced in DMD is profound. It is one of the major pathological factors

of DMD that brings about ultimate muscle dysfunction. Newly regenerated muscle tissue in

DMD patients is vulnerable to cell death, creating a cyclical state of degeneration. This produces

chronic inflammation characterized by incomplete muscle regeneration, and an absence of

extracellular matrix remodeling. Over time, muscle tissue is increasingly replaced by

extracellular matrix, further reducing the muscle strength, and making it prone to increased

damage in the future. The ability of satellite cells to repair the tissue deteriorates over time,

though there is some uncertainty whether this is either due to an inability to replicate, or an inability to produce additional functional muscle tissue[63,76,77]. There has been a long-standing body of evidence which suggests that, even before the onset of muscle loss, there is an increase in collagen deposition in the endomysium[78–81]. A 2009 study evaluated several histological features in DMD patients, including fibrosis, fatty degeneration, myofiber size, and necro/basophilic fibers, and compared these to several motor outcomes. These outcomes included quadriceps strength, ages at loss of walking and wheelchair confinement, scoliosis, and manual muscle testing. Of all the parameters assessed, only fibrosis in the endomysium correlated with poorer motor outcome. This was possibly mediated through fibrosis-induced separation of the muscle tissue from associated vessels. Layers of extracellular matrix would reduce the efficiency of oxygen diffusion to muscle, possibly causing ischemia of the muscle[80].

1.1.6 The Fibrotic Microenvironment in DMD

The normal muscle microenvironment is compromised in fibrosis, taking on characteristics which promote further fibrosis, rather than healing. There are shifts not only in the cell populations which compose the tissue, but also in the formulation of the extracellular matrix which is produced. In terms of cell types, the fibrotic microenvironment leads to changes in cells responsible for regeneration, for inflammation, and for production of extracellular matrix. There is evidence that the myoblast population's ability to replenish cells, and differentiation capability, may be altered in the fibrotic microenvironment. Although many mediators of this event have been identified, one major candidate has been TGF-β[73]. TGF-β has been shown to block myoblast differentiation[82], trigger its apoptosis[83] or myofibroblast transdifferentiation[84], and promote myostatin expression in myoblasts[85]. Hypoxia has also been implicated as a possible factor influencing the ability of myoblasts and muscle satellite cells to differentiate and

proliferate, though there is disagreement in the literature over whether it promotes stemness or differentiation in myoblasts[73,86–88]. The combination of these factors can result in imbalances in the myoblast population that can lead to exhaustion of the population, or, through interactions with other factors, overcrowding of the stem cell niche. As mentioned previously, inflammatory cells also play a key role in the fibrotic microenvironment, with persistence of the M1 macrophage population[55]. M2 macrophages also become elevated in dystrophic muscle, though this activity is insufficient to clear fibrosis[89]. Furthermore, M2 macrophages may actually contribute to the fibrotic microenvironment, as they produce a significant fraction of inflammatory cell derived TGF-β, thus promoting pro-fibrotic signalling[90]. With regards to other inflammatory cells, mice which have had their T and B cell populations depleted experience reduced fibrosis compared to control animals[91]. Although several cell types are responsible for the production of extracellular matrix in healthy skeletal muscle, the major cell candidate for type I collagen production, and basal lamina protein production in general, are fibro/adipogenic progenitor (FAP) cells[73,92]. After proliferating to support normal repair, FAP cells apoptose, but in the case of fibrosis, they remain chronically elevated without this apoptotic event[93–95]. This apoptosis is driven by tumour necrosis factor (TNF), but can be halted by overexpression of TGF-β, as takes place in fibrosis[96]. FAP cells are able to differentiate into adipocytes or myofibroblasts[73,93]. During fibrosis, it suggested that myofibroblasts can arise from many cells types besides FAP cells alone, including pericytes, resident fibroblasts, fibrocytes, endothelial cells, and epithelial cells, as well as locally specific cell types such as myoblasts[84,97,98].

Both the mechanical properties and the composition of the extracellular matrix are altered in fibrosis. Collagen content typically increases in fibrosis, with a greater degree of cross-linking, resulting in a dense collagen network[80,99,100]. DMD patients have additionally shown to have

several proteoglycans, the proteins responsible for water retention and viscous mechanical properties, enriched in their tissue[101]. Fibronectin is also increased in cases of DMD[73,102]. The secretion of matrix metalloproteinases (MMP)s into the extracellular matrix rises, and deletion of particular MMPs, such as MMP-9, has been shown to reduce levels of fibrosis[103,104]. The combination of these changes results in an extracellular matrix which is much stiffer than in healthy conditions. This not only reduces the function of the surrounding muscle tissue, but also has downstream effects due to the deleterious changes in mechanoregulation this has in other cell types. Stiffness has been shown to prompt macrophages to adopt a more M1 phenotype, and prevent differentiation and formation of contractile sarcomeres in myoblasts[73,105–107]. The recognition of the fact the microenvironment in DMD is transformed into one contributing to fibrosis is of vital importance, as it enables the tailoring of therapies to be able to function despite this impediment.

1.1.7 Detection of Fibrosis in DMD

In order to determine the progression of fibrosis, biopsy is often considered the gold standard for staging purposes[108,109]. Although this method does allow accurate assessment of fibrosis stage, it also comes with key downsides in the form of invasivity and limited accessibility. In some patient groups, biopsy may be considered an unnecessary risk due to complicating factors such as the chance of infection, or lasting damaging which the biopsy may produce. This is a concern for DMD patients[7,110]. Investigating other methods to analyze fibrosis, such as the use of imaging technologies or serological markers, is therefore pertinent.

With regards to current imaging technology, this takes several forms. Magnetic resonance imaging (MRI) is able to effectively resolve muscle, fat, and connective tissue, but suffers from difficulties separating fat from water. There is current work being done on fat suppression

techniques that allow better resolution of increased water content brought about by inflammation[81,111,112]. Unfortunately, equipment for MRI is often prohibitively expensive, and may not necessarily be available for DMD patients to use. Elastography-based techniques, which evaluate tissue stiffness using MRI or ultrasound imaging of mechanical sheer waves[113], and impedantometry, which examines tissue water content through propagation of electrical current, are both promising new techniques to examine muscle tissue[114,115]. However, little work has been conducted examining their use in DMD patients. Similarly, myography, which involves examining the physical properties of near-surface muscle through palpation, also shows promise, but requires investigation with regards to specific applications in DMD patients[81,116]. Positron emission tomography-computed tomography (PET-CT) techniques, combining modern imaging with radiolabeled substances which localize to fibrotic regions, have also seen some exploration in recent years[117]. However, little focused has been placed on PET-CT in DMD patients. In general, these imaging techniques are still in development, and may require combination with serological marker evaluation to accurately gather information about fibrosis.

In terms of current serological markers for fibrosis, a great deal of focus has been placed on liver and cardiac fibrosis markers, with a lesser, though still considerable, amount of analysis on skeletal muscle fibrosis markers. There have been several large-scale studies on markers in DMD patient and mouse model sera. A 2014 study which evaluated 355 mouse sera proteins found 23 which were significantly elevated in the *Mdx* mouse model, of which twenty were also elevated in serum derived from human DMD patients. These could be divided into several categories, and primarily consisted of glycolytic enzymes, transport proteins, and myofibrillar proteins. There were several possible candidate proteins detected which had links to fibrosis, as opposed to muscle degeneration alone. Some examples include thrombospondin 4 (TSP4), an

extracellular remodeling protein, and matrix metalloproteinase 9 (MMP9), an extracellular protease[118]. MMP9 has been previously correlated with DMD disease severity over time in patients[119]. Another study analyzing DMD and BMD patients found similar results with regards to markers of muscle degeneration, but elucidated difficulty with regards to separating cases of DMD from BMD utilizing MMP9 alone. It did not examine TSP4[73,120]. Exploration of these and similar markers in the future is vital to accurately determine levels of fibrosis. Combining multiple markers into a panel-based measure may be necessary.

1.1.8 Treatment

There are several treatments available for DMD. Corticosteroids are most commonly used to increase muscle strength and slow rate of decline, but often have complications. Other drug therapies, such as anabolic steroids and immunosuppressive agents, which attempt respectively to boost muscle strength, and prevent inflammatory responses, are in early stages of exploration. Respiratory dysfunction often results in repeated infections, necessitating chest physiotherapy and antibiotic use[4,7–9]. Cardiac symptoms also require monitoring, though treatment of these is limited to beta blockers and angiotensin converting enzyme inhibitors[7]. Despite advances in physical therapies and steroid treatments, no cure or long-term treatment for DMD has been found.

Several promising new therapies have also appeared in recent years, primarily in the form of gene therapy variants. Some of the most common versions of these are viral vector strategies, which normally make use of recombinant adeno-associated viral vectors carrying components of the dystrophin gene. These are capable of restoring some dystrophin expression in mouse models. However, the size of the dystrophin gene creates challenges for this therapy, as the normal gene is too large to be transported within adeno-associated virus. Attempts have been

made to supply truncated, but still functional, versions of the gene. However, many of these attempts result in either sacrifice of some dystrophin gene functions, or reduced transduction efficiency[121,122]. Nonetheless, there are ongoing clinical trials utilizing this technique, such as with rAAVrh74.MHCK7.micro-dystrophin or PF-06939926[123]. Another strategy which still utilizes adeno-associated viral vectors is CRISPR/Cas9 delivery. This can be targeted toward single mutations bringing about DMD, and past studies have showed some success in mouse models. This has included measures such as force generation, evaluation of CK level, and histological examinations such as rate of tissue necrosis[121,124–126]. Nonetheless, these strategies still face problems, generally associated with delivery and specificity. Fibrotic environments, such as those found in DMD, often have reduced blood perfusion, and therefore poorer delivery of viral carriers. Effectively targeting adeno-associated virus to a single cell type can also be challenging, Additionally, these strategies do not directly target the muscle microenvironment or the fibrosis that is associated with DMD. Even if these treatments were successful, loss of muscle strength may persist for months, or last indefinitely. Drugs which induce exon-skipping, such as Eteplirsen, are also under investigation[127]. These produce partially-functional dystrophin which ignores critically mutated exons. Unfortunately, only cases with mutations in particular vulnerable exons are possible candidates for this form of treatment. Stem cell therapy has been considered in the past as a possible treatment for DMD, but complications have arisen due to the nature of the therapy. Nonetheless, novel methods to adjust the therapy to make it suitable for DMD are still being studied. Stem cell therapy involves supplying DMD patients with new muscle stem cells which produce dystrophin, and which can replace their normal dystrophin null stem cells. However, immune responses to myogenic stem cells derived from donor sources limit their applicability, as the body may destroy these before any therapeutic benefit is yielded.

Additionally, the stem cell niche, which enables stem cell proliferation and differentiation, can often be destroyed through the process of fibrosis[73,128,129]. Autologous myogenic stem cell sources are a possible solution to the immune response issue. Ex vivo gene correction techniques, such as chimeraplasty and small fragment homologous replacement therapy, can be used prior to expansion of these myogenic stem cell colonies. These can then be transplanted back into the host from which the cells were derived. Unfortunately, dystrophic muscle often has a low population of myogenic stem cells, making it difficult to extract a sufficient number to begin this process[121,130–132]. Even techniques involving bone marrow-derived stem cells with myoremodeling capacity need other measures to acquire a sufficiently large population[133]. Satellite cell transplantation has been shown to be improved by initial treatment with a neutralizing antibody against connective tissue growth factor[73,134]. It is clear that these upcoming techniques still require refinement before being candidates for DMD treatment.

Another group of upcoming therapies, rather than focusing on correcting mutations in the dystrophin gene, attempt to address the fibrosis associated with the condition. Anti-inflammatory drugs, such as TNF inhibitors, and nuclear factor kappa-light-chain-enhancer of activated B cells (NF-κB) inhibitors, are possible candidates to be repurposed for an antifibrotic role[81,135].

TGF-β is a possible target for this therapy. In radiation-induced fibrosis in cancer treatment, and in scleroderma cases, halofuginone is able to block the canonical TGF-β pathway, inhibiting synthesis of type I collagen, slowing fibrosis[73,74]. Another activator of the MAPK and SMAD pathways is the renin-angiotensin system, where angiotensin-converting enzyme 1 (ACE1)-mediated conversion of angiotensin I into angiotensin II allows it to bind to the angiotensin II (AT1/2) receptors, which can promote these pathways[136]. Inhibitors of ACE1, such as Enalapril and Lisinopril, and the AT1/2 blocker Losartan, are all potential antifibrotic

treatments[73,137–139]. Nitric oxide enhancers such as the phosphodiesterase 5 inhibitor sildenafil may also serve a role, as hypoxia has been shown to increase fibrosis, and treatment with these enhancers may reduce it[140]. Antioxidants such as idebenone[141] and resveratrol[142], and mineralocorticoid antagonists like eplerenone[81,143], are also possible candidates. Combining nutrition, physiotherapy, and temperature-based techniques with these drugs can create a holistic approach to addressing fibrosis in DMD patients[81]. However, additional research will need to be conducted in order to determine how applicable these drugs are for use in DMD patients, and at what stages of fibrosis they can be used at.

This suggests two major directions in which to continue research. Firstly, to develop new treatments aimed at improving the microenvironment and reducing fibrosis. Secondly, to develop techniques to identify areas that will become fibrotic before permanent damage takes place. To meet these goals, it is necessary to identify biomarkers of the fibrotic microenvironment.

1.1 Wilms' Tumour 1 (Wt1)

1.1.1 Overview

Wilms' Tumour 1 (Wt1) is a zinc-finger transcription factor with additional roles in post-transcriptional regulation, and control of other transcription factors. In mammals, the gene is composed of ten exons, and is approximately 50 kb in length[144]. The human protein Wt1 was originally identified in Wilms' tumour, but has since been implicated as a factor in multiple other conditions, such as the Denys-Drash and Frasier syndromes[144–146]. It has numerous isoforms, which act in related but distinct cellular roles. Twenty-four different forms of Wt1 protein have been identified in murine and human models. However, recent research suggests that there are additional Wt1 isoforms which have so far been uncharacterized in the literature[147,148]. The different Wt1 isoforms arise primarily from alternative starts sites where translation of Wt1

protein takes place, and from alternative splicing, though there is some evidence that RNA editing may also play a role[148,149].

1.1.2 Wt1 Expression during Development

Wt1's most well-known functions, apart from pathogenesis, are its roles in the regulation of mammalian embryonic development. Wt1 has been found to have roles in several major organ systems, most prominently the gonads and kidneys, but also the cardiac, nervous, and respiratory systems. In mice with mutations in their Wilms' tumour 1 gene, *Wt1*, these organs often develop poorly, or not at all, resulting in embryonic lethality[148,150–152].

In the gonads and adrenal glands, Wt1 serves a variety of roles. It has been shown to reduce Leydig cell formation while promoting Sertoli cell differentiation through its promotion of the sex-determining region Y (SRY) gene[153]. Mice which are *Wt1* null fail to develop adrenal glands or the gonads[154]. In kidney development, Wt1 is expressed in the metanephric mesenchyme. There are multiple Wt1 target genes vital for proper mesenchymal function during this stage, including spalt-like transcription factor 1 (Sal1), bone morphogenetic protein 7 (Bmp7), and paired box gene 2 (PAX2). Wt1 also controls several other key regulators of mesenchymal proliferation and apoptosis[144,155,156]. Not only does Wt1 maintain the mesenchyme of the developing kidney, it also supports the formation of the proximal nephron and podocytes. Wt1 expression becomes localized to the arising nephron during nephrogenesis, and eventually is confined to the proximal developing nephron, and then the developing podocytes[144,152].

Wt1 expression during cardiac development is primarily in the epicardium. Eliminating expression of the Wt1 mouse protein has been shown to prevent proper cardiac vascularization. Wt1 appears to be required for epithelial and mesothelial to mesenchyme transitions, and this transition is necessary for epicardial derived coronary vascular cell progenitor formation[144,157].

Furthermore, Wt1 deletion can cause incomplete formation of the diaphragm, leading to herniation of the abdominal organs into the chest cavity[144,158].

1.1.3 Wt1 Expression during Adulthood

Beyond development, Wt1 and its isoforms also serve functions in adult organisms, primarily in the kidneys, gonads, and bone marrow. Deletion of Wt1 in adult mice triggers severe glomerulosclerosis in the kidney, as well as bone loss, and atrophy of the spleen and exocrine pancreas. Insulin growth factor 1 (IGF1), a regulator for both bone and fat growth, was reduced in circulation in these models, suggesting that Wt1 may serve a role in controlling it[159]. In the cortex of the adult adrenal gland, research has indicated the presence of rare Wt1 expressing cells which, through adulthood, can still differentiate into steroidogenic cells. Gonadectomy appears to stimulate this differentiation[144,160]. In the kidneys, Wt1 serves roles in regulating nephrin and podocalyxin in podocytes[144,161,162]. Expression of Wt1 additionally takes place in the adult mouse heart, serving a role in coronary vascular cell proliferation following ischemia[147,163]. There is evidence that transcription of the *Wt1* mouse gene can be directly upregulated by hypoxia-inducible factor 1 (HIF1)[144,164].

1.1.1 Wt1 Protein Structure

The role a particular Wt1 isoform fulfills is largely determined by how it has been post-transcriptionally modified, though there are nonetheless some common functions between variants. The capacity for Wt1 to bind certain DNA and RNA sequences is mediated through its zinc finger domains, and these are present in all major isoforms, though there is evidence the affinity for particular DNA or RNA sequences can differ between different Wt1 isoforms[165]. Wt1 isoforms can be divided into four major groups (Fig. 2), defined through their inclusion of exon

five (EX5), and through inclusion of a lysine, threonine, and serine (KTS) amino acid sequence toward the end of exon nine[147]. Commonly, the isoforms of Wt1 are referred to as A (EX5-/KTS-), B (EX5+/KTS-), C (EX5-/KTS+), and D (EX5+/KTS+).

Exon five enables interactions with prostate apoptosis response factor 4, by encoding a protein-protein interaction domain. This modulates the ability of Wt1 to regulate cell proliferation[144,166]. In the adult mammary glands, exon 5 bearing isoforms are expressed[167]. Furthermore, there is preliminary evidence that exon 5 appears to partially compensate for some zinc finger function. Natoli et al. showed that so long as exon 5 is present, both the third and fourth zinc fingers of Wt1 can be deleted, with normal viability and kidney histology maintained. However, additional work is necessary to confirm this[168].
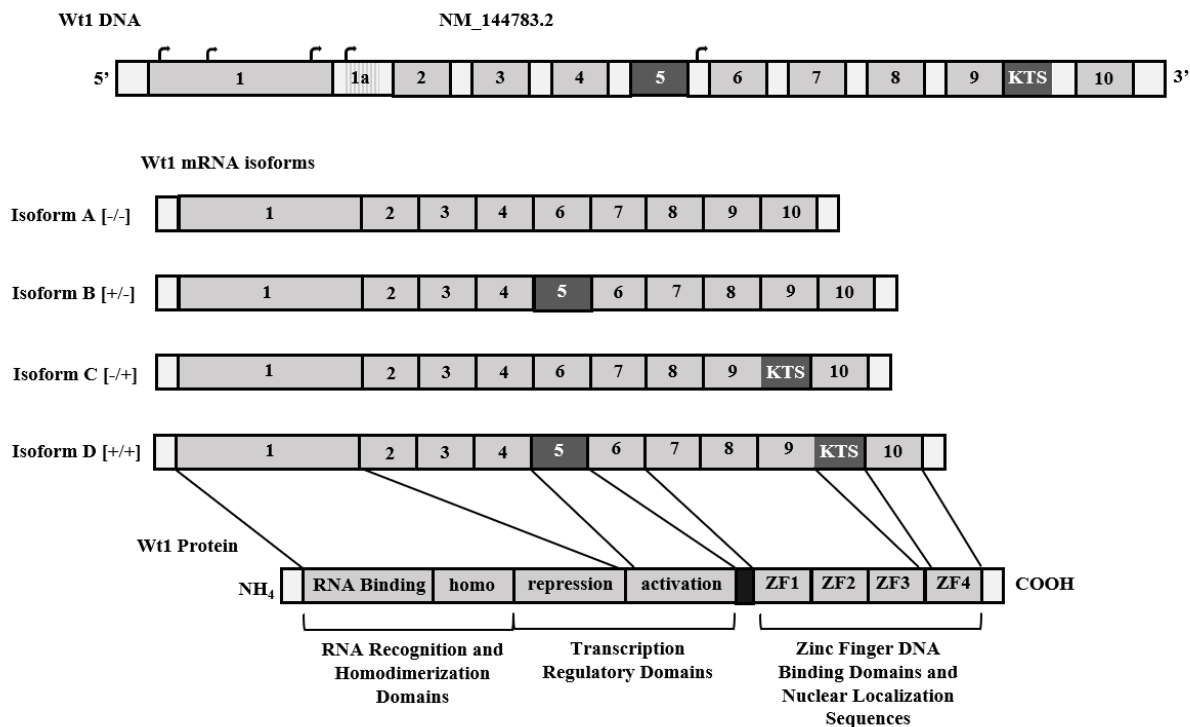
Figure 2. Wt1 and Isoforms

Diagram of *Wt1* gene, some of its mRNA products, and the translated protein. Alternative translation initiation sites are indicated by the black arrows, alternative splice sites are indicated by dark coloration, and an alternate exon produced by an alternative translation initiation site is indicated by vertical hatching. Portions of this figure adapted from Kramarzova (2012).

The KTS sequence is suspected to be involved with the splicing machinery itself, and its regulation. However, the two isoforms do have some degree of overlapping function, as studies evaluating developing mice where only one of the two isoforms have been expressed reveal little to no differences in the development of the cardiovascular or genitourinary systems. Isoforms with the KTS sequence show stronger affinity for insulin growth factor 2 (IGF2) RNA than those lacking the sequence. However, those without the sequence still maintain some binding affinity, likely mediated through zinc finger activity[165,169]. This activity can be modulated by post-transcriptional regulation. Inclusion of the KTS sequence likely limits the ability for Wt1 to bind early growth response-1 (EGR1) sequences in the genome. Wt1 increases the stability of p53, inhibiting its apoptotic effects[170]. This interaction not only has been shown to modulate the transcriptional activity of p53, but also that of the Wt1 isoform lacking the KTS sequence[171]. The binding partners of Wt1 may have distinct interactions with it dependent on the particular isoform to which they are bound.

Regardless of the presence of the KTS sequence, Wt1 can bind sequences for several other genes, including *IGF2*, platelet derived growth factor subunit A (*PDGF-A)*, *PAX2*, and its own *Wt1* gene sequence. Wt1 is capable of both transcriptional activation and repression, and debate is ongoing over which comprises its major role[147,172–176]. Although Wt1 has many roles in the nucleus, it is also found to some extent in the cytoplasm. For example, in developing skeletal muscle, myocardium, and the endothelial cells of blood vessels[177]. One possible explanation for this localization is interactions with translation. Wt1 has previously been shown to associate with translating polyribosomes, and that regardless of the presence of exon 5 or the KTS sequence, this activity is maintained. This may indicate active involvement of Wt1 with the translation of protein, or interactions with RNA outside the nucleus[178].

1.1.2 Wt1 in Fibrosis

Although its discovery was through its appearance in forms of cancer, recent research has shown Wt1 to also be involved with fibrosis, for example, in idiopathic pulmonary fibrosis and Dupuytren's Disease (DD). One 2015 study by Sontake and colleagues showed that Wt1 expression was present in subpleural fibrotic lesions in the lungs of human idiopathic pulmonary fibrosis patients, but not in healthy patients. Cultures of mesenchymal cells taken from these tissues showed increased *Wt1* transcript presence. When knocked down with siRNA against *Wt1*, these cultures showed significant decreases in production of several extracellular matrix genes. Mice which had subpleural fibrotic lesions induced by TGF-α overexpression showed similarly increased Wt1 expression in vimentin-positive mesenchymal cells and alpha smooth muscle actin (α-SMA) expressing myofibroblasts, though not in fibrocytes. However, fibrocyte infusion did appear to increase the number of Wt1 positive cells in mice[179]. Lineage tracing experiments have furthermore shown that Wt1-positive mesothelial cells are a major source of mesenchymal cells, and specifically, myofibroblasts, in subpleural fibrotic lung lesions. Transfection with Wt1-overexpressing lentivirus increased fibroblast-to-myofibroblasts transformations in fibroblast cultures derived from mice, and Wt1 knockdown is able to reduce rates of proliferation in fibroblast cultures derived from human idiopathic pulmonary fibrosis lung tissue. Partial knockout of Wt1 in TGF-α mice is able to reduce lung hydroxyproline levels and improve lung compliance, and reduce Masson's trichrome staining in bleomycin treated wildtype mice[180]. However, other research has run contrary to this narrative. A 2014 study by Karki and colleagues found reduced Wt1 expression in idiopathic pulmonary fibrosis lung tissue pleural mesothelial cells. Treatment of pleural mesothelial cells with shRNA against Wt1 was found to cause a mesothelial to mesenchymal transition, with upregulation of fibronectin and α-SMA, an altered

morphology, and increased collagen gel contractility[181]. Another area of particular interest has been research concerning the upregulation of Wt1 expression in primary fibroblasts derived from DD. Immunohistochemistry of fibrotic tissues taken from DD patients revealed clusters of cells expressing Wt1, and quantitative polymerase chain reaction (qPCR) analysis of Wt1 expression in fibroblast cultures derived from these tissues showed upregulation of Wt1 compared to control fibroblast cultures. Control cultures in this study were derived from syngeneic fibroblasts, suggesting that neither genetic variability or systemic effects were the cause of the Wt1 upregulation, but that it was brought about by fibrosis itself.[182]. This suggests that, if it is the case that Wt1 is a marker for fibrosis, it may be a marker in several fibrotic disorders, including fibrosis induced by DMD. Nonetheless, the literature is currently divided on this topic, so it would be worthwhile to gather a deeper understanding of Wt1 overall.

1.2   Animal Models of DMD

1.2.1 Dystrophin Knockout Mice

Numerous animal models of DMD have been engineered, across a range of species, but some of the most well-studied have been mice[183]. Particularly, the X chromosome-linked muscular dystrophy (*Mdx)* mouse, a dystrophin-null model, has received the most examination as a model of the disease (Fig. 3). The *Mdx* mouse model possesses a point mutation in the dystrophin gene, resulting in production of no functional dystrophin[184].

Figure 3. Different Mouse models of Duchenne Muscular Dystrophy

Representative images of wildtype (A), *Mdx* (B), *Mdx*/*Utrn*+/- (C), and *Mdx*/*Utrn*-/- (D) mice. Table depicting the number of alleles expressing dystrophin and utrophin, as well as the age ranges utilized, for each mouse model (E).

There are increased muscle creatine and pyruvate kinases in the *Mdx* mouse model, alongside muscle lesions typical of human DMD patients[185]. The *Mdx* model exhibits histological features characteristic of muscle degeneration, including centrally-nucleated myofibers and the presence of inflammatory infiltrate. Other DMD-like symptoms also occur, such as fibrosis, but not as extreme as in the case of most human DMD. Fibrosis is often limited to certain muscle groups, such as the diaphragm, with muscle groups like the hind limb experiencing negligible fibrosis. Furthermore, the *Mdx* mouse model exhibits little weakness[186–188]. A 2015 study characterized the *Mdx* model, alongside several others, compared to the wildtype. Examination of muscle weakness via a grip duration test, measuring the duration which mice can support their body weight by gripping to a mesh, showed only minor deficits in the *Mdx* mouse compared to the wildtype prior to six months of age. Furthermore, after six months, the durations both groups could grip the mesh had become indistinguishable. Rotarod testing, which evaluates how long a mouse can remain on a rotating rod, found similar results, with *Mdx* mice performing marginally poorer than the wildtype for the first six months of life, and then becoming similar to the wildtype thereafter. Triceps myofiber cross-sectional area was significantly smaller than the wildtype in the *Mdx* model until twelve months of age, and the distribution of different myofiber areas differed from the wildtype until approximately six months of age. Furthermore, the myosin isoforms expressed in this tissue did not differ in the *Mdx* model compared to the wildtype. In the *Mdx* mouse, density of collagen IV was shown to be significantly increased from the wildtype in the triceps after twelve months, though density of collagen I was increased from as early as three months[189]. The *Mdx* mouse model additionally has altered presentation of cardiac symptoms compared to human DMD patients. Cardiac fibrosis does not occur in this model until later in life, and furthermore exhibits other differences,

such as the absence of hypokinesia and dyskinesia, uniform distribution of the fibrotic material, and a reduced amount of fibrosis compared to DMD patients. Additionally, *Mdx* mice have an increased life expectancy compared to DMD patients, with a 25% reduction in life expectancy compared to wildtype mice, in contrast with the 75% reduction from normal life expectancy as seen in human DMD patients[183,190]. This makes the *Mdx* mouse an incomplete model for DMD, as the more severe features of the disease are not accurately represented. It is therefore pertinent that other models be utilized, in order to recapitulate the condition as seen in humans more clearly.

1.2.2 Dystrophin and Utrophin Knockout Mice

The literature suggests that, in mice, the presence of utrophin, a dystrophin homolog, provides a compensatory effect which alleviates some of the pathology produced by dystrophin loss. In mice, use of a utrophin transgene has been shown to ameliorate pathology caused by the absence of dystrophin. Furthermore, muscle regions which normally have high utrophin exhibit lower muscle degeneration in mice[188,191–193]. Knocking out utrophin, either partially, as in the case of *Mdx*/*Utrn*+/- mice, or totally, as in the case of *Mdx*/*Utrn*-/- mice, provides an avenue by which pathology more similar to human DMD can be evaluated.

The *Mdx*/*Utrn*+/- model has been shown to experience greater muscle weakness than *Mdx* or wildtype mice. In the 2015 study previously discussed, this was determined by grip duration and rotarod testing. Grip duration evaluations showed *Mdx/Utrn+/-* mice performing at less than a quarter of the ability of either the *Mdx* or wildtype mice at the initial one month of age examination point, and they remained lower than both of these other models effectively during all evaluation points. Rotarod testing indicated significant deficits for *Mdx/Utrn+/-* mice compared to both Wildtype and *Mdx* genotypes, until roughly eighteen months of age. The

Mdx/*Utrn*+/- model mice exhibit differences in the distribution of the sizes of their myofibers, as well as differences in the expression of myosin isoforms, which are not present in the *Mdx* model. Analysis of deposition of collagen I and collagen IV showed significant increases in this deposition compared to the wildtype at all of the age points examined in this study, as well as from the *Mdx* model, except for the 6 month age point for collagen I[189]. The differences in collagen deposition observed have been replicated in other studies, and indicate that particular tissues may become fibrotic in the utrophin knockout models which do not become fibrotic in the *Mdx* model. As fibrosis is a significant cause of human DMD patient mortality, this is an important feature to focus on[189,194]. An independent 2012 study showed similar results for rotarod and grip duration testing of *Mdx* mice, though it showed that all of *Mdx*, *Mdx/Utrn+/-,* and *Mdx/Utrn-/-* mice perform similar on fore limb grip strength tests. This study additionally showed a nonsignificant correlation between the number of utrophin alleles knocked out and the expression of inflammatory and fibrotic genes in mouse quadriceps muscle[195]. Single utrophin allele knockout in the *Mdx* model has been shown to significantly reduce diaphragm function, and causes both increased inflammation and fibrosis in the diaphragm and other skeletal muscle groups[186,187]. Some research has indicated that there is a correlation between the number of utrophin alleles knocked out, and the increasing presence of centrally-located nuclei indicative of muscle fiber regeneration[195]

In the *Mdx*/*Utrn*-/- model, where there is no utrophin or dystrophin expression, lifespan is reduced to 3-4 months, approximately only 11% of the normal lifespan of a wildtype mouse[183]. For the purposes of evaluating these mice, this can be problematic, as it limits long-term studies, and complicates animal care and handling. These mice experience severe muscle weakness at an age earlier than even that of the *Mdx*/*Utrn*+/- model. Examination has shown that these mice are

unable to maintain their grip or remain on a rotarod at even one month of age. Furthermore, they also experience different expression of myosin isoforms and distribution of myofiber sizes, similar to the *Mdx/Utrn+/-* model. Their collagen deposition is also not significantly different than that of the *Mdx/Utrn+/-* model[189]. Past research has shown that tibialis anterior muscle degeneration is only transient in the *Mdx* model, while persistent in the *Mdx*/*Utrn-/-* model, and furthermore that cardiac manifestations are more severe in the *Mdx*/*Utrn-/-* model[188]. Utilization of additional *Mdx*/*Utrn+/-* and *Mdx*/*Utrn-/-* models provides a deeper understanding of disease progression.

1.3   Research Outline

In this thesis, wildtype, *Mdx*, *Mdx*/*Utrn+/-*, and *Mdx*/*Utrn-/-* mice were utilized. Collectively, an analysis of all of these genotypes allow exploration of various DMD severities[194]. Furthermore, this study included mice at 4-5 weeks old, 8-10 weeks old, and 10-14 months old, representing immature, mature, and aged mice. These ages allow an interrogation of Wt1 expression changes with respect to the progression of fibrosis over time. Heart, diaphragm, and gastrocnemius muscle tissue were examined for these mice, as prior work suggests that fibrosis does not arise in all muscle groups in DMD model mice simultaneously, allowing examination of these differences. However, only 8-10 week old wildtype and *Mdx*/*Utrn+/-* gastrocnemius muscles were used to evaluate mRNA expression. This provides examples of non-fibrotic tissue, in the form of the 8-10 week old wildtype gastrocnemius muscle tissue, and fibrotic tissue, in the form of the 8-10 week old *Mdx*/*Utrn+/-* gastrocnemius muscle tissue[194].

2   HYPOTHESIS AND OBJECTIVES

2.1   Hypothesis

Previous studies indicating that Wt1 is both a marker for fibrosis in DD[182] and idiopathic pulmonary fibrosis[179,180] suggest that Wt1 may be a marker for multiple fibrotic conditions. Therefore, this has led to the hypothesis that Wt1 immunoreactivity is a marker for fibrosis in a mouse model of DMD.

2.2   Rationale and Objectives

1. To evaluate the timing and location of expression of Wt1 with respect to the onset of fibrosis in a mouse model of DMD.

   The rationale behind this objective was that it will provide a thorough understanding of the changes in Wt1 immunoreactivity throughout the aging process and at multiple levels of fibrosis in these models, allowing a comparison with DMD patient fibrosis more accurately. In order to address this objective, immunohistochemistry was used to assess Wt1 immunoreactivity location, as well as its quantity as a function of the proportion of a tissue and its structures which were immunoreactive for Wt1. Furthermore, Masson's trichrome staining was also used to determine the level of fibrosis, and hematoxylin and eosin staining was used to identify candidate cell types that Wt1 may be found in.

2. To determine which isoforms of Wt1 are altered during the onset of fibrosis in a mouse model of DMD.

   The rationale behind this objective was that it will elucidate how Wt1 expression changes with regards to the particular isoforms that are expressed in fibrotic conditions. This may enable more specific targeting in reference to treating isoforms responsible for tissue fibrosis. In order to address this objective, qPCR was utilized to assess total *Wt1* expression, as well as the fraction

of the sum of expression of its four major isoforms which each of the four major isoforms was responsible for.

3 MATERIALS AND METHODS

3.1 Samples

3.1.1 Animal Care and Tissues

All animal protocols were approved by the Institutional Animal Use Subcommittee (Western University, London, ON, Canada) and conducted according to guidelines set by the Canadian Council on Animal Care (CACC); ethics approval documentation can be found in Appendix A. Mice were maintained in the Animal Care Facility at St. Joseph's Health Care (SJHC), under controlled conditions (19–23˚C, 12 hour light/dark cycles), and allowed water and food *ad libitum*. Wildtype, *Mdx*, and *Mdx*/*Utrn*+/- mice were obtained from the Jackson Laboratory (Bar Harbor, ME), with additional wildtype mice purchased from Charles Rivers. An additional portion of the *Mdx*/*Utrn*+/- mice were provided by Dr. Robert Grange (Virginia Polytechnic and State University), originally generated by Dr.'s Mark Grady and Josh Sanes (Washington University, St. Louis)[188]. Production of *Mdx*/*Utrn*-/- mice was conducted by breeding together *Mdx*/*Utrn*+/- mice. Mice that declined in health, characterized by a loss of 15% body mass, lethargy, dehydration, labored breathing, and lack of appetite, were euthanized to prevent suffering. Genotyping was conducting by polymerase chain reaction (PCR), using tail snips or ear notch tissues.

Cohorts used in this study consisted of three mice of a particular age range, either 4-5 weeks old, 8-10 weeks old, or 10-14 months old, as well as a particular genotype, being either wildtype, *Mdx*, *Mdx*/*Utrn*+/-, or *Mdx*/*Utrn*-/- mice (n = 3 for all groups). However, 10-14 month old *Mdx*/*Utrn*-/- mice were not utilized due to a short life expectancy prohibiting study. Mice from a C57B1/6ScSn and C57B1/10ScSn background were pooled for each cohort. Upon reaching the desired age, mice were sacrificed through cervical dislocation following gas

euthanasia. Immediately after this, diaphragm, heart, and gastrocnemius muscles were dissected and fixed in 10% formalin for 24-48hrs. These tissues were then embedded in paraffin. For some of the 8-10 week old wildtype and *Mdx*/*Utrn*+/- mice, a second gastrocnemius muscle was extracted and either immediately flash frozen, or placed into RNA*later*™ (Thermo Fisher Scientific) reagent and stored at -20ºC, for later RNA extraction.

3.1.2 Human Tissues

Human muscle tissue samples were acquired from the University of Maryland Brain and Tissue Bank, fixed in 10% formalin, and embedded in paraffin. One sample of skeletal muscle from a DMD patient, and one from a healthy control, were used. These were subjected to staining in an identical fashion to the mouse tissue blocks, but were used exclusively for immunohistochemistry and Masson's trichrome staining. These samples underwent solely qualitative analysis through visual inspection.

3.2   Histology

3.2.1 Tissue Preparation

Immunohistochemical staining (performed in-house) and Masson's trichrome staining (performed at the Pathology Department at University Hospital, London, ON) were performed on all cohorts as well as on human DMD patient muscle tissue, with three biological replicates for each mouse cohort, and one biological replicate for human samples. Hematoxylin and eosin staining (performed at the Molecular Pathology Lab at Robarts Research Institute, London, ON) was performed on a single biological replicate for each mouse cohort. Furthermore, three technical replicates were utilized for Masson's trichrome and immunohistochemistry of mouse tissues. Single technical replicates were used for human tissues, as well as hematoxylin and eosin staining. Sections produced from each block were 5μm in thickness.

3.2.2 Immunohistochemistry

For those tissue sections proceeding with immunohistochemistry, a modified protocol based on Abcam standards was performed. The sections were first deparaffinized and rehydrated in a series of xylene and ethanol washes. This was followed by heat-mediated antigen retrieval in a Tris-ethylenediaminetetraacetic acid (EDTA) buffer for 20 minutes. Slides were then cooled slowly to room temperature, and incubated in a 3.0% hydrogen peroxide solution for 10 minutes to block endogenous peroxide activity. The slides then underwent nuclear permeabilization via treatment with 0.3% Triton X-100 in phosphate buffered saline (PBS) for 10 minutes, with an additional two washes for five minutes in PBS before and after this treatment. Background Sniper (Biocare Medical) was applied for 8.5 minutes as a blocking reagent to reduce non-specific background staining. Tissue sections were then incubated overnight with either anti-Wt1 (Abcam, 1:250), or no antibody, the latter as a negative control (Fig. 4). A negative control was conducted in this fashion for every tissue stained and quantified (Appendix B-D). The anti-Wt1 antibody is a rabbit monoclonal antibody against the 50-250 amino acids of the Wt1 protein. As a positive control and true negative control one section of mouse kidney was stained with anti-Wt1. This staining followed the same protocol, alongside each group of slides stained, for those slides which would be quantified. Kidney podocyte staining was used as a positive control, while negative staining of the medulla was used as a true negative control[144] (Fig. 5). Sequential dilutions of antibody were tested in order to determine 1:250 as an appropriate working concentration. All incubations were conducted in 1% bovine serum albumin (BSA) PBS. After washing twice in PBS for five minutes, tissue sections were then incubated with a biotinylated secondary antibody (Vector Labs, 1:200) for one hour, and following two additional five minutes PBS washes, with ExtrAvidin®−Peroxidase (Millipore Sigma, 1:100). Oxidization of 3,3′-

diaminobenzidine (DAB), with the substrate left on each sample for 2.5 minutes, was then used to visualize these sections, with nuclei counterstained using Carazzi's hematoxylin. Sample diaphragm and gastrocnemius tissue sections derived from 8-10 week old *Mdx*/*Utrn*-/- mice then underwent eosin staining to enable identification of cell types. Additionally, one sample of each tissue type did not undergo Carazzi's hematoxylin counterstaining (Appendix F-H)
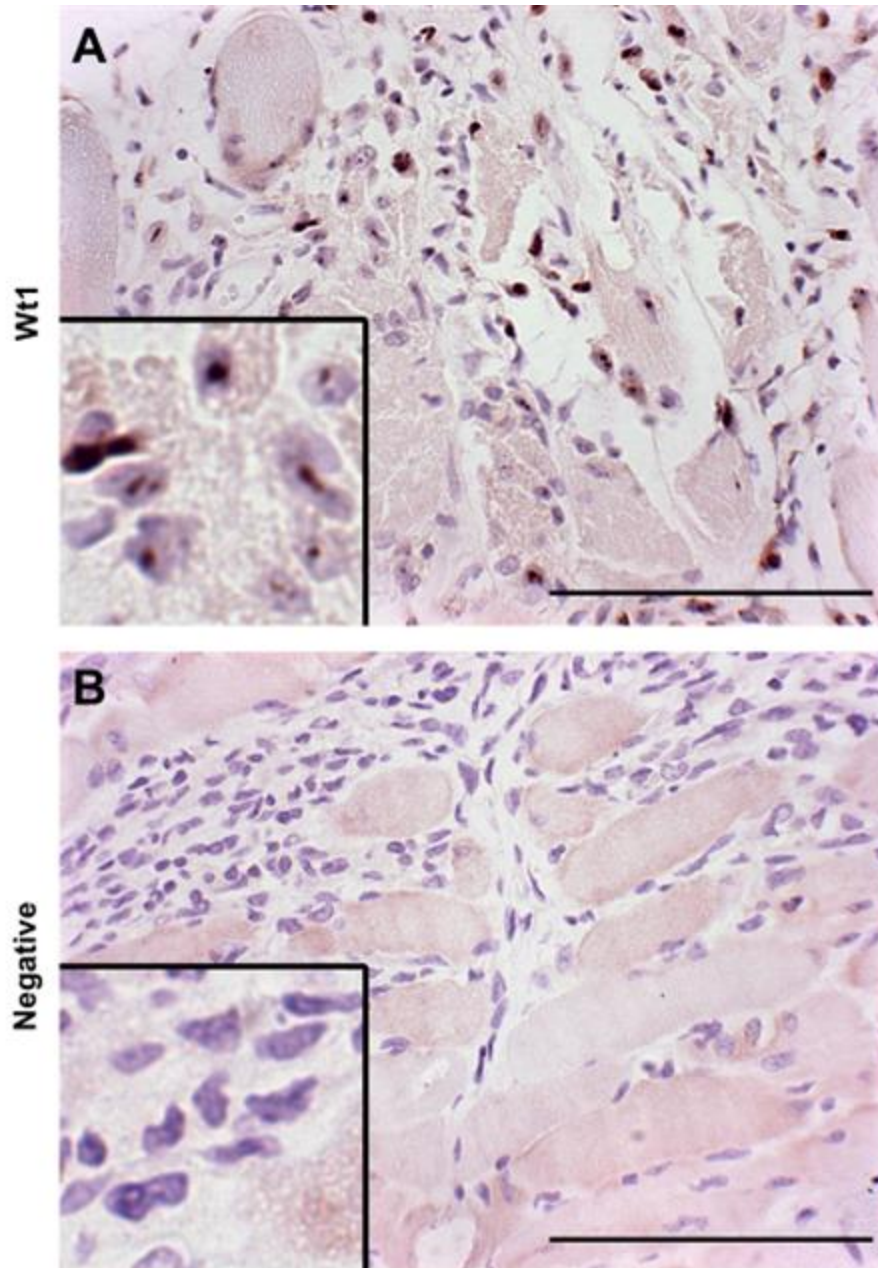
Figure 4. Representative images of diaphragm assessed for Wt1 immunoreactivity, alongside a negative control, in 8-10 week old *Mdx* mice.

An example section of 8-10 week old *Mdx* diaphragm evaluated immunohistochemically for Wt1, with nuclei counterstained using hematoxylin (A). Additionally, the same procedure was conducted without primary antibody as a negative control (B). In the bottom left corner, a section of magnified nuclei are provided for examination (scale bar = 100μm).
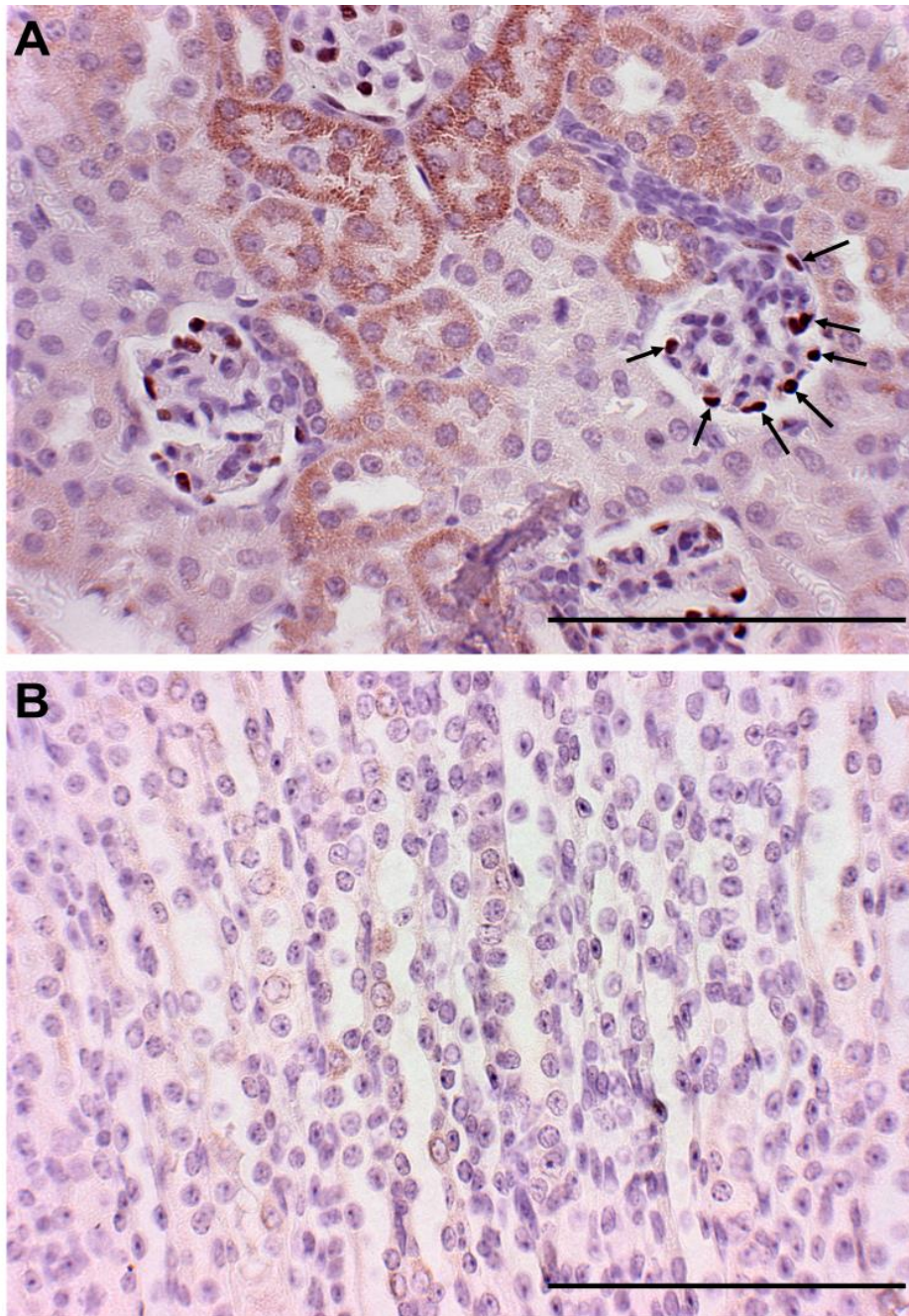
Figure 5. Positive control validation of Wt1 antibody binding in kidney podocytes, and negative control validation of Wt1 antibody binding in kidney medulla.

An example section of 4-5 week old *Mdx/Utrn-/-* kidney evaluated immunohistochemically for Wt1, with nuclei counterstained using hematoxylin. Podocytes immunoreactive for Wt1 can be identified in the clustered regions of nuclei indicative of Bowman's capsules, one of which have been identified with arrows, while Wt1 immunoreactive cytoplasm can be identified in the proximal portion of developing nephrons (A). Additionally, an image of the medulla of this same section, showing no Wt1 immunoreactivity (B) (scale bar = 100μm).

3.2.3 Microscopy and Image Analysis

For imaging of collagen content, and Wt1 DAB stain intensity, images were acquired on a Zeiss Axioskop 50 Microscope under a 40x objective, for Wt1, or a 20x objective, for collagen content, using Eclipse Image Software. Up to ten images were taken from each tissue section, with a minimum of five images. For immunohistochemistry images, care was taken not to image regions of fat where false-positive signal was generated due to sequestering of DAB reagents.

For nuclear Wt1 quantification in tissue sections, nuclei and the number of nuclei positive for Wt1 were quantified using Fiji[196,197] and QuPath[198]. Images were pre-processed in Fiji, through background subtraction, and manual selection of the tissue component of the image and application of a color balancing macro. This was to ensure that nuclei were considered positive only if they have darker staining than the surrounding region. Positive nuclei were then determined through the positive cell detection module in QuPath, first quantifying the number of nuclei by identifying regions of the image which were significantly 'blue' compared to the background, and then determining if those nuclei were positive for Wt1 by either having a mean or max 'brown' color above two separate threshold parameters (Fig. 6).

For muscle cytoplasm and non-muscle tissue quantification, regions of tissue positive for Wt1 were assessed using a simple thresholding algorithm in Fiji. Images were pre-processed in Fiji, through background subtraction, and manual selection of the non-tissue component of the image and application of a color balancing macro. For each image, if possible, separate regions of interest were manually outlined containing muscle cytoplasm or non-muscle tissue. This was determined through examination of these regions for typical histological features of muscle and non-muscle tissues (Appendix E). Images which did not contain one of these regions were not included in the evaluation of that region for the respective tissue section. These regions were,

after selection, then given a standard threshold, to determine the percent area which is sufficiently brown, deemed Wt1 positive. This was conducted for both the experimental sections as well as the negative controls for each sample. The negative control signal was subtracted from the experimental sections, to yield a true Wt1 immunoreactivity (Appendix B-D).

Collagen content was assessed across all Masson's trichrome images for a particular slide and automatically quantified using an in-house colour thresholding algorithm written in MATLAB 2019b (Mathworks, Natick, MA, USA). Briefly, all images were transformed into Lab colour space allowing the isolation of the colour and lightness components of each pixel. A k-means clustering algorithm was then applied to the colour components of each individual image to partition the pixels into groups of relatively 'red' or 'blue' colour values. A uniform threshold was applied to all images to mask regions with high lightness (appearing as white). Finally, morphological closing operations were performed on the 'red' and 'blue' regions to fill any gaps less than 3 pixels in radius. The area of the image which was composed of tissue was determined by brightness threshold. The percent of collagen present in each image was calculated as the area of the remaining 'blue' region divided by the area considered tissue. Automatic thresholds were manually verified with labelled colour overlays on the original histology images to ensure that collagen presence was accurately identified (Fig. 7).
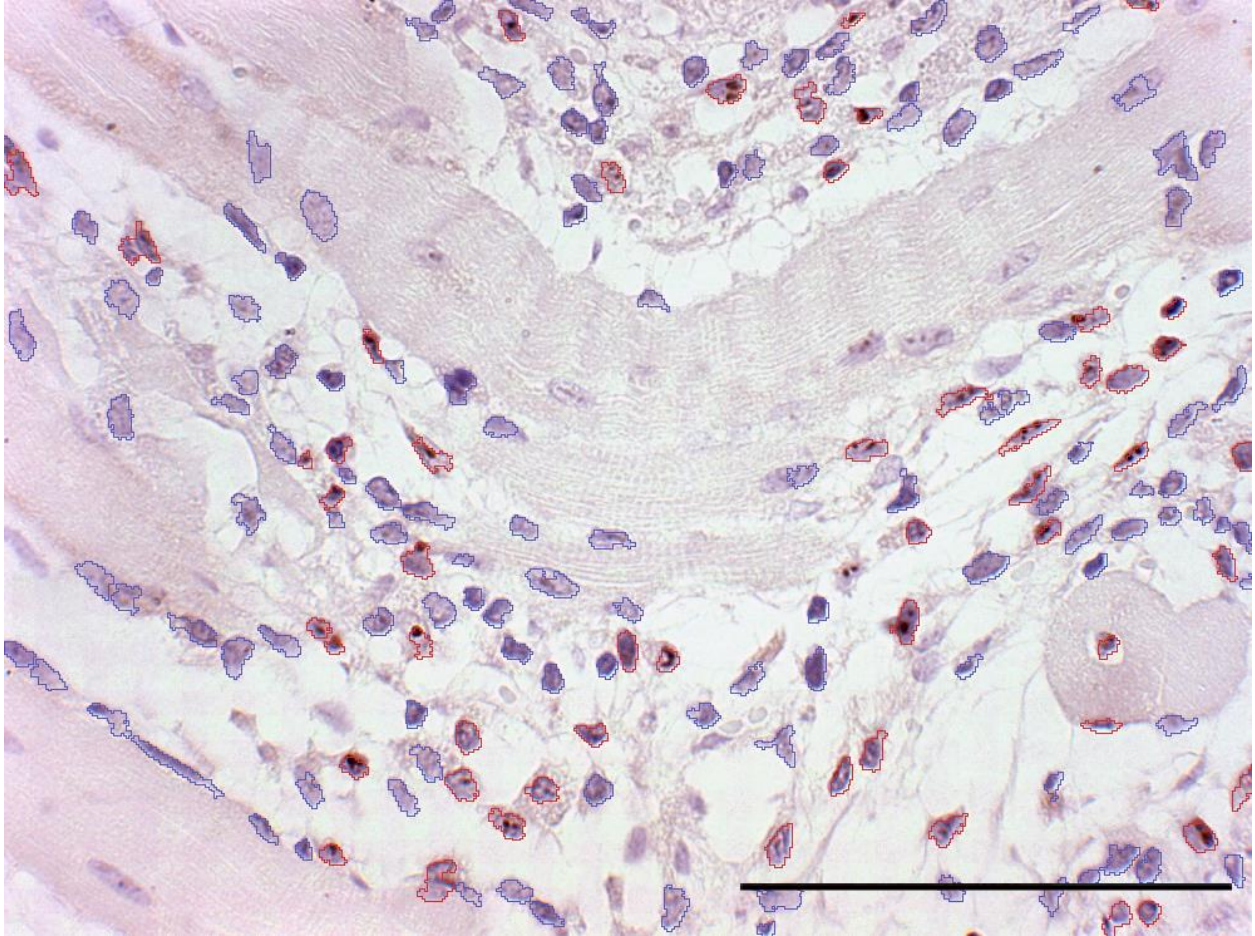
Figure 6. Example division of image into Wt1 immunoreactive and Wt1 non-immunoreactive nuclei.

An example of 4-5 week old *Mdx/Utrn+/-* gastrocnemius stained immunohistochemically for Wt1, with nuclei counterstained using hematoxylin. QuPath positive cell detection has identified negative nuclei in blue, and positive nuclei in red, with 181 nuclei detected, at a 29.83% immunoreactivity rate. Manual quantification by eye found 178 nuclei, at a 26.40% immunoreactivity rate (scale bar = 100µm).
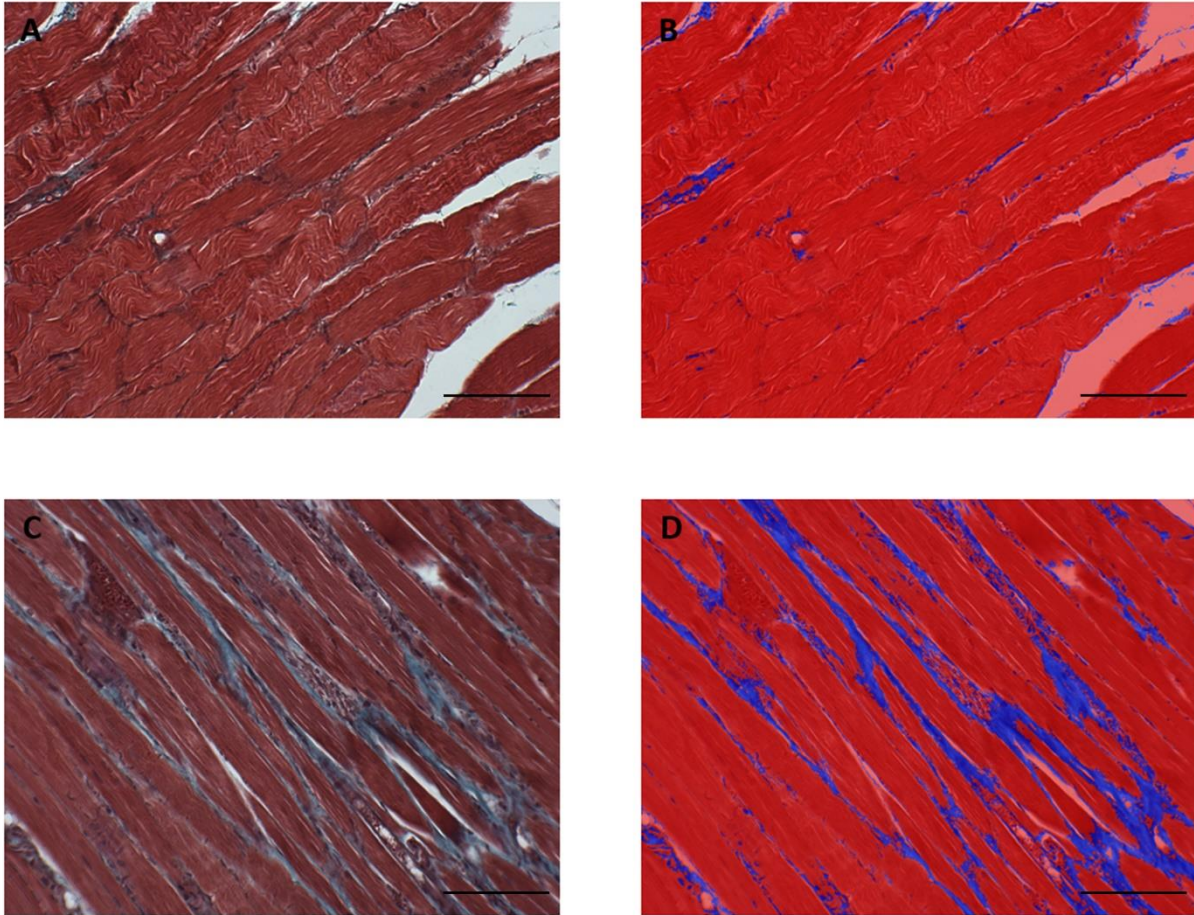
Figure 7. Quantification of collagen content in Masson's trichrome stained muscle tissue sections.

Sections of 10-14 month old gastrocnemius tissue stained with Masson's trichrome, either wildtype (A) or *Mdx*/*Utrn*+/- (C). Images were transformed into Lab colour space, allowing the isolation of the colour and lightness components of each pixel. A k-means clustering algorithm was then applied to the colour components of each individual image to partition the pixels into groups of relatively 'red' or 'blue' colour values (B, D) (scale bar = 100μm).

3.3   Quantification of mRNA

3.3.1 RNA Extraction and Preparation

Samples of gastrocnemius tissue up to 50mg in size were weighed and homogenized in Trizol Reagent (Ambion), using an Ultra-Turrax T25 Homogenizer. Samples were then transferred to Phasemaker Tubes (Invitrogen), mixed with chloroform, and centrifuged at 16000G at 4°C for 15 minutes. The aqueous layer was then pipetted off into a new tube, combined with an equal volume of isopropanol, and incubated for 20 minutes at room temperature. Following centrifugation at 16000G at 4°C for 10 minutes, samples were washed twice in chilled 70% ethanol, with this centrifugation step repeated at the end of each wash. Samples were allowed to dry for 15 minutes after removal of ethanol, and then resuspended in 40ul RNAse free water through a 10 minute incubation at 60°C. The amount of RNA in these samples was then quantified through analysis on a DeNovix DS-11 spectrophotometer.

RNA was then converted into cDNA using a High Capacity cDNA Reverse Transcription Kit (Applied Biosystems), in accordance with the manufacturer's instructions.

3.3.2 Primer Creation and Validation

For the purposes of quantifying total Wt1 and its isoforms, the primers and probe published by Kramarzova et. al (2012), originally for use in humans, were adopted[199]. Primers and probe were adjusted to match the mouse genome, and ordered from Sigma-Aldrich. This consisted of a 6FAM-TAMRA conjugated fluorescent probe, and two groups of forward and reverse primers. The first primer group is a primer pair to quantify total Wt1. The second primer group are two sets of two primers, one set being forward primers for the presence and absence of exon 5, and the other being reverse primers for the presence and absence of the KTS sequence.

Combining the primers in the latter group allows amplification of all the major isoforms of Wt1 (Table 1). These primer combinations were assayed using PCR on a mouse cDNA sample. The PCR products were then run on a 2.0% agarose gel in tris-acetate-EDTA (TAE) buffer at 80V. After the bands had been adequately separated, those bands reflecting the molecular weight of the PCR products were extracted and processed using the QIAEX II gel extraction kit according to the manufacturer's instructions. The PCR products were then sequenced (performed at the DNA Sequencing Facility at Robarts Research Institute, London, ON) to confirm that the correct region of the genome was being amplified.

3.3.3 qPCR

With three technical replicates each, qPCR runs for total Wt1, as well as for each major Wt1 isoform, were conducted for 8-10 week old wildtype and *Mdx/Utrn+/-* gastrocnemius samples. The qPCR and fluorescence quantification was conducted using the QuantStudio5 system, with Taqman Fast Advanced Master Mix (Applied Biosystems) used for the reaction. The reactions were considered positive if at least one of the technical replicates yielded fluorescent signal. Wt1 isoform fluorescence was normalized as a fraction of the sum of all isoforms for a particular sample. Total Wt1 was normalized based on the geometric mean of three control genes: glyceraldehyde 3-phosphate dehydrogenase (*Gapdh*), β-Actin (*Actb*), and Cyclophilin A (*Ppia*). These were chosen due to their past history of use as control genes for examination of RNA in the *Mdx* mouse, as well as their individual efficiencies and the geometric mean's efficiency being similar to that of the primers used to quantify total Wt1 (Appendix I).

Primers and Probes

Primer/probe code	5' Position (size)	Sequence 5'-3' and exon location
Wt1-fwd	1335 (21)	TAC ACA C<u>C</u>C ACG G<u>G</u>G TCT TC<u>C</u> exon 6
Wt1-rvs	1420 (21)	<u>T</u>TC AGA TGC <u>T</u>GA CCA <u>G</u>AC AAG exon 7
EX5(-)-fwd	1203 (19)	GAG C<u>T</u>A CCT TAA AGG GCC A exon 4 exon 9
EX5(+)-fwd	1249 (20)	ATG GAC AGA AGG GCA GAG CA exon 5
KTS(-)-rvs	1717 (22)	GCT GAA GGG CTT TTC ACC TGT A exon 10 exon 9
KTS(+)-rvs	1716 (25)	CTG AAG GGC TTT TCA CTT GTT TTA C exon 10 KTS
Wt1-probe	1357 (25)	6FAM-AGG CAT TCA GGA TGT GCG <u>G</u>CG TGT A-TAMRA exon 6 exon 7

Wt1 Variants Detected

Wt1 variant	Fwd primer	Rvs primer	Size of qPCR Product
Wt1—total	Wt1-fwd	Wt1-rvs	86
Wt1—isoform A(-/-)	EX5(-)-fwd	KTS(-)-rvs	455
Wt1—isoform B(+/-)	EX5(+)-fwd	KTS(-)-rvs	460
Wt1—isoform C(-/+)	EX5(-)-fwd	KTS(+)-rvs	463
Wt1—isoform D(+/+)	EX5(+)-fwd	KTS(+)-rvs	468

Table 1. qPCR primers and probes for total Wt1 and major isoforms

Table listing the sequences for the primers and probes used in this experiment. Exons spanned by primers or probes are defined below the relevant sequence by arrows. Bases which have been changed between human and mouse primers and probe are underlined, showing conversion of human sequence into homologus mouse sequence. Portions of this figure adapted from Kramarzova (2012).

3.4   Data Analysis

For quantified images, one of two analysis techniques were used. For comparisons between the wildtype and disease models within an age group, a standard one-way analysis of variance (ANOVA) was performed. If significant differences were detected, this was followed by Bonferroni's post-hoc test to determine differences between the wildtype and disease models. For comparisons between age groups and tissue types, Brown-Forsythe and Welch ANOVA tests, and Welch's t-tests, were used. Where significant differences were found in the former case, Dunnett's T3 multiple comparison test was used to determine differences between different age groups and tissue types. In both forms of ANOVA analysis, data are assumed to be normally distributed, with each sample independent from each other. However, in the case of comparing samples at different time points, the third requirement for standard ANOVA, that there be equal variances between treatments, may be violated here. With increased age, there is more time for samples to diverge, hence older samples would have more variance than younger samples, and so this assumption would be violated. Different tissue types may diverge within an animal at different rates as well, so they would not have consistent variances between them. Hence, Brown-Forsythe and Welch ANOVA, or Welch's t-tests, which compensates for this, must be utilized. A two-way ANOVA was additionally conducted, to evaluate the strength of associations of time and genotype to the outcomes analyzed, though this does not account for the differences in variation (Appendix J).

For qPCR, student's t-tests were used to compare the differences in the mean expression of Wt1 and its isoforms between the 8-10 week old wildtype and *Mdx*/*Utrn*+/- gastrocnemius tissue. Differences between groups were considered significant at a p-value less than 0.05.

4   RESULTS

4.1   Relative to the age-matched wildtype, the proportion of Wt1 immunoreactive nuclei is increased in the absence of collagen deposition in 4-5 week old mouse skeletal muscle

In order to determine whether the proportion of Wt1 immunoreactive nuclei was increased in the absence of collagen deposition in disease model muscle, gastrocnemius, diaphragm, and heart muscle in 4-5 week old wildtype, *Mdx*, *Mdx*/*Utrn*+/-, and *Mdx*/*Utrn*-/- mice were evaluated, examining general histology (Fig. 8), tissue collagen deposition (Fig. 9), and nuclei positive for Wt1 (Fig. 10) .

Evaluation of general histological features of these gastrocnemius (Fig. 8A, D, G, J), diaphragm (Fig. 8B, E, H, K), and heart (Fig. 8C, F, I, L) tissues was conducted to determine patterns in tissue organization and nuclear Wt1 immunoreactivity. Primarily peripheral nuclei were observed in wildtype diaphragm and gastrocnemius tissues (Fig. 8A-B). Central nuclei, typical of regenerating skeletal muscle, were observed in all disease models, in both the diaphragm and gastrocnemius (Fig. 8D-E, G-H, J-K). However, particularly for the *Mdx* model, these myofibers with central nuclei were uncommon (Fig. 8D, E). Histology characteristic of inflammatory infiltrate, such as increased cellularity and polymorphonuclear cells, was visible in both the *Mdx*/*Utrn*+/- and *Mdx*/*Utrn*-/- model skeletal muscle (Fig. 8G-H, J-K), while none was found in the wildtype model (Fig. 8A-B). Nuclear Wt1 immunoreactivity was often observed to be more abundant than that of the surrounding muscle in these regions (Fig. 10J). However, the presence of these infiltrates alone did not appear to prompt nuclear Wt1 immunoreactivity. Muscle cells undergoing active degeneration were common in skeletal muscle of all disease

models (Fig. 8D-E, G-H, J-K). Tissue morphology characteristic of the presence of adipocytes was observed only in *Mdx*/*Utrn*+/- and *Mdx*/*Utrn*-/- diaphragm tissue (Fig. 8H, K). In contrast to the skeletal muscle, the heart muscle examined showed negligible pathological changes at this age (Fig. 8F, I, L).

At this age, the diaphragm exhibited a significant increase in collagen deposition in the *Mdx/Utrn-/-* ($p = 0.019$) model compared to the wildtype, as well as significant increases in proportion of Wt1 immunoreactive nuclei in the *Mdx* ($p = 0.021$), *Mdx*/*Utrn*+/- ($p = 0.048$) and *Mdx*/*Utrn*-/- ($p = 0.003$) models. The gastrocnemius exhibited statistically significant collagen deposition in the *Mdx*/*Utrn*+/- model ($p < 0.001$), and significant increases in proportion of Wt1 immunoreactive nuclei in the *Mdx*/*Utrn*+/- ($p < 0.001$) and *Mdx*/*Utrn*-/- ($p < 0.001$) models. The heart exhibited neither significant differences in collagen deposition nor changes in proportion of Wt1 immunoreactive nuclei across all models assessed ($p > 0.050$) (Fig. 11A-C).

Figure 8. *Mdx*, *Mdx/Utrn+/-*, and *Mdx/Utrn-/-* **mice demonstrate histopathological changes in the diaphragm and gastrocnemius at 4-5 weeks of age.**

Gastrocnemius, diaphragm, and heart muscle was acquired from 4-5 week old mice of several genotypes, and stained with hematoxylin and eosin (H&E) to characterize general muscle histology. Representative H&E stained sections for wildtype (A-C), *Mdx* (D-F), *Mdx/Utrn+/-* (G-I), and *Mdx/Utrn-/-* (J-L) mice (scale bar = 100μm) One biological and one technical replicate was used.

Figure 9. *Mdx/Utrn+/-* **gastrocnemius muscle and** *Mdx/Utrn-/-* **diaphragm muscle demonstrate collagen deposition at 4-5 weeks of age.**

Gastrocnemius, diaphragm, and heart muscle was acquired from 4-5 week old mice of several genotypes, and stained with Masson's trichrome to distinguish collagen deposition (blue) from muscle (red). Representative images of Masson's trichrome stained muscle are shown for wildtype (A-C), *Mdx* (D-F), *Mdx/Utrn+/-* (G-I), and *Mdx/Utrn-/-* (J-L) mice (scale bar = 100μm). Three biological and three technical replicates were used.

Figure 10. Relative to the age-matched wildtype, there is an increase in number of Wt1 immunoreactive nuclei in the *Mdx* diaphragm, as well as both the *Mdx/Utrn+/-* and *Mdx/Utrn-/-* diaphragm and gastrocnemius, at 4-5 weeks of age.

Gastrocnemius, diaphragm, and heart muscle was acquired from 4-5 week old mice and assessed for Wt1 immunoreactivity. Representative images of Wt1 IHC analysis of muscle are shown for wildtype (A-C), *Mdx* (D-F), *Mdx/Utrn+/-* (G-I), and *Mdx/Utrn-/-* (J-L) mice. In the bottom left corner, a section of magnified nuclei are provided for examination. Asterisks indicate large example regions containing cells resembling inflammatory infiltrate (scale bar = 100μm). Three biological and three technical replicates were used.

Figure 11. Relative to age-matched wildtype, there is an increased proportion of Wt1 immunoreactive nuclei in the absence of collagen deposition in 4-5 week old skeletal muscle, as examined in wildtype, *Mdx*, *Mdx/Utrn+/-*, and *Mdx/Utrn-/-* mice.

Following immunostaining or Masson's trichrome staining, percent of tissue area composed of collagen, and percent of nuclei positive for Wt1, was determined, and is expressed as mean +SD. This is displayed for the gastrocnemius (A), diaphragm (B), and heart (C). Asterisks indicate significant differences with wildtype (* < 0.050, ** < 0.010, *** < 0.001). Three biological and three technical replicates were used.

4.2   Relative to the age-matched wildtype, the proportion of Wt1
        immunoreactive nuclei is increased during early collagen deposition
        in 8-10 week old mouse skeletal muscle

That the proportion of Wt1 immunoreactive nuclei was increased in *Mdx/Utrn-/-*
diaphragm and *Mdx/Utrn+/-* gastrocnemius at 4-5 weeks of age despite significant collagen
deposition suggested that this increase might persist during early collagen deposition. To explore
this, gastrocnemius, diaphragm, and heart muscle in 8-10 week old wildtype, *Mdx*, *Mdx*/*Utrn+/-*,
and *Mdx*/*Utrn-/-* mice were evaluated for general histology (Fig. 12), collagen deposition (Fig.
13), and nuclei positive for Wt1 (Fig. 14).

Once again, gastrocnemius (Fig. 12A, D, G, J), diaphragm (Fig. 12B, E, H, K), and heart
(Fig. 12C, F, I, L) tissue general histology was evaluated. Wildtype skeletal muscle showed
primarily peripheral nuclei (Fig. 12A-B), with central nuclei observed in all disease model
skeletal muscle (Fig. 12D-E, G-H, J-K). To a small extent in the *Mdx* model, and to a greater
extent in both the *Mdx*/*Utrn+/-* and *Mdx*/*Utrn-/-* models, histology was exhibited in skeletal
muscle which was characteristic of inflammatory infiltrate, such as increased cellularity and
polymorphonuclear cells (Fig. 8G-H, J-K). In these inflammatory infiltrate candidate regions,
nuclear Wt1 immunoreactivity was often observed to be higher than that of the surrounding
muscle. However, the presence of these infiltrates did not alone appear to prompt Wt1 expression
(Fig. 14E, J). Muscle cells undergoing active degeneration were common in skeletal muscle of
all disease models (Fig. 12D-E, G-H, J-K). Tissue morphology characteristic of the presence of
adipocytes was observed only in *Mdx*/*Utrn+/-* and *Mdx*/*Utrn-/-* diaphragm tissue (Fig. 12H, K).
In contrast to the skeletal muscle, the heart muscle examined showed negligible pathological
changes at this age (Fig. 12F, I, L).

At this age, the diaphragm exhibited significant increases in collagen deposition in the *Mdx*/*Utrn*+/- (p = 0.006) and *Mdx*/*Utrn*-/- (p < 0.001) models compared to the age-matched wildtype control, and showed significant increases in the proportion of Wt1 immunoreactive nuclei in the *Mdx* (p < 0.001), *Mdx*/*Utrn*+/- (p = 0.004), and *Mdx*/*Utrn*-/- (p < 0.001) models. The gastrocnemius exhibited statistically significant increases in collagen deposition in the *Mdx*/*Utrn*+/- (p < 0.001) and *Mdx*/*Utrn*-/- (p = 0.001) models, and showed a significantly increased proportion of Wt1 immunoreactive nuclei in the *Mdx*/*Utrn*+/- (p < 0.014) model. The heart exhibited neither significant differences in collagen deposition nor changes in the proportion of Wt1 immunoreactive nuclei (p > 0.050) (Fig. 15A-C).

This corroborates past research in the Hoffman lab which describe the diaphragm and gastrocnemius muscles of these mice models at these ages, indicating a fibrotic phenotype at a similar timepoint[194].
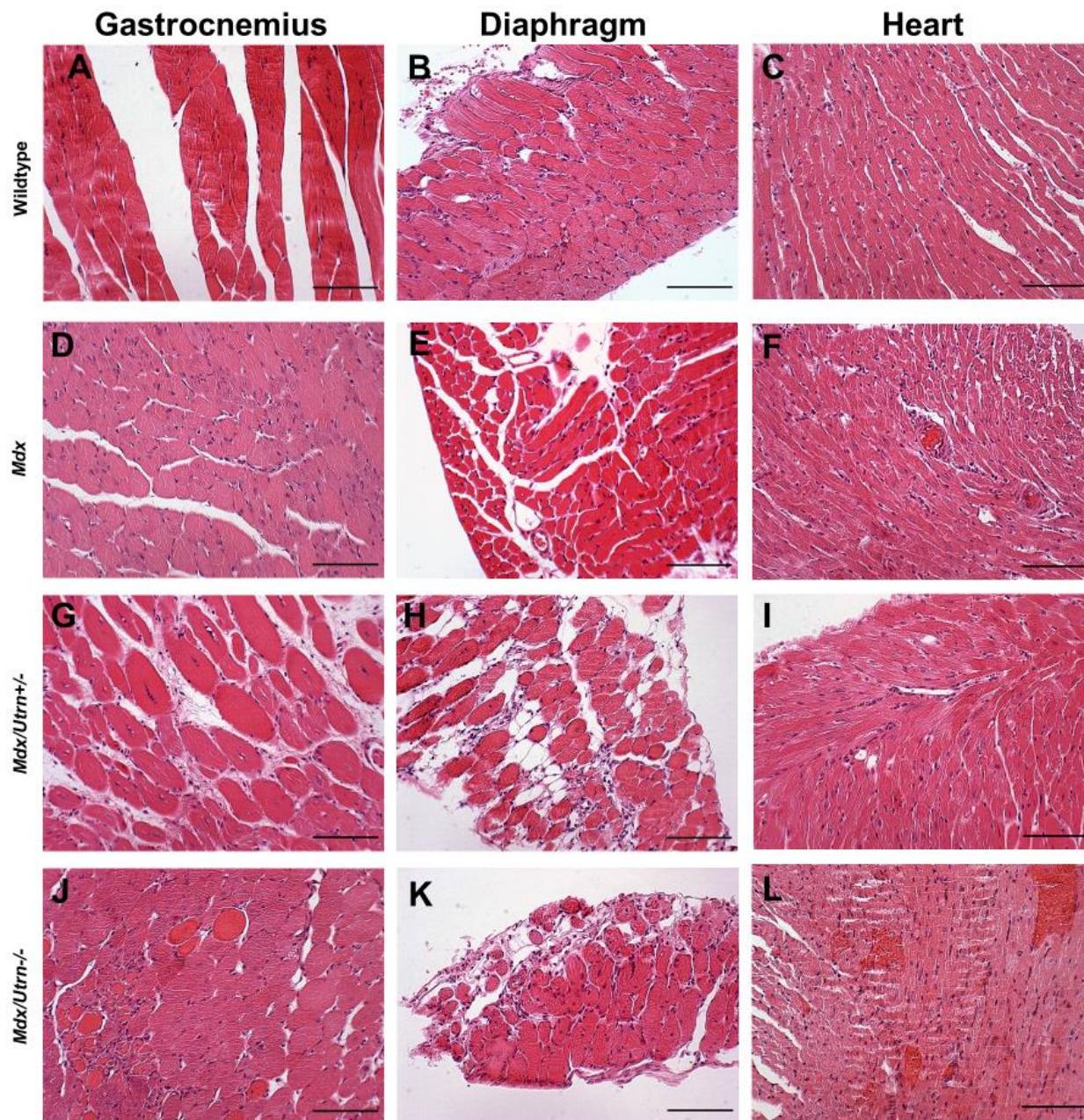
Figure 12. *Mdx*, *Mdx/Utrn+/-*, **and** *Mdx/Utrn-/-* **mice demonstrate histopathological changes in the diaphragm and gastrocnemius at 8-10 weeks of age.**

Gastrocnemius, diaphragm, and heart muscle was acquired from 8-10 week old mice of several genotypes, and stained with hematoxylin and eosin (H&E) to characterize general muscle histology. Representative H&E stained sections for wildtype (A-C), *Mdx* (D-F), *Mdx/Utrn+/-* (G-I), and *Mdx/Utrn-/-* (J-L) mice (scale bar = 100µm). One biological and one technical replicate was used.

Figure 13. *Mdx/Utrn+/-* **and** *Mdx/Utrn-/-* **gastrocnemius muscle and diaphragm muscle demonstrate collagen deposition at 8-10 weeks of age.**

Gastrocnemius, diaphragm, and heart muscle was acquired from 8-10 week old mice of several genotypes, and stained with Masson's trichrome to distinguish collagen deposition (blue) from muscle (red). Representative images of Masson's trichrome stained muscle are shown for wildtype (A-C), *Mdx* (D-F), *Mdx/Utrn+/-* (G-I), and *Mdx/Utrn-/-* (J-L) mice (scale bar = 100μm). Three biological and three technical replicates were used.
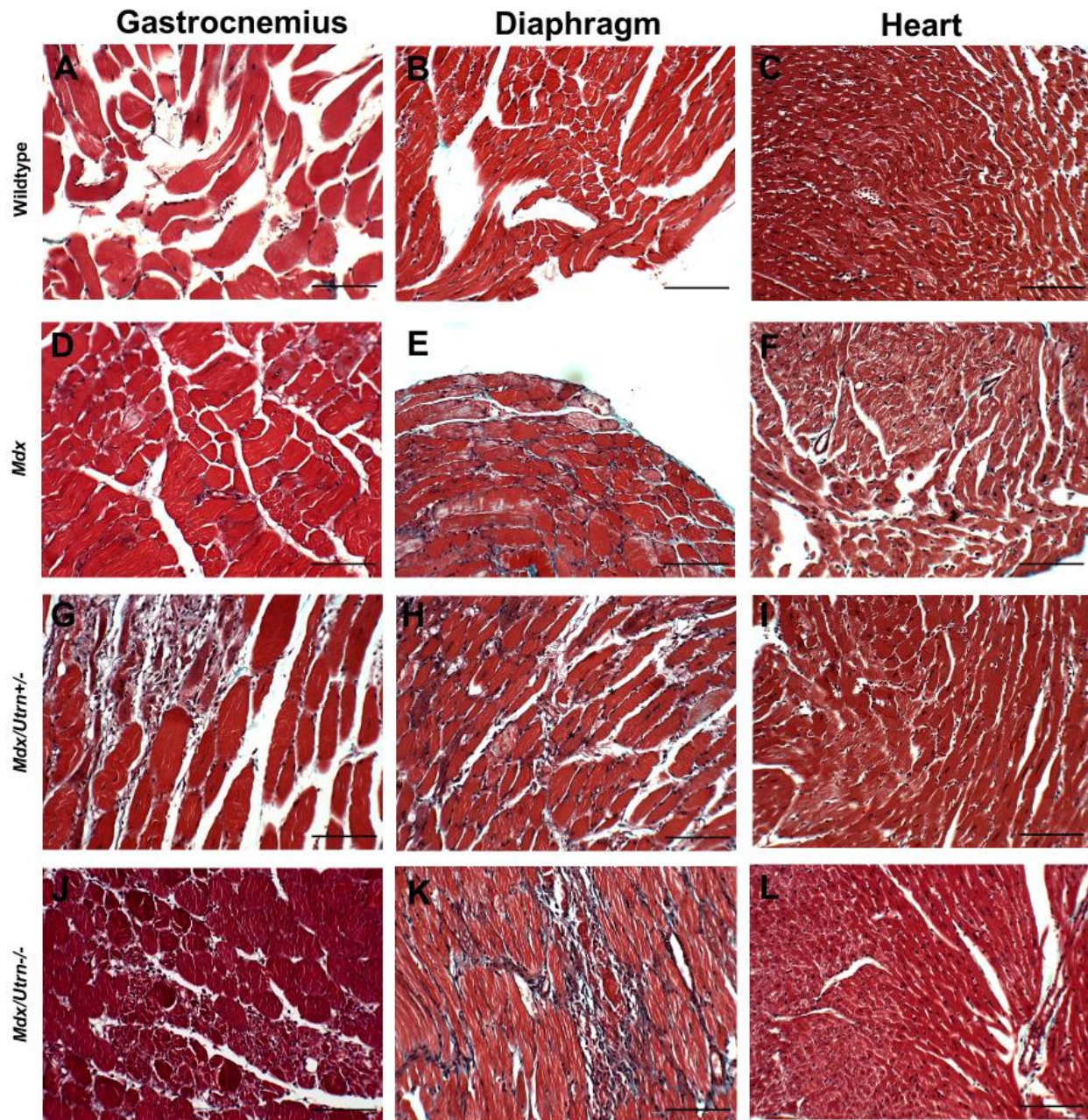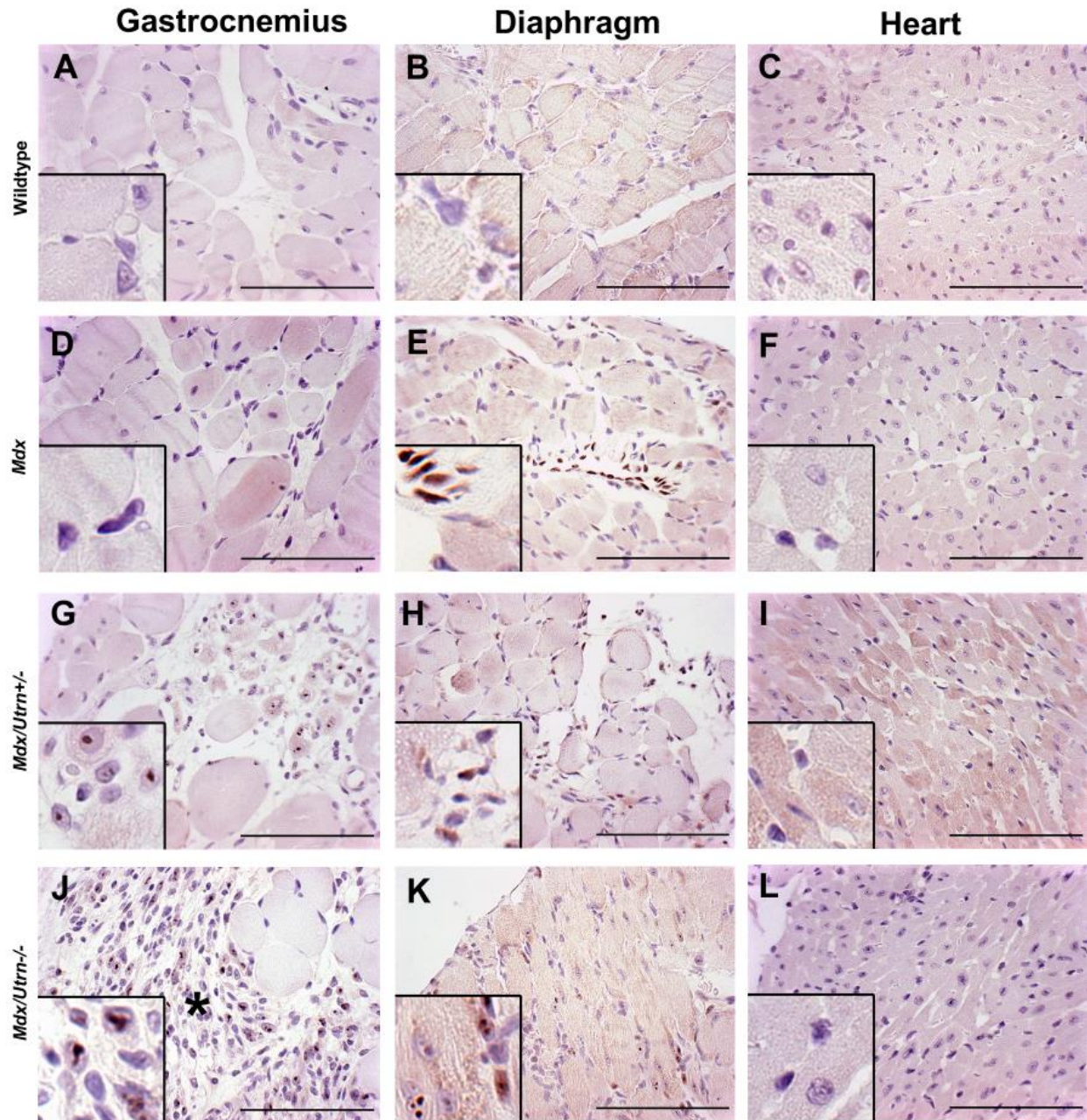
Figure 14. Relative to the age-matched wildtype, there is an increase in number of Wt1 immunoreactive nuclei in *Mdx*, *Mdx/Utrn+/-* and *Mdx/Utrn-/-* diaphragm, and *Mdx/Utrn+/-* gastrocnemius, at 8-10 weeks of age.

Gastrocnemius, diaphragm, and heart muscle was acquired from 8-10 week old mice and assessed for Wt1 immunoreactivity. Representative images of Wt1 IHC analysis of muscle are shown for wildtype (A-C), *Mdx* (D-F), *Mdx/Utrn+/-* (G-I), and *Mdx/Utrn-/-* (J-L) mice. In the bottom left corner, a section of magnified nuclei are provided for examination. Asterisks indicate large example regions containing cells resembling inflammatory infiltrate (scale bar = 100µm). Three biological and three technical replicates were used.
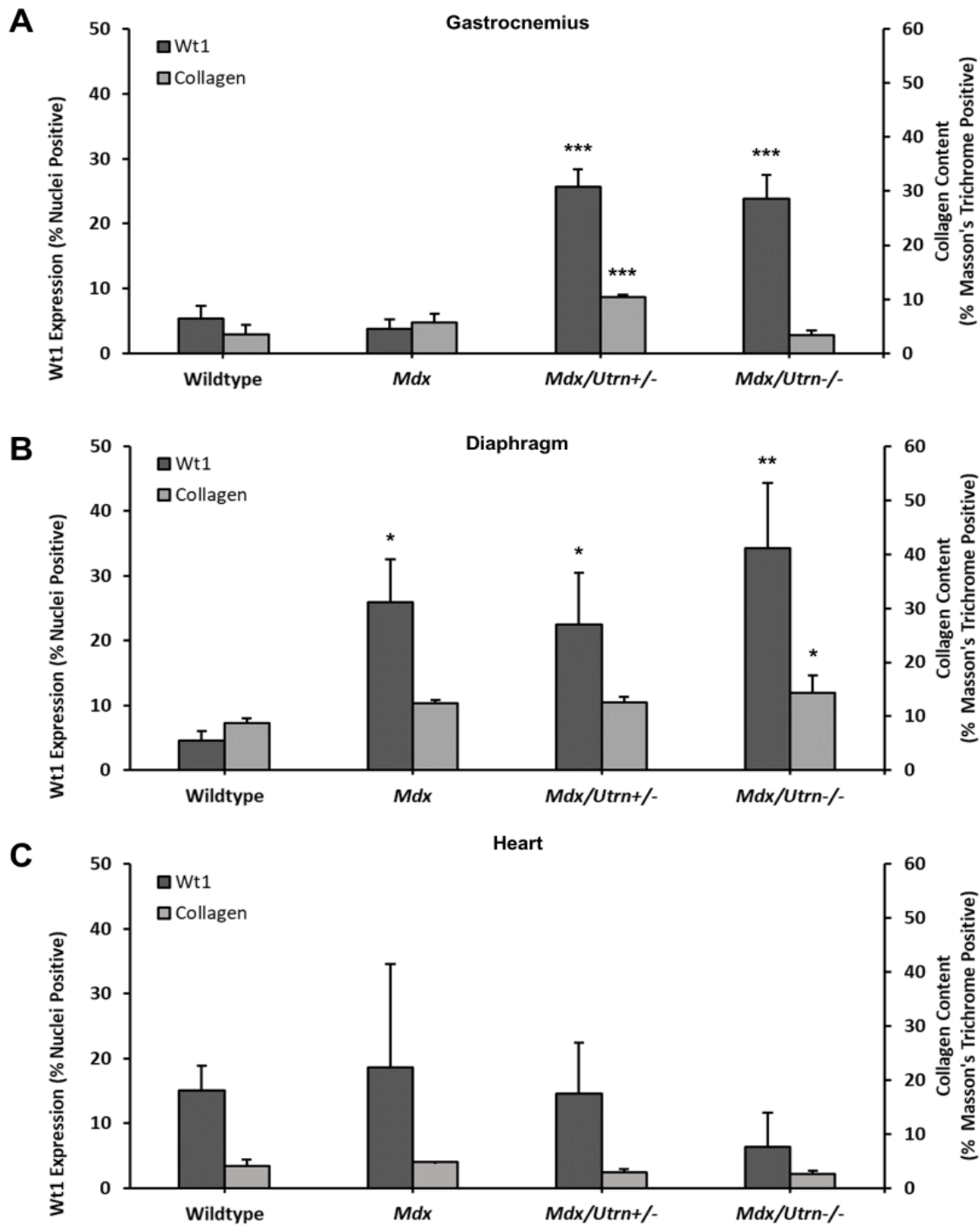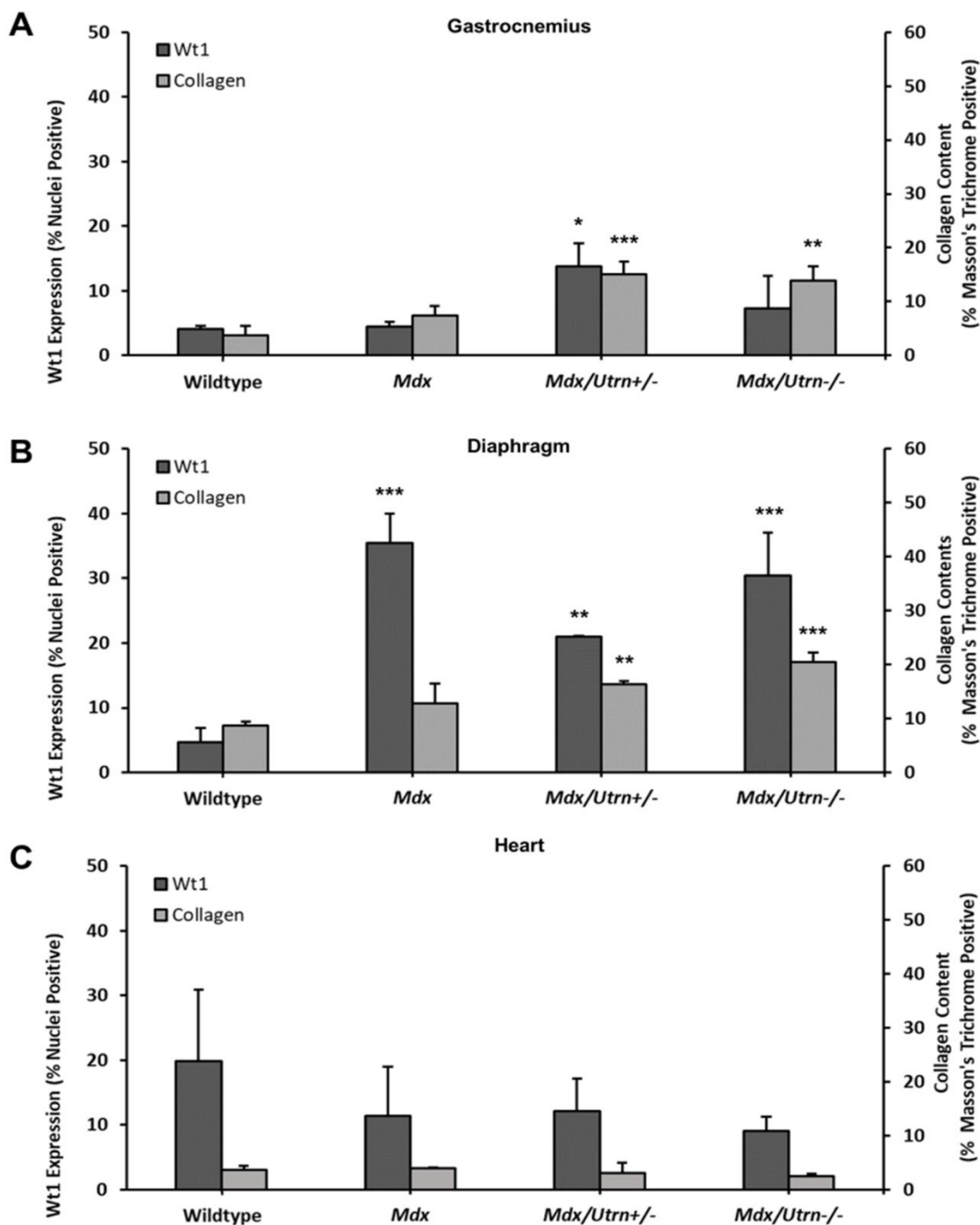
Figure 15. Relative to the age-matched wildtype, there is an increased proportion of Wt1 immunoreactive nuclei during early collagen deposition in skeletal muscle, as examined in 8-10 week old wildtype, *Mdx*, *Mdx/Utrn+/-*, and *Mdx/Utrn-/-* mice.

Following immunostaining or Masson's trichrome staining, percent of tissue area composed of collagen, and percent of nuclei positive for Wt1, was determined, and is expressed as mean +SD. This is displayed for the gastrocnemius (A), diaphragm (B), and heart (C). Asterisks indicate significant differences with wildtype (* < 0.050, ** < 0.010, *** < 0.001). Three biological and three technical replicates were used.

4.3   Relative to the age-matched wildtype, the proportion of Wt1 immunoreactive nuclei is not increased during late collagen deposition in 10-14 month old mouse skeletal muscle

Finally, it was important to determine whether the increase in proportion of Wt1 immunoreactive nuclei remained during late collagen deposition in skeletal muscle. Therefore, 10-14 month old wildtype, *Mdx*, and *Mdx*/*Utrn*+/- gastrocnemius, diaphragm, and heart muscle proportion of Wt1 immunoreactive nuclei and tissue collagen deposition were quantified. To explore this, gastrocnemius, diaphragm, and heart muscle in 10-14 month old wildtype, *Mdx*, *Mdx*/*Utrn*+/-, and *Mdx*/*Utrn*-/- mice were evaluated for general histology (Fig. 16), tissue collagen deposition (Fig. 17) and nuclei positive for Wt1 (Fig. 18).

General histological features of these gastrocnemius (Fig. 16A, D, G, J), diaphragm (Fig. 16B, E, H, K), and heart (Fig. 16C, F, I, L) tissues were examined, once again showing primarily peripheral nuclei in wildtype skeletal muscle tissues (Fig. 16A-B) and central nuclei in all disease model skeletal muscle (Fig. 16D-E, G-H). Histology characteristic of inflammatory infiltrate, such as increased cellularity and polymorphonuclear cells, were common in the skeletal muscle of the *Mdx*/*Utrn*+/- model, and to a lesser extent in the *Mdx* model (Fig. 16D-E, G-H). However, no differences were found in Wt1 immunoreactivity patterns across these regions. Muscle cells undergoing active degeneration were found in the skeletal muscle of all disease models (Fig. 16D-E, G-H). Tissue morphology consistent with adipocyte presence, was present in disease model skeletal muscle, aside from the *Mdx* gastrocnemius (Fig. 16E, E-H). All disease models showed muscle cells undergoing active degeneration (Fig. 16D-E, G-H). The *Mdx/Utrn*+/-, but not *Mdx*, heart, was observed to have small, localized regions of inflammatory infiltrate and fatty deposition (Fig. 16I).

At this age, the diaphragm exhibited significant tissue collagen deposition in the *Mdx* (p < 0.001) and *Mdx*/*Utrn*+/- (p < 0.001) models, compared to the wildtype, but did not show differences in the proportion of Wt1 immunoreactive nuclei (p > 0.050). The gastrocnemius exhibited a statistically significant increase in collagen deposition in only the *Mdx*/*Utrn*+/- model (p < 0.001), but similarly did not show differences in proportion of Wt1 immunoreactive nuclei (p > 0.050). The heart exhibited neither significant differences in collagen deposition nor changes in proportion of Wt1 immunoreactive nuclei (p > 0.050) (Fig. 19A-C).

In all of the tissues which would become fibrotic by the 10-14 month old timepoint, those being the *Mdx* diaphragm, as well as the *Mdx*/*Utrn*+/- and *Mdx*/*Utrn*-/- diaphragm and gastrocnemius, there was a statistically significant increase in proportion of Wt1 immunoreactive nuclei at the 4-5 week old timepoint.

The patterns of fibrosis described here corroborates past research in the Hoffman lab which describe the diaphragm and gastrocnemius muscles of these mice models at these ages, indicating a fibrotic phenotype at a similar timepoint[194].
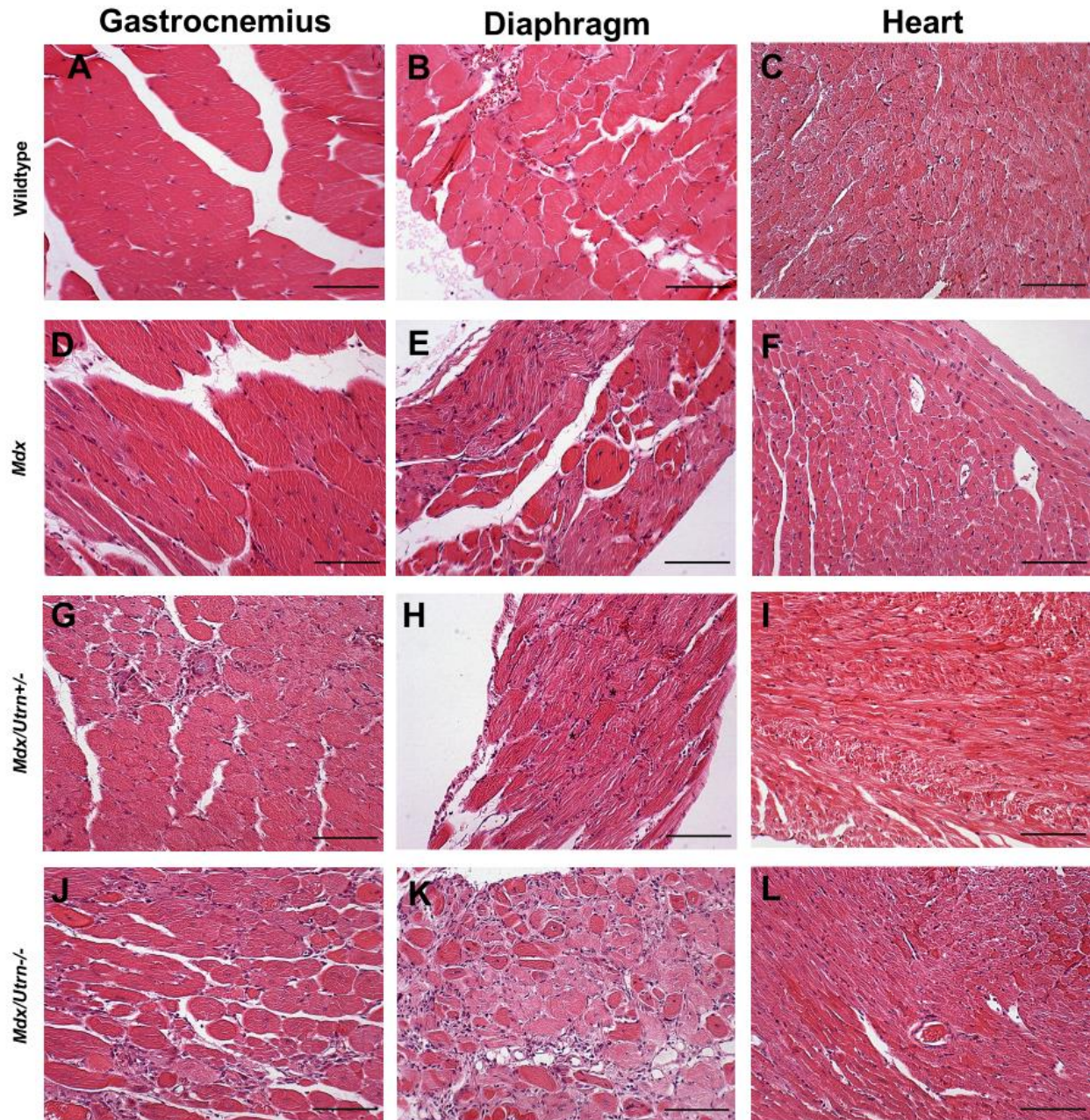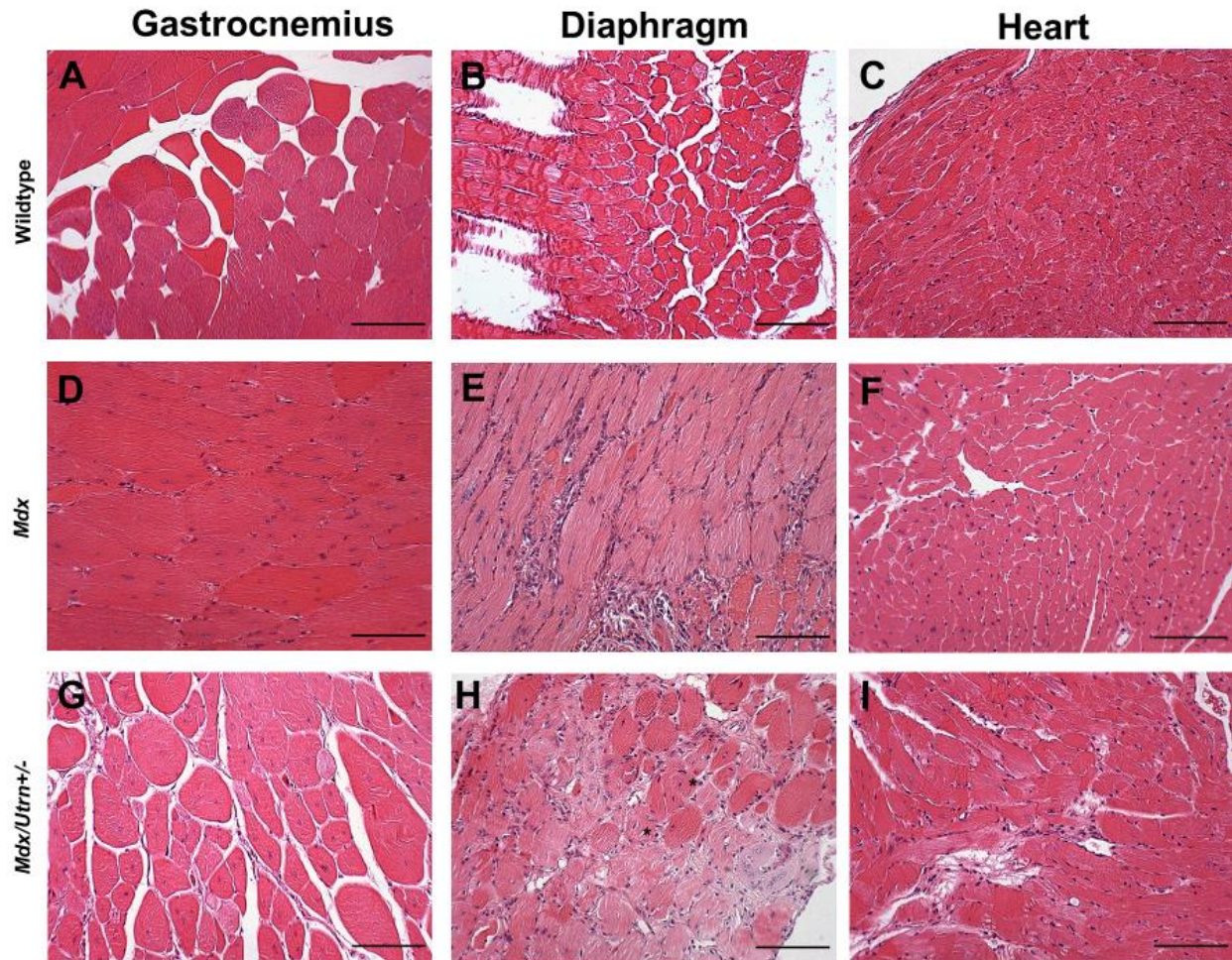
Figure 16. *Mdx* and *Mdx/Utrn+/-* mice demonstrate histopathological changes in the diaphragm and gastrocnemius, and *Mdx/Utrn+/-* mice additionally in the heart, at 10-14 month of age.

Gastrocnemius, diaphragm, and heart muscle was acquired from 10-14 month old mice of several genotypes, and stained with hematoxylin and eosin (H&E) to characterize general muscle histology. Representative H&E stained sections for wildtype (A-C), *Mdx* (D-F), and *Mdx/Utrn+/-* (G-I) mice (scale bar = 100μm). One biological and one technical replicate was used.
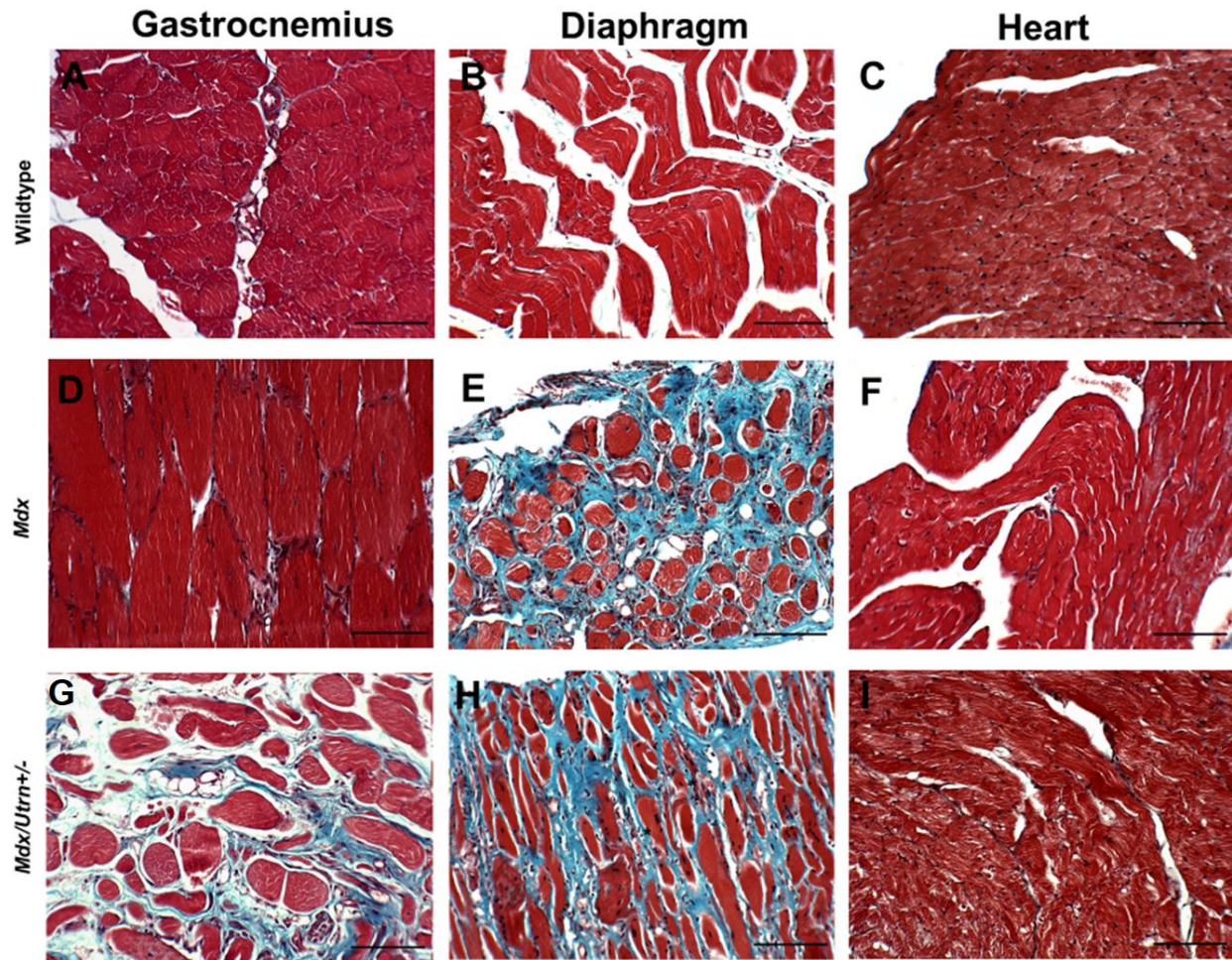
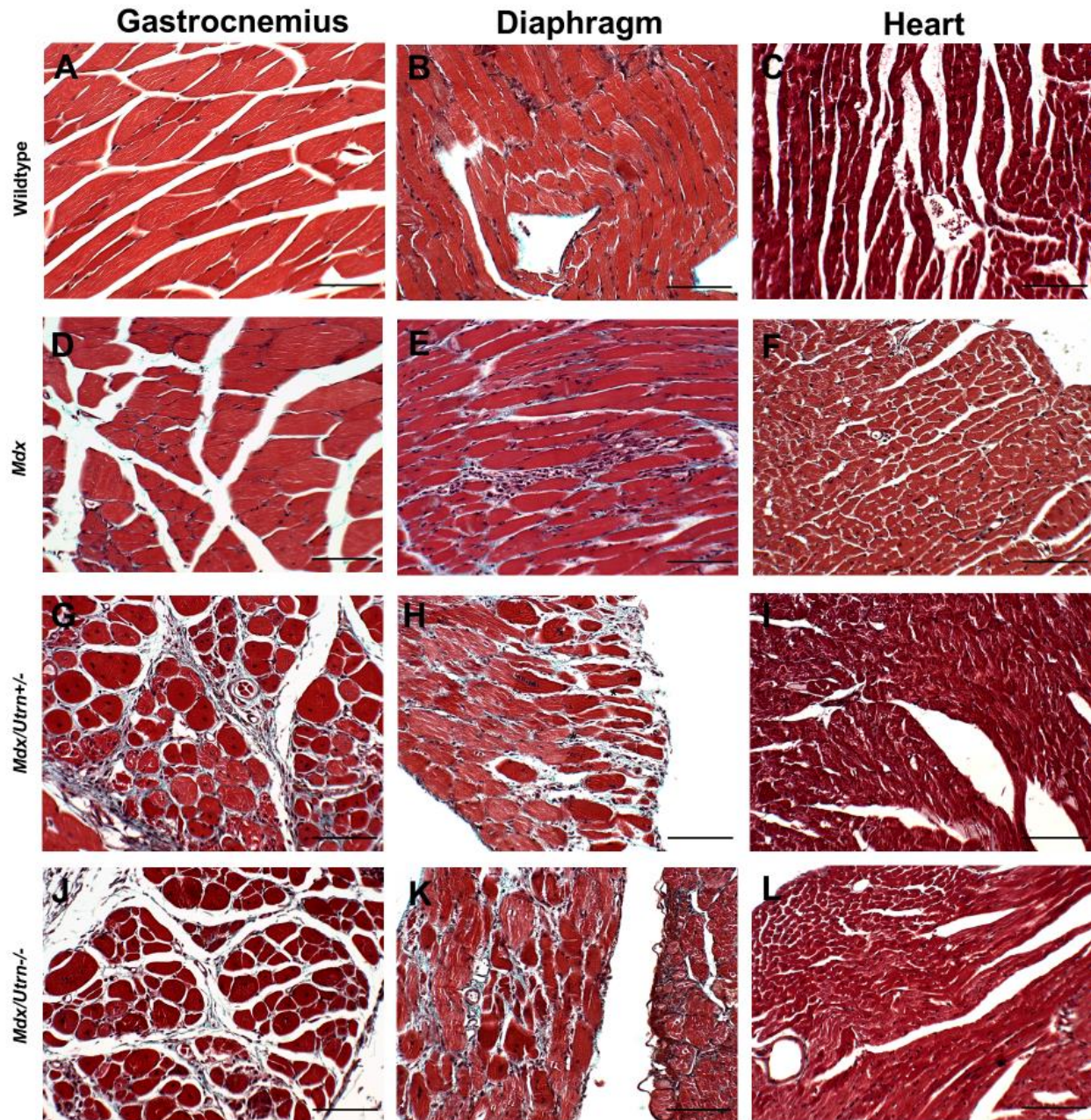**Figure 17. *Mdx* and *Mdx/Utrn+/-* mice demonstrate collagen deposition in the diaphragm, and *Mdx/Utrn+/-* mice additionally in the gastrocnemius, at 10-14 month of age.**

Gastrocnemius, diaphragm, and heart muscle was acquired from 10-14 month old mice of several genotypes, and stained with Masson's trichrome to distinguish collagen deposition (blue) from muscle (red). Representative images of Masson's trichrome stained muscle are shown for wildtype (A-C), *Mdx* (D-F), and *Mdx/Utrn+/-* (G-I) (scale bar = 100µm). Three biological and three technical replicates were used.
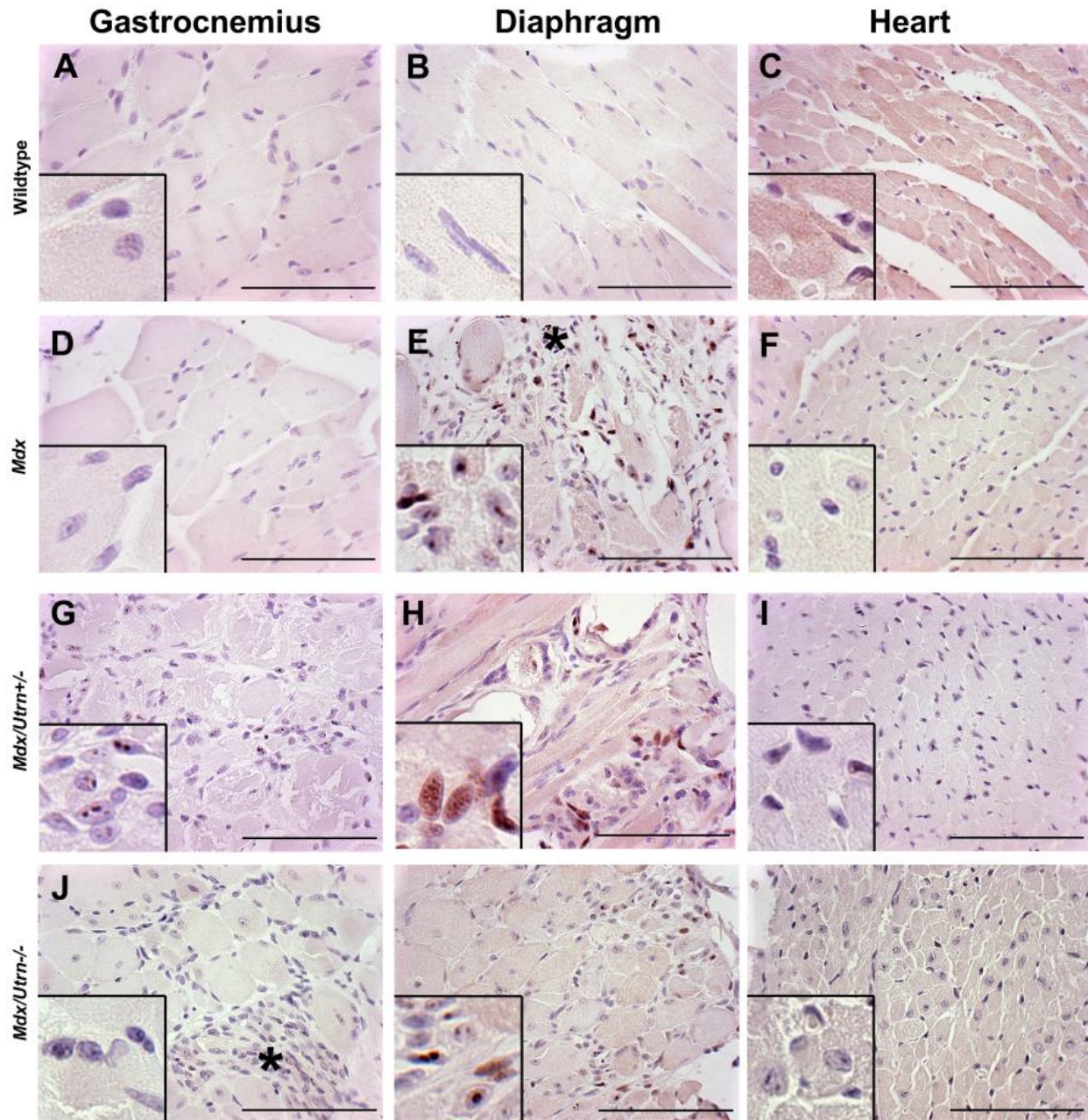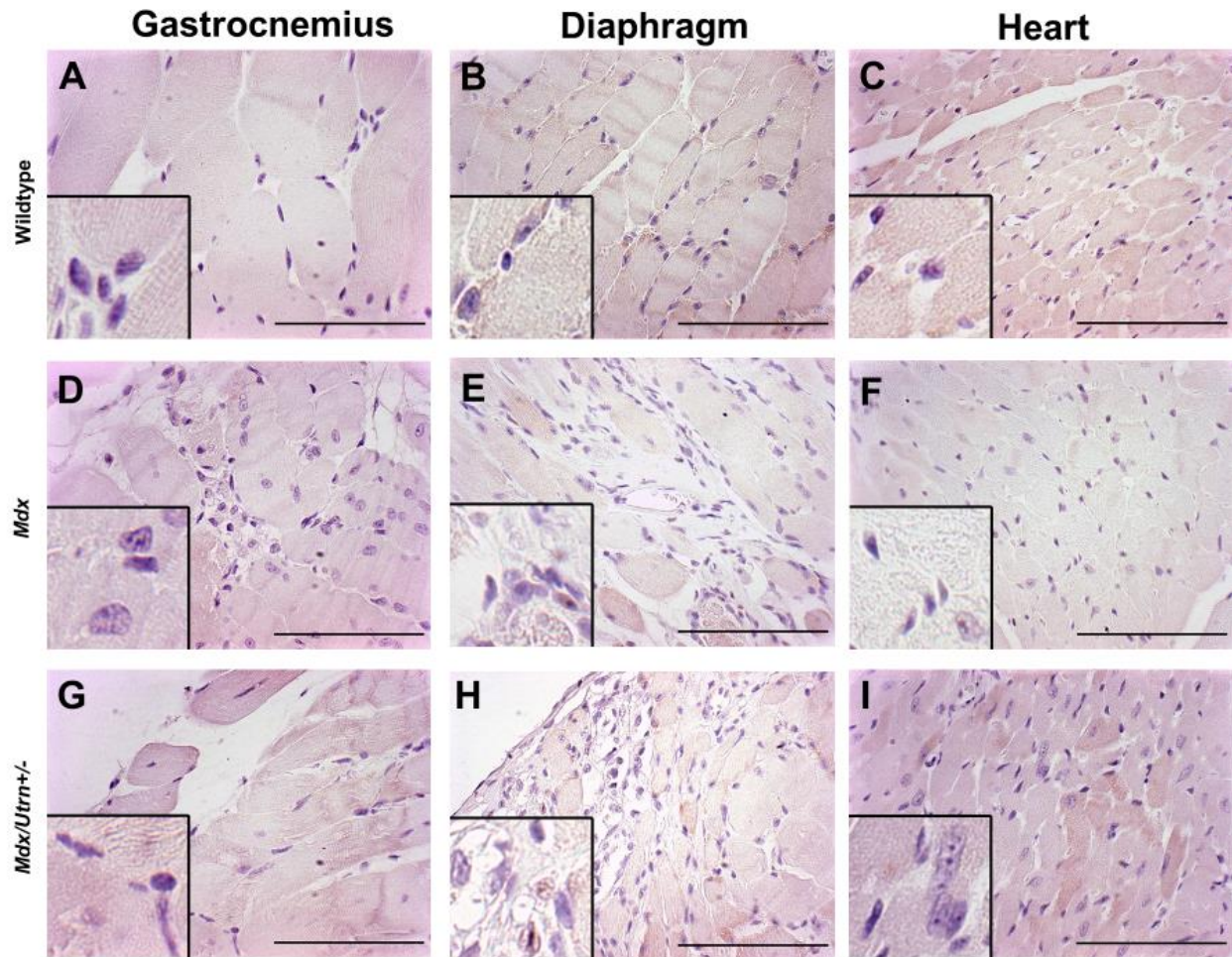
Figure 18. Relative to the age-matched wildtype, there are no differences in number of Wt1 immunoreactive nuclei in *Mdx*, or *Mdx/Utrn+/-* diaphragm, gastrocnemius, or heart, at 10-14 months of age.

Gastrocnemius, diaphragm, and heart muscle was acquired from 10-14 month old mice and assessed for Wt1 immunoreactivity. Representative images of Wt1 IHC analysis of muscle are shown for wildtype (A-C), *Mdx* (D-F), and *Mdx/Utrn+/-* (G-I) mice. In the bottom left corner, a section of magnified nuclei are provided for examination. Asterisks indicate large example regions containing cells resembling inflammatory infiltrate (scale bar = 100μm). Three biological and three technical replicates were used.
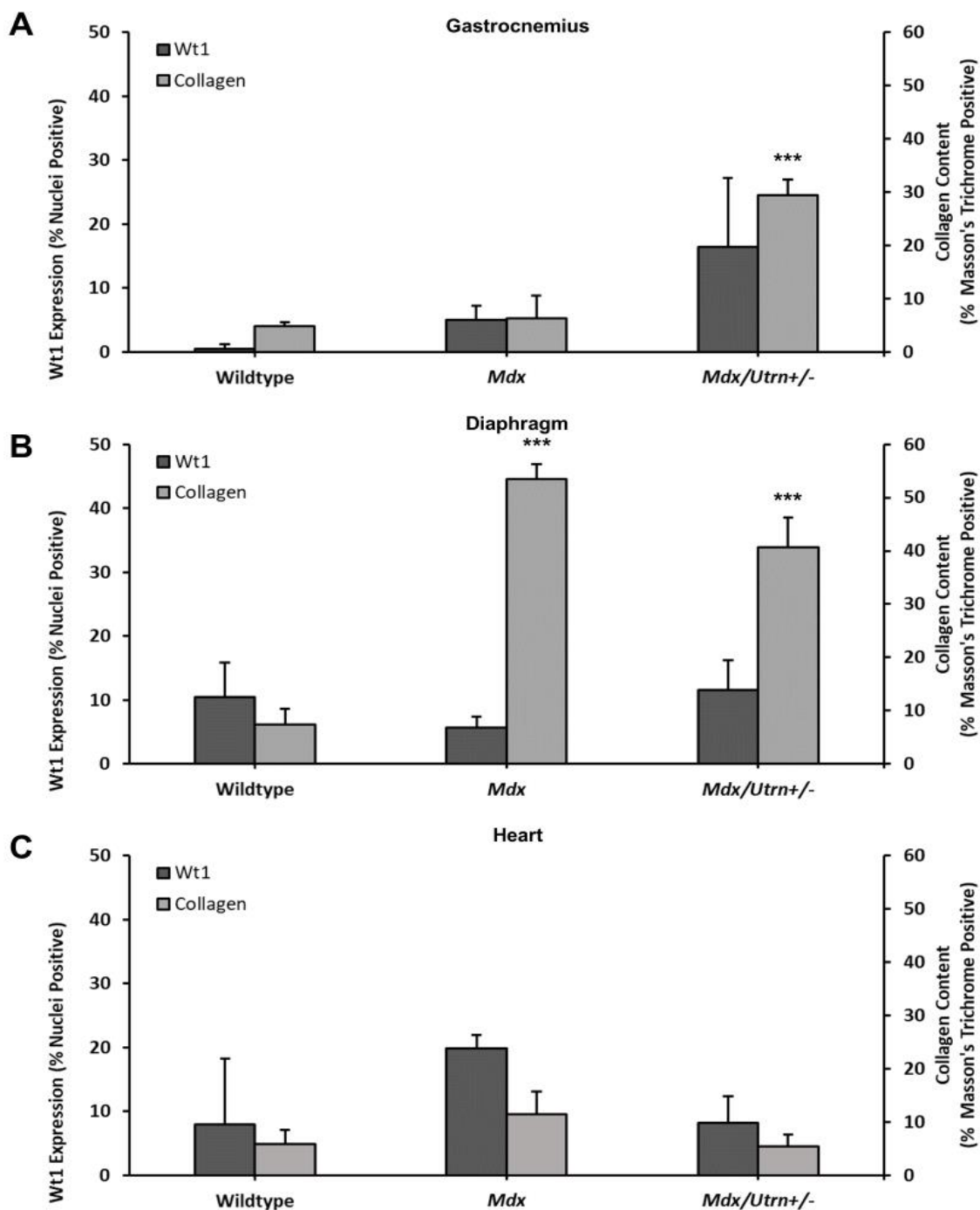
Figure 19. Relative to the age-matched wildtype, there are no differences in proportion of Wt1 immunoreactive nuclei during late collagen deposition in skeletal muscle, as examined in 10-14 month old wildtype, *Mdx*, *Mdx/Utrn+/-*, and *Mdx/Utrn-/-* mice.

Following immunostaining or Masson's trichrome staining, percent of tissue area composed of collagen, and percent of nuclei positive for Wt1, was determined, and is expressed as mean +SD. This is displayed for the gastrocnemius (A) and diaphragm (B). Asterisks indicate significant differences with wildtype (* < 0.050, ** < 0.010, *** < 0.001). Three biological and three technical replicates were used.

4.4   Wt1 immunoreactivity patterns in muscle cytoplasm and non-muscle

tissue do not change in mouse skeletal and cardiac muscle, and are not

significantly different from an absence of expression

Although Wt1's principle function is as a transcription factor, it was nonetheless important to also characterize its appearance in areas outside the nucleus. Wt1 is also found to a degree in the cytoplasm, and furthermore has been shown to possibly be involved in translation, such as through interactions with translating polyribosomes[177,178].

The percent of the muscle cytoplasm and non-muscle tissue was thus also evaluated for the presence of Wt1 in 4-5 week old (Fig. 10), 8-10 week old (Fig. 14), and 10-14 month old (Fig. 18) *Mdx*, *Mdx*/*Utrn*+/-, and *Mdx*/*Utrn*-/- gastrocnemius, diaphragm, and heart tissue, comparing them with age-matched wildtype controls. These analyses were conducted on the sections previously presented.

No statistically significant differences in either the percent area positive for Wt1 in the muscle cytoplasm or non-muscle tissue were found ($p > 0.050$). For several of these tissues, subtraction with the negative control showed no area positive for Wt1 whatsoever, and that none of the other tissues are significantly different from these suggest that there is no significant Wt1 immunoreactivity in the muscle cytoplasm or non-muscle tissue (Appendix K).

4.5 Proportion of Wt1 immunoreactive nuclei and collagen deposition patterns show weak respective trends over time toward decreasing and increasing in skeletal muscle

As collagen deposition has previously been identified to differ between ages and disease models, it was important to determine whether the proportion of Wt1 immunoreactive nuclei varied over time in skeletal or cardiac muscle, and how this related to collagen deposition[194]. Therefore, the proportion of Wt1 immunoreactive nuclei, as well as well as collagen deposition throughout the tissue, were evaluated for 4-5 week old, 8-10 week old, and 10-14 month old wildtype (Fig. 20A, C, E), *Mdx* (Fig. 20B, D, F), *Mdx*/*Utrn*+/- (Fig. 20G, I, K), and *Mdx*/*Utrn*-/- (Fig. 20H, J, L) gastrocnemius, diaphragm, and heart. For each measure, within each tissue and genotype, all age points were compared to all other age points. These analyses were conducted on the sections previously presented (Fig. 9-10, 13-14, 17-18).

Of the wildtype tissues, only the gastrocnemius showed significant differences. The 8-10 week old wildtype gastrocnemius was found to have a significantly higher proportion of Wt1 immunoreactive nuclei ($p = 0.008$) than the 10-14 month old wildtype gastrocnemius, though no differences ($p > 0.050$) were found in the wildtype collagen deposition (Fig. 20C).

With regards to the *Mdx* tissues, only the diaphragm showed significant differences. The 8-10 week old *Mdx* diaphragm was found to have a significantly higher proportion of Wt1 immunoreactive nuclei than the 10-14 month old *Mdx* diaphragm ($p = 0.004$), while the 10-14 month old *Mdx* diaphragm was found to have significantly greater collagen deposition than at either the 4-5 week old ($p = 0.003$), or 8-10 week old ($p < 0.001$) timepoints (Fig. 20B).

Turning attention to the *Mdx/Utrn*+/- tissues, both the diaphragm and gastrocnemius showed significant differences, though only for collagen deposition. For the gastrocnemius, the

10-14 month old tissue was found to have significantly more collagen deposition than both the 4-5 week old (p = 0.016) and 8-10 week old (p = 0.007) timepoints (Fig. 20I). The 4-5 week old *Mdx/Utrn+/-* diaphragm was found to have significantly less collagen deposition compared to the 8-10 week old (p = 0.030) and the 10-14 month old (p = 0.029) diaphragm, and the 8-10 week old *Mdx/Utrn+/-* diaphragm was similarly found to have significantly less collagen deposition compared to the 10-14 month old (p = 0.037) diaphragm (Fig. 20G).

Finally, turning focus to the *Mdx/Utrn-/-* tissue, only the gastrocnemius showed significant differences. The 4-5 week old *Mdx/Utrn-/-* gastrocnemius was found to have a significantly higher proportion of Wt1 immunoreactive nuclei (p = 0.012), and lower collagen deposition (p = 0.013), compared with the 8-10 week old *Mdx/Utrn-/-* gastrocnemius (Fig. 20J).

In contrast to these results, relative to the age-matched wildtype, proportion of Wt1 immunoreactive nuclear was consistently elevated prior to, or at the same time as, increases in collagen deposition throughout affected models, for both forms of skeletal muscle examined. However, that the significant differences in proportion of Wt1 immunoreactive nuclei and collagen deposition relative to the age-matched wildtype respectively occur earlier, and later, would support the results of the time-based analysis (Fig. 22).

The topic of time-based variation was also examined in the muscle cytoplasm and non-muscle tissue, with each timepoint compared against each other timepoint within each genotype, for the diaphragm, gastrocnemius, and heart. No significant differences were found (p > 0.050) (Appendix L).

Wildtype

A Diaphragm

B *Mdx* Diaphragm

C Gastrocnemius

D Gastrocnemius

E Heart

F Heart
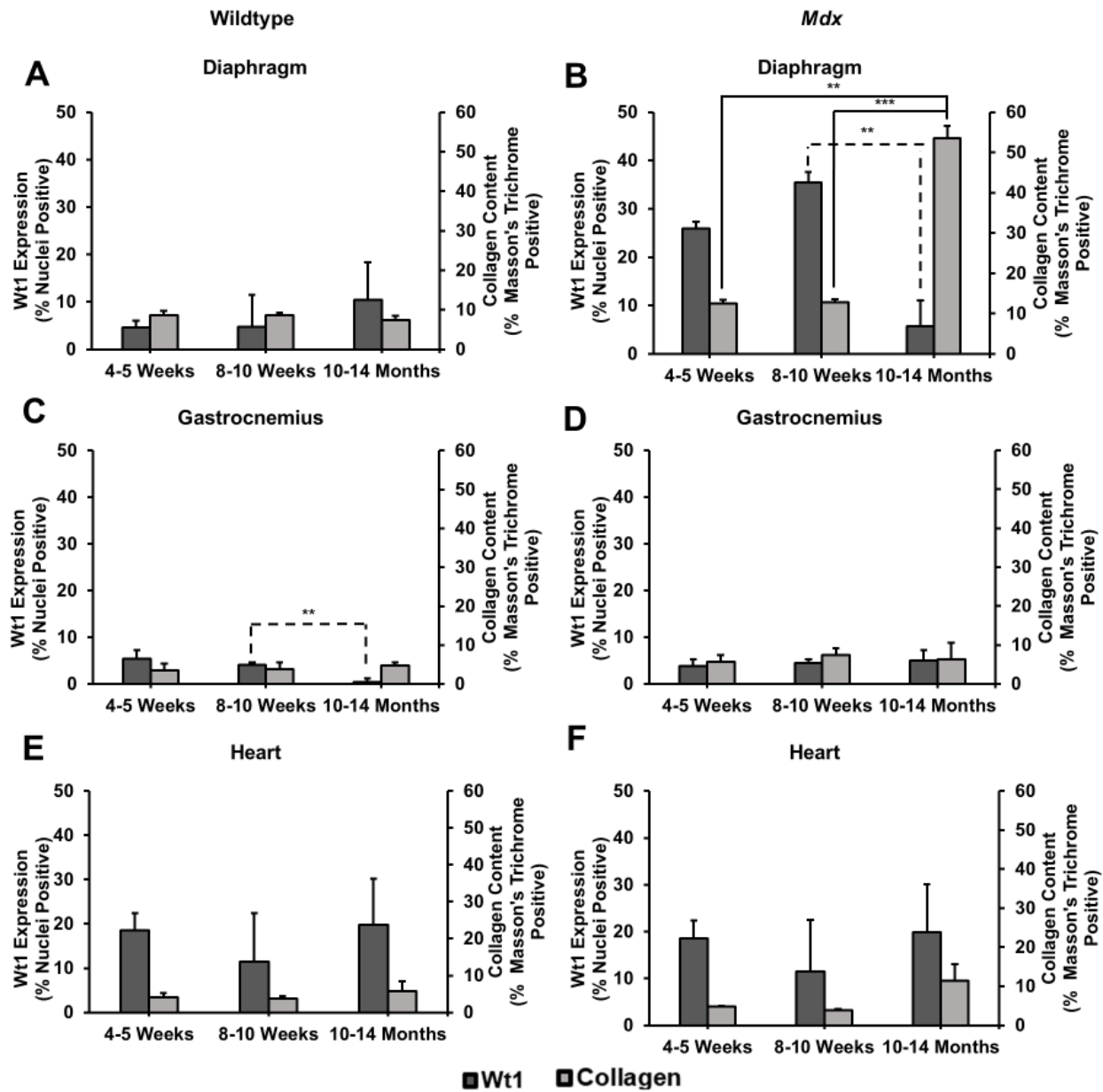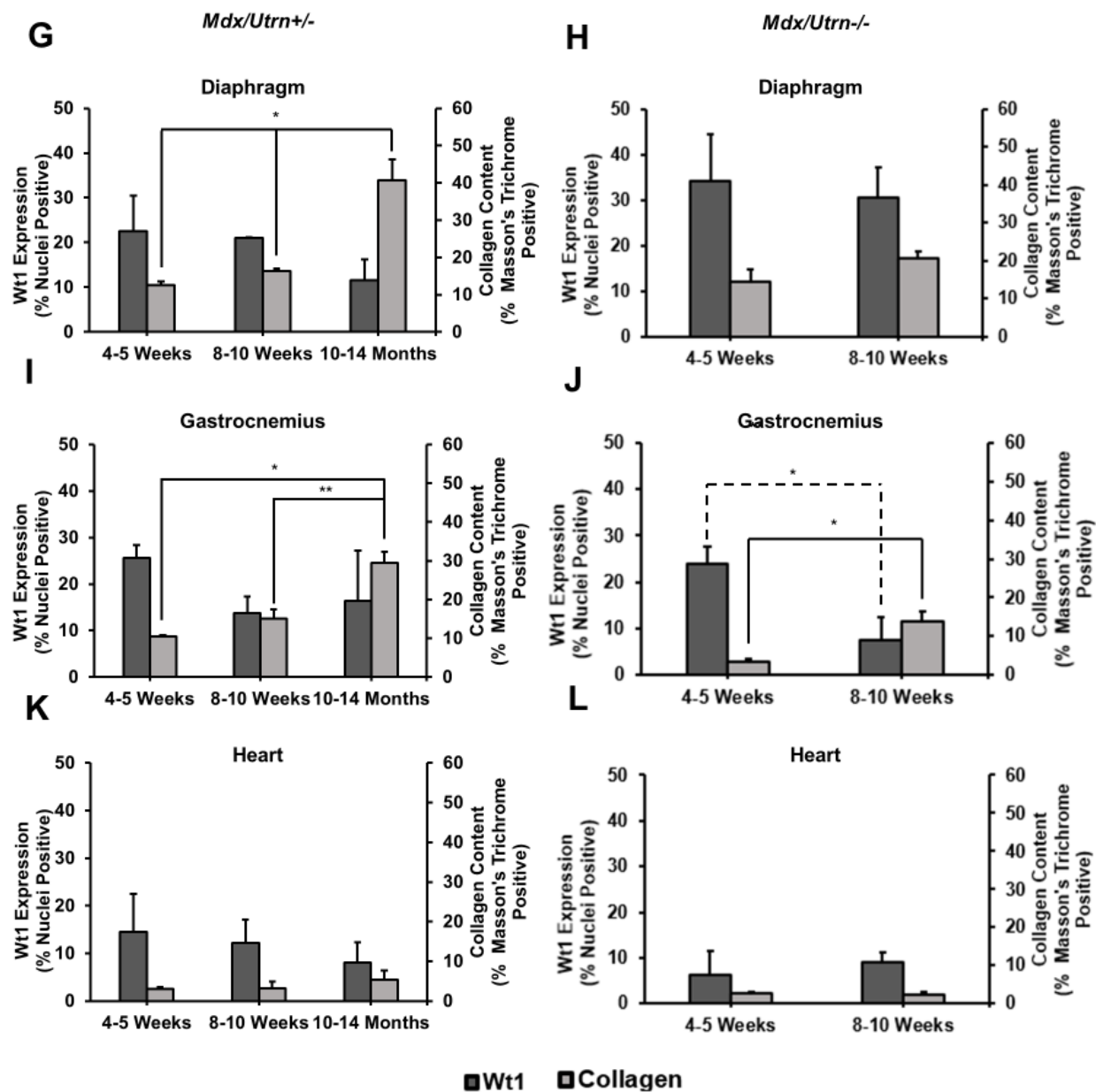
■Wt1   □Collagen

Figure 20. Over time, proportion of Wt1 immunoreactive nuclei, and tissue collagen content, show weak relationships toward decreasing and increasing, respectively.

Graphs depicting proportion of Wt1 immunoreactive nuclei as a percent of nuclei positive, along with the collagen content of the tissue as a percent of the tissue, for wildtype (A, C, E), *Mdx* (B, D, F), *Mdx/Utrn+/-* (G, I, K), and *Mdx/Utrn-/-* (H, J, L) diaphragm, gastrocnemius, and heart. Percent of positive nuclei or tissue area is expressed as mean +SD. Solid lines are used for comparisons between collagen at different timepoints, while dotted lines are used for comparisons between proportion of Wt1 immunoreactive nuclei at different timepoints. Asterisks indicate significant differences (* < 0.050, ** < 0.010, *** < 0.001). Three biological and three technical replicates were used.
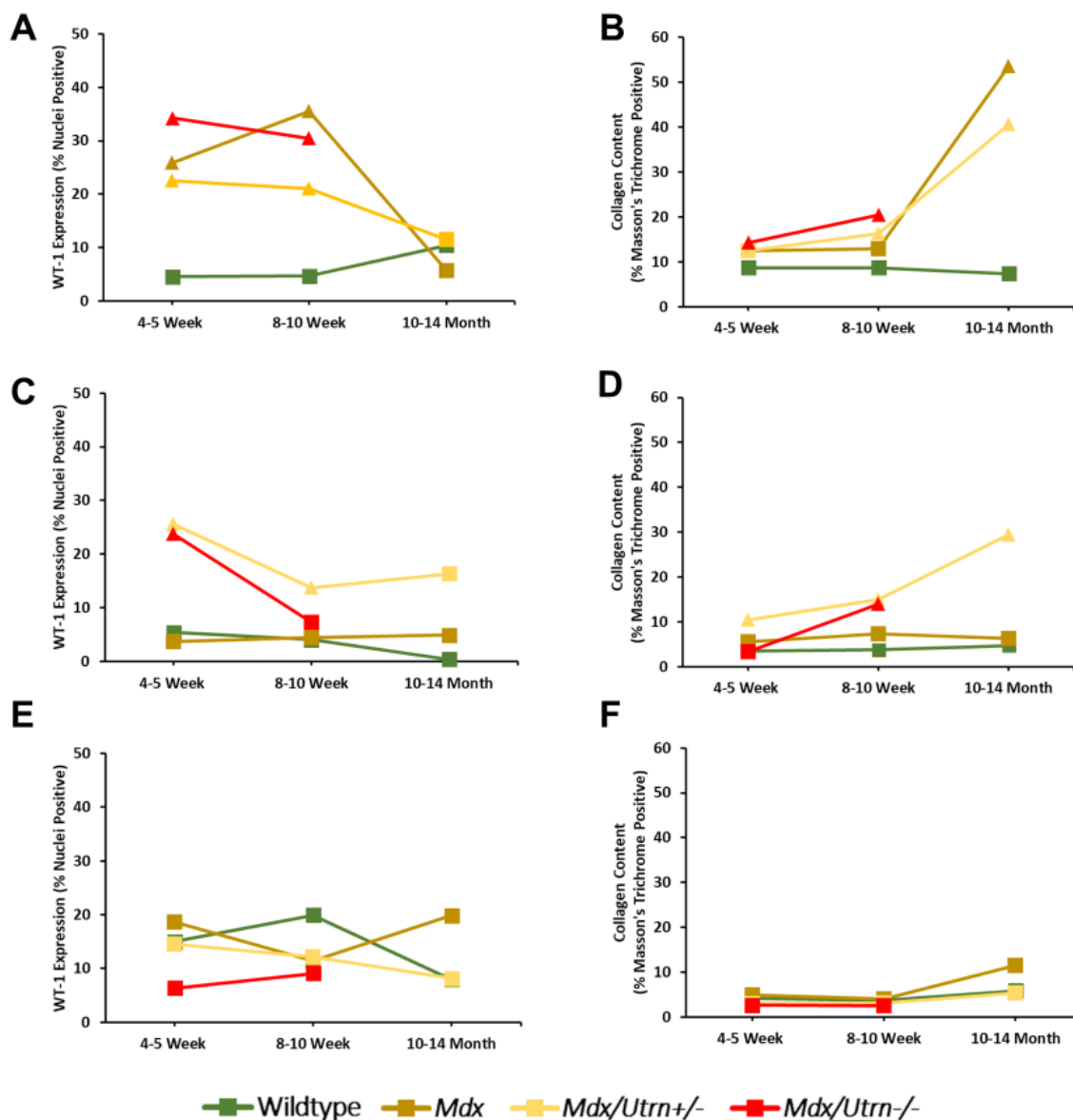
Figure 21. Line-graph summary showing that, relative to the age-matched wildtype, for the examined muscles in a model which developed significant collagen deposition, proportion of Wt1 immunoreactive nuclei was also significantly increased at either the same, or an earlier, timepoint.

Graphs depicting proportion of Wt1 immunoreactive nuclei as a percent of nuclei positive, along with the collagen content of the tissue as a percent of the tissue, for diaphragm (A, B), gastrocnemius (C, D), and heart (E, F), of wildtype, *Mdx*, *Mdx/Utrn+/-*, and *Mdx/Utrn-/-* mice. Percent of positive nuclei or tissue area is expressed as a mean. Triangle markers indicate a significant difference, with $p < 0.050$. Three biological and three technical replicates were used.

4.6   Collagen deposition, but not Wt1 immunoreactivity patterns, differ between healthy diaphragm, gastrocnemius, and heart tissue

To explore whether Wt1 immunoreactivity differed with respect to the level of collagen deposition in different tissues, Wt1 immunoreactivity in the nucleus, muscle cytoplasm, and non-muscle tissue, as well as collagen deposition throughout the tissue, were compared for 8-10 week old wildtype diaphragm, gastrocnemius, and heart. For each measure, each tissue type was compared to all other tissue types. These analyses were conducted on the sections previously presented (Fig. 9-10, 13-14, 17-18).

A significantly greater amount of collagen was found in the diaphragm than the heart (p = 0.003) (Appendix M).

4.7 Total Wt1 mRNA is upregulated during early collagen deposition in mouse skeletal muscle without a change in the ratios of its major isoforms

In order to determine whether the increase in proportion of Wt1 immunoreactive nuclei was accompanied by an increase in *Wt1* mRNA, primers were first generated for *Wt1* and its isoforms. To confirm they amplified the correct sequence, the PCR product of these primers was first separated on a gel, extracted, and sequenced (Fig. 22A-B). Following this confirmation, qPCR was used to compare expression of *Wt1* mRNA in gastrocnemius of 8-10 week old *Mdx*/*Utrn*+/- mice with the expression in age-matched wildtype control gastrocnemius (Fig. 22C). There was a statistically significant increase in *Wt1* mRNA expression (p = 0.049).

To examine this question further, it was important to analyze how the individual isoforms of *Wt1* mRNA varied. Therefore, whether there was a particular *Wt1* isoform which was upregulated was analyzed, quantifying the mRNA of each isoform in the same tissue as the total *Wt1* mRNA was quantified (Fig. 22D). However, no significant differences were found in the ratios of the isoforms expressed (p > 0.050).

Figure 22. Wt1 total mRNA increases with respect to an age-matched wildtype control in gastrocnemius muscle of 8-10 week old *Mdx/Utrn+/-* mice.

Following PCR amplification, total Wt1 and Wt1 isoform PCR products were separated on 2.0% agarose gel (A). Bands at molecular weights corresponding to total Wt1 and each of the Wt1 isoforms were then excised and sequenced to confirm amplification. Alignment of sequencing results on the top with the correct sequences is shown (B). Additionally, graphs are presented depicting Wt1 mRNA expression. For total Wt1, this is represented as the concentration relative to the wildtype (C). For Wt1 isoform comparison, this is represented as the fraction of the sum of the isoforms which a particular isoform makes up (D). Values are expressed as mean +SD. Asterisks indicate significant differences with age-matched wildtype. (* < 0.050, ** < 0.010, *** < 0.001). Three biological and three technical replicates were used.

4.8 Wt1 immunoreactivity in mouse skeletal muscle during early collagen deposition is also present in myotubes

In order to determine which cell types were immunoreactive for Wt1, an examination of differences in histology of 8-10 week old wildtype and *Mdx*, *Mdx/Ut*rn+/-, and *Mdx/Utrn-/-* diaphragm and gastrocnemius tissues (Fig. 15A-B, D-E, G-H, J-K) was conducted to establish changes between tissue which were not dependent on immunostaining. To expand on this, immunostaining of diaphragm and gastrocnemius muscle derived from 8-10 week old *Mdx*/*Utrn-/-* mice was followed with counterstaining of this tissue with Carazzi's hematoxylin and eosin. Nuclear Wt1 immunoreactivity was not only limited to the nuclei of cells external to the muscle, but also within the nuclei of developing myotubes (Fig. 23A-B).
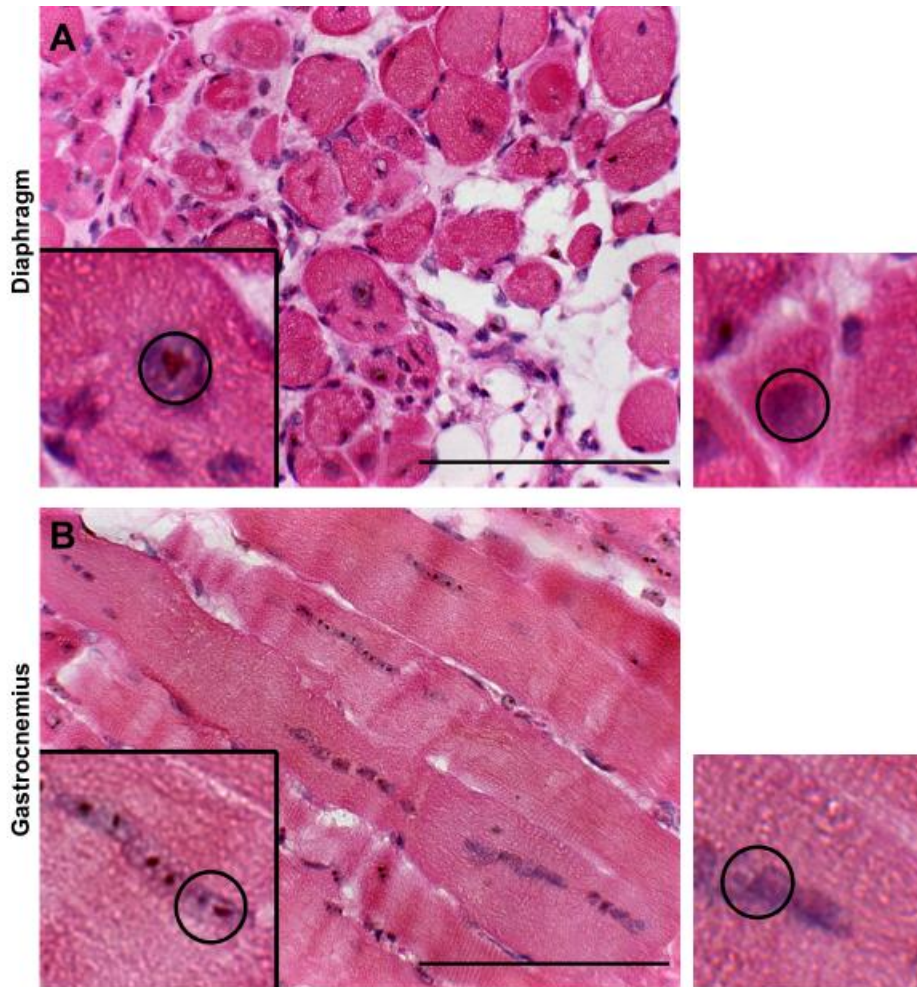
Figure 23. Wt1 immunoreactivity is present in myotube nuclei of eosin counterstained Wt1 immunostained diaphragm and gastrocnemius of 8-10 week old *Mdx/Utrn-/-* mice.

Representative images of 8-10 week old *Mdx/Utrn-/-* diaphragm (A) and gastrocnemius (B), already immunostained for Wt1, which was counterstained with Carazzi's hematoxylin and eosin. In the bottom left corner, a section of magnified immunoreactive nuclei are provided for examination. To the right of each image, a section of magnified non-immunoreactive nuclei are provided for examination. For further clarity, example immunoreactive and non-immunoreactive nuclei are circled in black (scale bar = 100μm). One biological and one technical replicate was used.

4.9 There is nuclear Wt1 immunoreactivity in late-stage DMD human skeletal muscle, where the tissue has been replaced primarily by fibrosis and adipose tissue

In order to determine whether these results applied to human cases of DMD, Wt1 expression and tissue collagen deposition in healthy human muscle and highly fibrotic human DMD muscle was examined. Wt1 immunoreactivity was not detected in the healthy human muscle, but was detected in nuclei in the highly fibrotic human DMD muscle (Fig. 24A-D). At this advanced stage, most of the tissue had been replaced by fibrosis and adipose tissue.
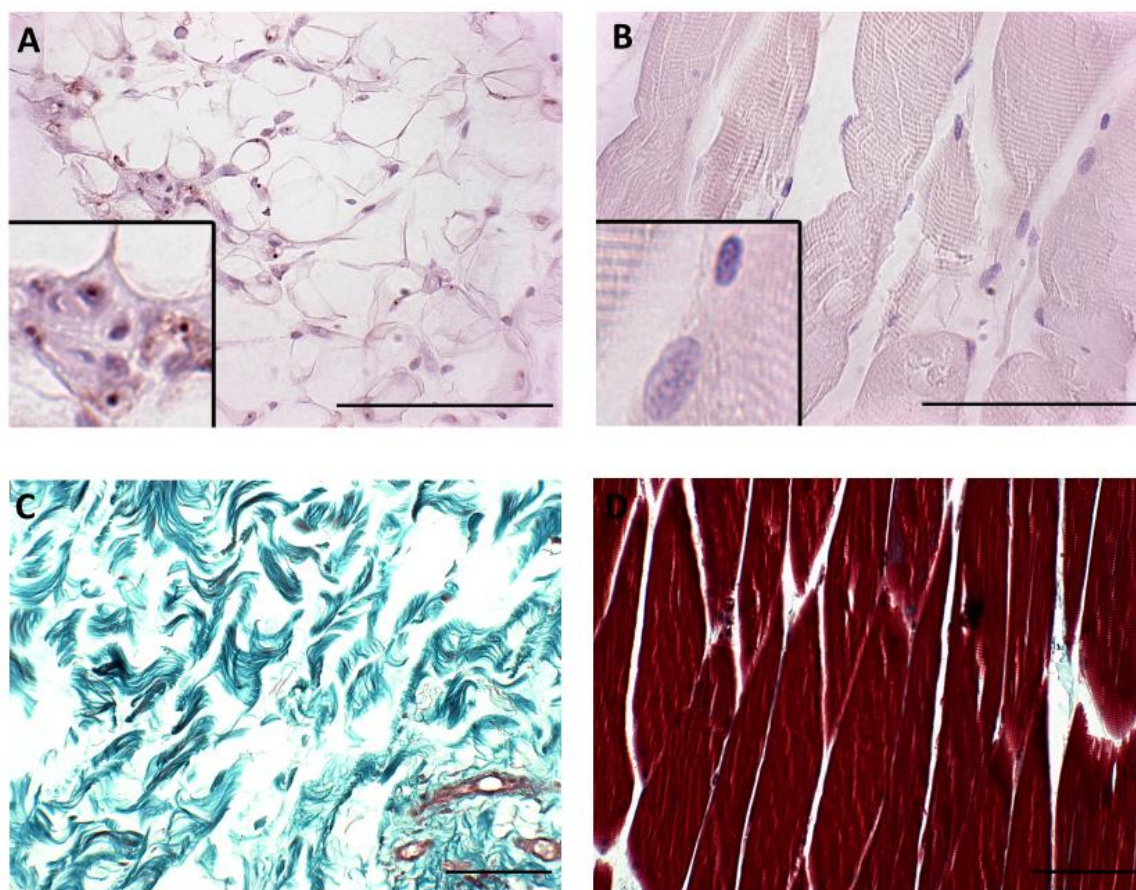
Figure 24. Wt1 immunoreactivity is present in late-stage DMD human skeletal muscle, where the muscle has been replaced primarily by fibrotic and adipose tissues.

Representative images of Wt1 immunostained human skeletal muscle, in highly fibrotic human DMD tissue (A), and in healthy tissue (B). In the bottom left corner, a section of magnified nuclei are provided for examination. Additionally, representative images of Masson's trichrome stained human skeletal muscle, in highly fibrotic human DMD tissue (C), and in healthy tissue (D) (scale bar = 100μm). One biological and one technical replicate was used.

5   DISCUSSION

5.1   Summary

Adequate treatment of Duchenne muscular dystrophy (DMD) and other muscular dystrophies is often impeded due to extensive muscle fibrosis throughout the body, reducing the ability of therapeutic agents to penetrate affected tissues. It is therefore a high priority to determine biomarkers for pre-fibrotic and early fibrotic states, as well as therapy candidates to reduce fibrosis. Wt1 is a protein which can potentially address both of these issues, having been linked to fibrosis in idiopathic pulmonary fibrosis, and DD[179,181]. This has led to the hypothesis that Wt1 immunoreactivity is a marker for fibrosis in a mouse model of DMD. The specific aims of this study, to address this hypothesis, were to evaluate the timing and location of expression of Wt1 with respect to the onset of fibrosis in a mouse model of DMD, and to determine which isoforms of Wt1 are altered during the onset of fibrosis.

This study has produced several major results concerning Wt1 expression in DMD. Firstly, it demonstrated that the proportion of Wt1 immunoreactive nuclei is increased prior to and during the onset of fibrosis in the diaphragm and gastrocnemius skeletal muscles. Secondly, it showed that the proportion of Wt1 immunoreactive nuclei, following a period of increase, returns to wildtype levels after the onset of skeletal muscle fibrosis. Thirdly, it showed that proportion of Wt1 immunoreactive nuclei does not change in *Mdx, Mdx/Utrn+/-, or Mdx/Utrn-/-* heart tissue, but that it is nonetheless expressed in these tissues, possibly indicative of some roles in the maintenance of these tissues. Thirdly, it indicated that neither in the gastrocnemius, diaphragm, or heart, are there significant changes in Wt1 immunoreactivity in the muscle cytoplasm or non-muscle tissue. Additionally, it provided initial evidence that *Wt1* mRNA upregulation may coincide with the increase in proportion of Wt1 immunoreactive nuclei, but

that there is no change in ratio of major *Wt1* isoforms. Furthermore, it indicated that nuclear Wt1 immunoreactivity takes place in developing myotubes, in addition to possibly fibrogenic cells or cells present in inflammatory infiltrate. Finally, it demonstrated that there is nuclear Wt1 immunoreactivity in fibrosis produced by DMD in human patient muscle.

5.2 Implications of Experimental Findings

5.2.1 Proportion of Wt1 immunoreactive nuclei is increased prior to and during early collagen deposition in mouse skeletal muscle, but not during late collagen deposition

In order to begin addressing the timing and location of Wt1 immunoreactivity with respect to the onset of fibrosis, the proportion of Wt1 immunoreactive nuclei, and collagen deposition, were evaluated in skeletal muscle.

Aside from the *Mdx* gastrocnemius, the disease model skeletal muscles examined all expressed a significantly increased proportion of Wt1 immunoreactive nuclei relative to the age-matched wildtype at some timepoint. Either simultaneously, or at an older timepoint, these tissues also showed significant collagen deposition relative to the age-matched wildtype (Fig. 11, 15, 19). This is the first study to indicate the expression of Wt1 in a disease model of DMD. Wt1 is a complex protein with conflicting past research suggesting it may both promote and inhibit fibrosis. Much of this prior body of work has focused primarily on its contribution to lung fibrosis. One such study by Sontake and colleagues found that Wt1 was upregulated in mesenchymal and mesothelial cells in idiopathic pulmonary fibrosis. Transduction of human fibroblasts with lentivirus containing Wt1 was shown to increase expression of a major myofibroblast marker, α-SMA, and its knockdown with siRNA was shown to decrease it. This knockdown additionally downregulated many transcripts associated with extracellular matrix

production, including integrin 7 (*Itg7*), integrin 2 (*Itg2*), and collagen 4 (*Col14*)[180]. In contrast to this, a 2014 study investigating pleural mesothelial cell plasticity suggested that Wt1 serves a role in preventing conversion of cells into a myofibroblast phenotype. Loss of Wt1, through short hairpin knockdown, was shown to promote this transformation, and actually led to an increase in α-SMA expression[181]. Past research by the O'Gorman lab examining fibrosis in DD patients indicated that Wt1 is expressed in fibrotic palmar fascia of the hand in DD patients. This was shown through both qPCR and immunohistochemical staining. However, no difference in Wt1 expression compared to the control, either through qPCR or through immunohistochemical staining, was found in palmar fascia of DD patients which had not already become fibrotic[182]. In order to acquire an adequate understanding of Wt1, these conflicts will need to be resolved. In the context of this literature, this study's results agree with those of the Sontake and O'Gorman groups, that the expression of Wt1 is increased in association with fibrosis.

In several of the tissues examined, such as the *Mdx* and *Mdx/Utrn+/-* diaphragm, and the *Mdx/Utrn-/-* gastrocnemius, the increase in proportion of Wt1 immunoreactive nuclei occurred in the absence of a significant increase in collagen deposition. The significant increase in collagen deposition was only detected, instead, at a later timepoint. This contrasts the results from the O'Gorman lab, as the non-fibrotic palmar fascia of DD patients which had not already become fibrotic showed no increase in nuclear Wt1 immunoreactivity[182]. This may speak to the differences in Wt1 expression in the fibrosis of different tissues, or it may indicate that nuclear Wt1 immunoreactivity is increased only immediately antecedent to fibrosis. The syngeneic tissues evaluated in the O'Gorman study may not have yet reached this antecedent point, or were not to become fibrotic at all. Nevertheless, the results of this study indicate that the proportion of Wt1 immunoreactive nuclei may be increased by pre-fibrotic conditions that persist into the early

stages of fibrosis. These may be the same conditions which prompt fibrosis itself, but additional research would be required before this could be confirmed.

Of all the disease models analyzed, the only skeletal muscle which did not show a significant increase in the proportion of Wt1 immunoreactive nuclei, or a significant increase in collagen deposition, was the *Mdx* gastrocnemius. The differences in proportion of Wt1 immunoreactive nuclei and collagen deposition between diaphragm and gastrocnemius muscle in the *Mdx* model may be explained through differences in progression of fibrosis. This may additionally elucidate the differences between the *Mdx* gastrocnemius muscle and the other disease models' examined skeletal muscles. The *Mdx* mouse model does not perfectly recapitulate the pathology of DMD as seen in humans. Instead, it experiences lower rates of limb fibrosis, as the presence of utrophin within this model is suggested to ameliorate muscle cell death[186–188]. Past work in the Hoffman lab has indicated that the 10 month old *Mdx* diaphragm (Fig. 17E), but not the *Mdx* gastrocnemius (Fig. 17D), becomes fibrotic. This past work has also found that both skeletal muscles have similar rates of regeneration as quantified by the percent of centrally-nucleated myofibers. This would suggest that it is fibrosis, and not muscle regeneration, which is triggering this increase in proportion of Wt1 immunoreactive nuclei[194]. Established literature exists describing the expression of Wt1 in developing, though not regenerating, skeletal muscle. There is immunohistochemical evidence for Wt1 being upregulated in the cytoplasm of muscle cells during development. However, an absence of nuclear Wt1 expression was also found in these studies, which would appear to contradict the nuclear immunoreactivity pattern in this study[200]. Other past research does show the presence of nuclear Wt1 in developing skeletal muscle, though does not describe its presence in regenerating

muscle[201]. It may the case that some form of cross-talk occurs where regenerating skeletal muscle expresses Wt1 only in the presence of the pre-fibrotic, or early fibrotic, environment.

The return in proportion of Wt1 immunoreactive nuclei to levels similar to the wildtype in the 10-14 month old skeletal muscle during late collagen deposition is a novel finding (Fig. 19A-B). This supports, though does not confirm, its role as a protein expressed in advance of fibrosis. Were the proportion of Wt1 immunoreactive nuclei increased as a result of fibrosis, it would consistently occur regardless of the time after fibrosis onset. This would suggest that it is the early fibrotic environment which promotes, or at least tolerates, nuclear Wt1 immunoreactivity. The proportion of Wt1 immunoreactive nuclei may be reduced once the fibroblast population ceases to divide and enters quiescence[181]. Another possibility is that the nuclear Wt1 immunoreactivity that took place in developing myotubes may no longer be visible, as the regenerative capacity of the muscle tissue is exhausted, but this seems unlikely due to the presence of developing myotubes at the 10-14 month timepoint.

5.2.2 Proportion of Wt1 immunoreactive nuclei does not change in *Mdx*, *Mdx/Utrn+/-*, or *Mdx/Utrn-/-* heart tissue

Beyond skeletal muscle, it was also important to evaluate the timing and location of changes in the proportion of Wt1 immunoreactive nuclei with respect to the onset of fibrosis in cardiac muscle. Quantification of collagen deposition in the heart showed surprising results, with none of the cohorts showing a statistically significant difference in collagen deposition compared to their age-matched wildtype controls (Fig. 11C, 15C, 19C). Earlier data on 4-5 week old and 8-10 week old heart collagen deposition corresponded well with the literature, but past studies evaluating the hearts of aged *Mdx* and *Mdx*/*Utrn*+/- mice have indicated that beyond ten months, the organ is fibrotic[202,203]. The small sample size and increased age range utilized in this study

may be one possible explanation for this, as the average collagen deposition present in the 10-14 month old *Mdx* and *Mdx*/*Utrn*+/- hearts was still higher than that of the 10-14 month old wildtype hearts. The lack of a statistically significant increase in proportion of Wt1 immunoreactive nuclei in 8-10 week old *Mdx*/*Utrn*-/- mice hearts furthermore compounds this issue. This absence is peculiar, as previous work has suggested that as early as 16 weeks of age, *Mdx*/*Utrn*-/- hearts are fibrotic[204]. As collagen deposition and the proportion of Wt1 immunoreactive nuclei in both ventricles was evaluated as part of this study, and past work primarily evaluated left ventricle fibrosis, it may be pertinent to evaluate the proportion of Wt1 immunoreactive nuclei and its relationship to fibrosis in this component of the heart alone.

An alternative explanation for the differences in proportion of Wt1 immunoreactive nuclei when compared to the skeletal muscle is that there appears to be a higher, though not significantly so, basal level of nuclear Wt1 immunoreactivity in the heart than in either skeletal muscles analyzed. This may mask slight changes in the proportion of Wt1 immunoreactive nuclei which arise as a result of fibrosis initiation. The existing literature supports Wt1 upregulation in the heart following myocardial infarction and ensuing hypoxia. Primarily, this is through Wt1's roles in managing the proliferation of coronary vascular cells[148,157,163,205]. This study's results, however, show high basal nuclear Wt1 immunoreactivity even in the wildtype, which may be indicative of other unknown roles Wt1 may be playing in adult cardiac muscle. To address the issue of statistical power with this particular outcome, it will be necessary to explore Wt1's role in the heart to a greater extent in the future.

5.2.3 Wt1 immunoreactivity patterns in muscle cytoplasm and non-muscle tissue do not change in mouse skeletal and cardiac muscle, and are not significantly different from an absence of expression

Although Wt1's principal role is often thought to be in the nucleus, it is important nonetheless to also consider its possible roles in the muscle cytoplasm and non-muscle tissue. With regards to Wt1 immunoreactivity in the skeletal muscle cytoplasm, results indicated no significant differences in the area positive for Wt1 in any of the disease models compared to the age-matched wildtype control (Appendix K). In many of the tissues examined, the presence of Wt1 in the muscle cytoplasm and non-muscle tissue were low enough that they were indistinguishable from the signal in the negative control (Appendix B-D). None of the other tissues compared showed significant difference from tissues where this was the case.

Wt1 has previously been identified to be expressed in the cytoplasm in other muscle groups. Expression of Wt1 is linked to skeletal muscle development, so its elevation earlier in development would be in accordance with established literature[177]. One possibility is that the antibody used in this study may not necessarily target all isoforms of Wt1, and that those isoforms which localize to the cytoplasm are not among the ones targeted. Alternatively, Wt1 expression may be low enough that only when a significant amount of the protein localizes to a relatively small location, such as the nucleus, is the immunohistochemical system that was utilized sensitive enough to pick it up.

Turning attention to Wt1 immunoreactivity in the cardiac muscle cytoplasm, results indicated, similar to the skeletal muscle, that there were no significant differences in the area positive for Wt1 in any of the disease model tissue compared to the age-matched wildtype control (Appendix K). Wt1 has been shown to be associated with early cardiac development.

Particularly, it plays roles in vascular cell proliferation, and its knockout causes reduced coronary vascularization, as well as epicardial thinning and smaller ventricles[152]. As little cardiac damage was observed in the models utilized, it may be possible that a more severely affected model, such as an older *Mdx/Utrn-/-* or *Mdx/Utrn+/-* model, may have Wt1 signal in the muscle cytoplasm of the heart. With increased cardiac injury, Wt1 expression may be more greatly promoted so as to prompt vascularization.

The absence of any change in percent immunoreactivity for Wt1 in the non-muscle tissue seems to conflict with prior observations in DD patients[182]. However, it may be the case that the possible Wt1 upregulation found in DMD tissues is not high enough, is not of the proper isoforms, or is not in the proper cell types, that it would appear in non-muscle tissues.

5.2.4 Proportion of Wt1 immunoreactive nuclei and collagen deposition patterns show weak respective trends over time toward decreasing and increasing in skeletal muscle

As it had been determined that proportion of Wt1 immunoreactive nuclei and collagen deposition varied compared to the wildtype in several of the disease models, it became worthwhile to examine if Wt1 immunoreactivity and collagen deposition formed any pattern over time. Proportion of Wt1 immunoreactive nuclei in skeletal muscle showed a weak trend toward decreasing over time, with several earlier timepoints showing significantly greater signal than later timepoints. In contrast, tissue collagen deposition showed a weak trend toward increasing over time, with several earlier timepoints showing a significantly lower signal than later timepoints (Fig. 20). This may speak to Wt1's roles in early disease progression, and potentially cell proliferation. As an organism ages, the number of cells which actively divide, or which begin to divide when stimulated by inflammation, may be reduced[181]. If it is the case that

these cells are the ones expressing Wt1, then it would be reasonable to see this reduction with time. The increase in collagen deposition with time seems to occur solely for the disease models, and is likely representative of the gradual production of collagen.

However, it should be noted that for both proportion of Wt1 immunoreactive nuclei and collagen deposition, these observed patterns were weak. Although there was never a case of a later timepoint showing lower collagen deposition, or greater Wt1 expression, there were many cases where a significant difference was not found whatsoever. This speaks to the need for additional power when conducting an analysis in this fashion, as well as the importance of putting the tissue signal in the context of the age-matched wildtype control.

5.2.5 Total Wt1 mRNA is upregulated during early collagen deposition in mouse skeletal muscle without a change in the ratios of its major isoforms.

To explore which of the different isoforms of Wt1 were being upregulated, as well as changes in total *Wt1* expression, both of these measures were evaluated through qPCR. An approximately 6-fold upregulation in total *Wt1* mRNA in the *Mdx/Utrn+/-* model gastrocnemius muscle at 8-10 weeks of age was identified. This corresponds well with past literature evaluating other forms of fibrosis (Fig. 22C)[182].

Examination of whether the four major isoforms of *Wt1* changed in ratio showed no significant differences between the 8-10 week old wildtype and *Mdx/Utrn+/-* models (Fig. 22D). As mentioned previously, Wt1 has numerous isoforms with multiple distinct roles, largely divisible into four major groups. Its roles envelope transcriptional regulation, post-transcriptional modification, and the binding of other proteins, giving it a wide range of means to enact its

function. The role Wt1 plays in fibrosis may be mediated by only a single isoform of the protein. However, these results suggest that either the upregulation of Wt1 that is associated with fibrosis is across all variants of the protein or that an isoform, distinct from the four major forms, is being upregulated.

Another interesting result of note is that the observed ratio of the isoforms, for A, B, C, and D, was 0.32:0.19:0.27:0.22. This is in contrast to past research studying *Wt1* isoforms in certain forms of cancer, and may reflect changes of the isoform ratios between different tissues[199].

5.2.6 Nuclear Wt1 immunoreactivity in mouse skeletal muscle during early collagen deposition is also present in myotubes

Nuclear Wt1 immunoreactivity in developing myotubes was also noted, identified through the central positions of the nuclei, both in tissues which showed (Fig. 23A) and did not show (Fig. 23B) significant increases in proportion of Wt1 immunoreactive nuclei overall. This provides evidence that the muscle is recapitulating part of development during the regeneration process, as Wt1 immunoreactivity has previously been seen to be upregulated during early skeletal muscle development. However, this upregulation in past investigations has been subject to some debate. Studies on the topic disagree on whether Wt1 is expressed primarily in the cytoplasm or the nuclei of developing muscle tissues[200,201]. It may be that with the recapitulation of development during the regeneration process, there is increased overall expression of Wt1. This may promote not only cytoplasmic Wt1, but also nuclear Wt1, resulting in increased nuclear Wt1 signal in skeletal muscle. The absence of a significant increase in proportion of Wt1 immunoreactive nuclei in the *Mdx* gastrocnemius, despite its undergoing muscle regeneration, further complicates this issue. This may play back into the possibility of cross-talk where

regenerating skeletal muscle expresses Wt1 only in the pre-fibrotic, or early fibrotic, environment.

However, not all of the nuclear Wt1 immunoreactivity detected was found in skeletal muscle, as a significant portion was also present in areas of inflammatory infiltrate (Fig. 10J, 15E). Although this may be possible fibroblast expression of Wt1, there are other potential cell candidates in these regions. These include mast cells, neutrophils, basophils, eosinophils, macrophages, and lymphocytes. These areas of inflammation may, furthermore, be the arrival site of fibrocytes, and the location where pericytes migrate to after beginning their transition into myofibroblasts[55,206]. One cell type of interest in this location that may be Wt1 positive are lymphocytes. A 2006 study showed that Wt1 was expressed in adult human lymphocytes, but additionally indicated that neither monocytes nor granulocytes express the protein[207]. There are, additionally, Wt1 positive cells on the periphery of myofibers (Fig. 10, 14). This expression may instead be endogenous fibroblasts, FAP cells, or satellite muscle cells, which are exiting quiescence and either beginning to divide, differentiate, or participate in the inflammatory and fibrotic processes.

5.2.7 There is nuclear Wt1 immunoreactivity in late-stage DMD human skeletal muscle, where the muscle has been replaced primarily by fibrotic and adipose tissues

In order to determine how well the results found carried over from the mouse model to human subjects, highly fibrotic DMD patient muscle tissue and non-fibrotic human muscle tissue were evaluated for Wt1 immunoreactivity. While immunoreactivity in the highly fibrotic human DMD patient muscle tissue was found, no immunoreactivity was found in the non-fibrotic tissue (Fig. 24). This contrasts the results in the mouse model in this study, which would indicate that

immunoreactivity in humans should become absent toward the peak of fibrosis. A greater replicative capacity in human fibroblasts, or a greater resistance to initial muscle death, may be possible explanations, though this would require additional human samples for statistical power.

5.3   Limitations

There are some limitations associated with this project which will need to be resolved in future experiments. Several of these issues concern immunohistochemical work. The immunohistochemistry performed to detect the presence of Wt1 is problematic in that the fibrogenic process is inherently heterogeneous throughout muscle tissue, with particular sections of the tissue becoming fibrotic long before others[55]. Some parts of the tissue may never become fibrotic. For this reason, only in regions of the tissue where fibrosis begins, or will begin, can expression of Wt1 be expected. This may lead to an inaccurate assessment of Wt1 expression across the entire tissue, should an appropriate proportion of fibrotic regions not be captured during sectioning. Addressing this may necessitate additional immunohistochemical staining, or alternative whole-tissue based analyses, such as western blotting. The antibody used for this evaluation was a rabbit monoclonal antibody against the 50-250 amino acids of the Wt1 protein. This may introduce some uncertainty, as well. The isoforms adopted by the protein may not necessarily still maintain the epitope for this antibody to bind to, so particular forms of Wt1 may be undetected by this antibody. This may be a possible explanation for why the heart showed no significant differences in Wt1 positivity in the affected tissues, if the Wt1 isoform which increased in expression in the heart was not one to which the antibody bound. Furthermore, this may explain why the overall Wt1 positivity in the diaphragm tended to be higher than that of the gastrocnemius. The isoforms that the antibody detects may not be as highly expressed in the gastrocnemius, compared to the diaphragm. A possible solution to the antibody issue may be

through using a polyclonal antibody against the whole Wt1 protein, though this would introduce potential off-targeting effects. An additional issue with the immunohistochemistry performed is that it takes the form of DAB staining, which is only semi-quantitative. The absorbance of light by oxidized DAB is not linear with respect to the quantity of DAB present. Therefore, quantification of total DAB stain intensity is not a direct measure for Wt1 expression, and instead it is only possible to identify whether particular nuclei are positive for Wt1, or whether a region is positive for Wt1. This can introduce uncertainty regarding whether Wt1 is being upregulated, as it may be the case that it is merely being localized to the nucleus or cytoplasm instead. This is in contrast with fluorescent immunohistochemistry, where the fluorescent signal is proportional to the number of fluorophores bound to the protein of interest. A fluorescent signal produced in this fashion is representative of the total amount of that protein present. Unfortunately, for proteins which are expressed in very small quantities, such as transcription factors like Wt1, fluorescent techniques may not be strong enough to resolve the protein. Thus, chromogenic reporters such as DAB must be used, as in the case of this study. Western blotting may be a potential supplementary technique to address this in the future. Finally, as Wt1 was identified in cell types besides only what were apparently fibroblasts, we cannot say for certain that the proportion of Wt1 immunoreactive nuclei was increased in fibroblasts. It may be the case that this increase was exclusively limited to non-fibroblast cell types. In order to address this in the future, co-staining for other markers of fibroblasts would be required.

Regarding limitations concerning Masson's trichrome staining, other literature identifies 10-14 month old *Mdx* and *Mdx*/*Utrn*+/- heart tissue as being fibrotic, while the results produced by this study indicated otherwise[202,203]. This is possibly explained through the increased age range and smaller sample size used in this study. The variation introduced by these factors may

be enough to make the differences between 10-14 month old *Mdx* and *Mdx*/*Utrn*+/- heart tissue and 10-14 month old wildtype heart tissue insignificant. Addressing this limitation would require additional samples of aged tissue in order to determine if the 10-14 month old heart tissue is fibrotic.

Concerning additional limitations regarding the heart, it may be the case that the basal Wt1 expression is high enough as to mask increases in Wt1 expression in the disease models. Fortunately, much as is the case with the Masson's trichrome staining, addressing this limitation would involve utilizing additional samples of heart in these age ranges. This would be able to identify whether or not there are significant differences in Wt1 immunoreactivity between these ages and genotypes.

Finally, regarding limitations in qPCR, there are some issues with respect to quantifying the total amount of each *Wt1* isoform. Although the inclusion of exon 5 and the KTS sequence are often considered the major features which differentiate isoforms, these are not the only features which can differ among isoforms. Wt1 has multiple start sites for translation, capable of producing isoforms of different lengths. This may play a role in altering the ultimate function of the protein[208]. In order to address this issue, designing primers which are capable of reliably performing qPCR on the differing *Wt1* isoforms will be a priority in the future.

5.4   Future Directions

With regards to future research, the next experiments to perform to expand on this project, besides those listed in the previous section, can take several forms. The evidence of substantial inflammatory infiltrate suggests that exploring immune cells, such as macrophages and lymphocytes, may be one possible future path to pursue. These cells may become Wt1 positive either as a result of expressing Wt1 themselves or phagocytosing it. Secondary

infiltration of immune cells which have phagocytosed Wt1 and then travelled into a nearby lymph node may provide a unique diagnostic tool, as sampling of lymph node fluid for Wt1 positive immune cells would allow detection of fibrotic tissue downstream of the node. Western blots can be performed to analyze differences in Wt1 level in the diaphragm as well as in the gastrocnemius muscle. This would provide definitive evidence regarding in which genotypes and age groups Wt1 is upregulated. Expanding the qPCR exploration to include variants of *Wt1* mRNA that begin at different start sites may also be a future direction. Rather than analyze all *Wt1* isoforms, however, it may be beneficial to evaluate the *Wt1* isoforms that begin at different start sites independently of those created through the selective inclusion of exon five and the KTS sequence. Another possible experiment is fluorescence activated cell sorting, followed by western blots, in order to separate out different cell types and quantify differences in Wt1 expression within them. This could target cells such as developing myotubes, fibroblasts, or immune cells. RNAseq is also a possible follow-up to fluorescence activated cell sorting, as it would allow determination of differences in mRNA variant regulation in fibroblasts, and allow us to determine which mRNAs are upregulated or downregulated in response to, or alongside, Wt1 upregulation. Examining different ages of tissues through this method would allow us to determine which Wt1 isoforms are upregulated at the start and end of fibrosis, and determine if any isoforms remain upregulated following the broad downregulation at 10-14 months of age. A final experiment to pursue, prior to trials using Wt1 immunotherapy in *Mdx*, *Mdx*/*Utrn*+/-, and *Mdx*/*Utrn*-/- mice, is the creation of conditional knockout mice. This involves the crossing of *Wt1* conditional knockout mice with *Mdx*, *Mdx*/*Utrn*+/-, or *Mdx*/*Utrn*-/- mice, in order to produce a murine model which can be used to simulate Wt1 inhibition by an external method. Following induction of Wt1 knockout, these mice can be evaluated for performance in muscle strength and

endurance tests. Furthermore, they can be sacrificed such that their muscle tissue can be examined for fibrosis compared to the wildtype control and mice which do not have Wt1 knocked out. Expanding on this, specifying this conditional knockout exclusively to fibroblasts may be beneficial in elucidating the function of Wt1 in fibrogenesis, but would require that future therapies also be fibroblast-specific. A number of existing therapies which downregulate Wt1 in cancers, such as Wt1 peptide vaccines and anti-Wt1 immunotherapies, may still be potentially used in treatments for fibrosis[209,210]. That Wt1 was shown to be upregulated in this model of fibrosis bodes well for this, as targeting Wt1 for downregulation may serve as a general therapy for fibrosis, as opposed to one for several specific fibrosis forms.

5.5 Significance

Significance for this research can be found primarily in how an understanding of fibrosis may benefit a number of novel and existing therapies for DMD. Existing therapies are largely palliative, intended to reduce symptoms of DMD. At the least, being able to determine when fibrosis is occurring will allow rapid treatment in order to delay the onset of symptoms and guarantee a higher quality of life. This supports early corticosteroid use when the microvasculature of the muscle is not damaged due to excessive buildup of extracellular matrix, allowing better perfusion of the tissue. If the case is that Wt1, or other proteins, may act as a marker for skeletal muscle fibrosis, but not cardiac fibrosis, then treatments can be refined to explicitly target those muscle groups undergoing fibrosis. Corticosteroids and physical therapy can be employed solely to affect those regions which are at highest risk of progressing to true fibrosis. This will reduce strain on the health care system, as it will no longer need to contribute resources to target many muscle groups simultaneously. Furthermore, this will reduce the need

for high corticosteroid use, moderating side effects such as weight gain and Cushingoid symptoms[9].

In terms of novel therapies, there are several techniques which may benefit from this research. As mentioned previously, viral vector strategies normally make use of recombinant adeno-associated viral vectors which carry components of the DMD gene, and have been shown to be able to restore dystrophin expression in mouse models. Challenges in delivery due to tissue fibrosis may be alleviated by identifying tissues which will become fibrotic early on in this process, allowing treatment before these difficulties arise. Other strategies involving delivery of key components, such as CRISPR/Cas9 delivery, may also appreciate accurate identification of fibrotic and pre-fibrotic regions[121]. Stem cell therapy is another exciting domain in which fibrosis detection may find substantial use. Myogenic stem cells from donors suffer from immune responses which limit their applicability, whereas autologous stem cells do not cause immune responses. Chimeraplasty and small fragment homologous replacement therapy, forms of ex vivo gene correction technique, can be used in autologous colonies to correct the dystrophin gene. Transplantation without an immune response then becomes possible, but low numbers of myogenic stem cells present in dystrophic muscle makes this process a challenge[121,130,131]. Through examination of biomarkers predictive of muscle fibrosis, myogenic stem cells can be harvested early on, allowing for circumvention of this issue entirely[7]. It is clear that an understanding of fibrosis, including its biomarkers, has innumerable benefits for health care, not just for DMD patients, but for all patients with progressive fibrotic conditions.

5.6   Conclusions

In conclusion, the hypothesis that Wt1 immunoreactivity is a marker for fibrosis in a mouse model of DMD was supported. The results obtained suggest that Wt1 levels do increase

prior to onset of fibrosis in the gastrocnemius and diaphragm muscles of a DMD mouse model. It is clear that the mechanisms regulating Wt1 expression are complex, and future research will be needed to understand them in full.

REFERENCES

1.	Moat, S. J., Bradley, D. M., Salmon, R., Clarke, A. & Hartley, L. Newborn bloodspot screening for Duchenne muscular dystrophy: 21 years experience in Wales. *Eur. J. Hum. Genet.* **21**, 1049–1053 (2013).

2.	Darras, B. T. *Neuromuscular disorders of infancy, childhood, and adolescence: A clinician's approach.* (Elsevier/Academic Press., 2015).

3.	Ciafaloni MD, E. *et al.* Delayed Diagnosis in Duchenne Muscular Dystrophy: Data from the Muscular Dystrophy Surveillance, Tracking, and Research Network. *J. Pediatr.* **155**, 380–385 (2009).

4.	Mercuri, E. & Muntoni, F. Muscular dystrophies. *Lancet* **381**, 845–860 (2013).

5.	Eagle, M. *et al.* Managing Duchenne muscular dystrophy - the additive effect of spinal surgery and home nocturnal ventilation in improving survival. *Neuromuscul. Disord.* **17**, 470–475 (2007).

6.	Eagle, M. *et al.* Survival in Duchenne muscular dystrophy: improvements in life expectancy since 1967 and the impact of home nocturnal ventilation. *Neuromuscul. Disord.* **12**, 926–929 (2002).

7.	Yiu, E. M. & Kornberg, A. J. Duchenne muscular dystrophy. *J. Paediatr. Child Health* **51**, 759–764 (2015).

8.	Bach, J. & Martinez, D. Duchenne muscular dystrophy: continuous noninvasive ventilatory support prolongs survival. *Respir. Care* **56**, 744–750 (2011).

9.	Bushby, K. *et al.* Diagnosis and management of Duchenne muscular dystrophy, part 1: Diagnosis, and pharmacological and psychosocial management. *Lancet Neurol.* **9**, 77–93 (2010).

10.	Bernardini, C. *Duchenne Muscular Dystrophy: Methods and Protocols*. **1687**, (Springer New York, 2018).

11.	Griggs, R. C., Mendell, J. R. & Miller, R. G. *Evaluation and Treatment of Myopathies*. **44**, (F.A. Davis, 1995).

12.	Hsu, J. D. The natural history of spine curvature progression in the nonambulatory Duchenne muscular dystrophy patient. *Spine (Phila. Pa. 1976).* **8**, 771–775 (1983).

13.	Choi, Y.-A., Chun, S.-M., Kim, Y. & Shin, H.-I. Lower extremity joint contracture according to ambulatory status in children with Duchenne muscular dystrophy. *BMC Musculoskelet. Disord.* **19**, 286–287 (2018).

14.	Suresh, S., Wales, P., Dakin, C., Harris, M. & Cooper, D. M. Sleep-related breathing disorder in Duchenne muscular dystrophy: Disease spectrum in the paediatric population. *J. Paediatr. Child Health* **41**, 500–503 (2005).

15.	Nigro, G., Comi, L. I., Politano, L. & Ban, R. J. I. The incidence and evolution of cardiomyopathy in Duchenne muscular dystrophy. *Int. J. Cardiol.* **26**, 271–277 (1990).

16.	Hoogerwaard, E. *et al.* Signs and symptoms of Duchenne muscular dystrophy and Becker muscular dystrophy among carriers in the Netherlands: a cohort study. *Lancet* **353**, 2116–2119 (1999).

17.	Hoogerwaard, E. M. *et al.* Cardiac involvement in carriers of Duchenne and Becker muscular dystrophy. *Neuromuscul. Disord.* **9**, 347–351 (1999).

18.	Brooke, M. H. *et al.* Clinical investigation in Duchenne dystrophy: II. Determination of the 'power' of therapeutic trials based on the natural history. *Muscle and Nerve* **6**, 91–103

(1983).

19. Laing, N. G., Davis, M. R., Bayley, K., Fletcher, S. & Wilton, S. D. Molecular diagnosis of Duchenne muscular dystrophy: past, present and future in relation to implementing therapies. *Clin. Biochem. Rev.* **32**, 129 (2011).

20. Worton, R. G. & Thompson, M. W. Genetics of Duchenne Muscular Dystrophy. *Annu. Rev. Genet.* **22**, 601–629 (1988).

21. Belfall, B. *et al.* The Duchenne muscular dystrophy gene product is localized in sarcolemma of human skeletal muscle. *Nature* **333**, 466–469 (1988).

22. Hoffman, E. P. *et al.* Characterization of Dystrophin in Muscle-Biopsy Specimens from Patients with Duchenne's or Becker's Muscular Dystrophy. *N. Engl. J. Med.* **318**, 1363–1368 (1988).

23. Aartsma-Rus, A., Van Deutekom, J. C., Fokkema, I. F., Van Ommen, G. B. & Den Dunnen, J. T. Entries in the Leiden Duchenne muscular dystrophy mutation database: An overview of mutation types and paradoxical cases that confirm the reading-frame rule. *Muscle and Nerve* **34**, 135–144 (2006).

24. Blake, D. J., Weir, A., Newey, S. E. & Davies, K. E. Function and genetics of dystrophin and dystrophin-related proteins in muscle. *Physiol. Rev.* **82**, 291–329 (2002).

25. Abbs, S. *et al.* Best Practice Guidelines on molecular diagnostics in Duchenne/Becker muscular dystrophies . *Neuromuscular Disorders* **20**, 422–427 (2010).

26. Clerk, A., Strong, P. N. & Sewry, C. A. Characterisation of dystrophin during development of human skeletal muscle . *Development* **114**, 395 (1992).

27. Muntoni, F., Torelli, S. & Ferlini, A. Dystrophin and mutations: one gene, several proteins, multiple phenotypes. *Lancet Neurology* **2**, 731–740 (2003).

28. Flanigan, K. M. *et al.* Nonsense mutation-associated Becker muscular dystrophy: interplay between exon definition and splicing regulatory elements within the DMD gene. *Hum. Mutat.* **32**, 299–308 (2011).

29. Flanigan, K. M. *et al.* Mutational spectrum of DMD mutations in dystrophinopathy patients: application of modern diagnostic techniques to a large cohort. *Hum. Mutat.* **30**, 1657–1666 (2009).

30. Tuffery-Giraud, S. *et al.* Genotype-phenotype analysis in 2,405 patients with a dystrophinopathy using the UMD-DMD database: a model of nationwide knowledgebase. *Hum. Mutat.* **30**, 934–945 (2009).

31. Gao, Q. & McNally, E. M. The Dystrophin Complex: structure, function and implications for therapy. *Compr. Physiol.* **5**, 1223–1239 (2015).

32. Bushby, K. M. D. & Gardner-Medwin, D. The clinical, genetic and dystrophin characteristics of Becker muscular dystrophy: I. Natural history. *J. Neurol.* **240**, 98–104 (1993).

33. Hoffman, E. P. & Dressman, D. Molecular pathophysiology and targeted therapeutics for muscular dystrophy. *Trends Pharmacol. Sci.* **22**, 465–470 (2001).

34. Campbell, K. P. *et al.* Primary structure of dystrophin-associated glycoproteins linking dystrophin to the extracellular matrix. *Nature* **355**, 696–702 (1992).

35. Yoshida, M. *et al.* Biochemical evidence for association of dystrobrevin with the sarcoglycan-sarcospan complex as a basis for understanding sarcoglycanopathy. *Hum. Mol. Genet.* **9**, 1033–1040 (2000).

36. Miller, G., Wang, E. L., Nassar, K. L., Peter, A. K. & Crosbie, R. H. Structural and functional analysis of the sarcoglycan–sarcospan subcomplex. *Exp. Cell Res.* **313**, 639–

651 (2007).

37. Braun, R., Wang, Z., Mack, D. & Childers, M. Gene therapy for inherited muscle diseases: where genetics meets rehabilitation medicine. *Am. J. Phys. Med. Rehabil.* **93**, 97–107 (2014).

38. Williamson, R. A. *et al.* Dystroglycan is essential for early embryonic development: disruption of Reichert's membrane in Dag1-null mice. *Hum. Mol. Genet.* **6**, 831–841 (1997).

39. Belanto, J. J. *et al.* Microtubule binding distinguishes dystrophin from utrophin. *Proc. Natl. Acad. Sci. U. S. A.* **111**, 5723–5728 (2014).

40. Prins, K. W. *et al.* Dystrophin Is a Microtubule-Associated Protein. *J. Cell Biol.* **186**, 363–369 (2009).

41. Rybakova, I. N., Patel, J. R. & Ervasti, J. M. The Dystrophin Complex Forms a Mechanically Strong Link between the Sarcolemma and Costameric Actin . *The Journal of Cell Biology* **150**, 1209–1214 (2000).

42. Pardo, J. V., Siliciano, J. D. & Craig, S. W. A vinculin-containing cortical lattice in skeletal muscle: Transverse lattice elements ("Costameres") mark sites of attachment between myofibrils and sarcolemma. *Proc. Natl. Acad. Sci. United States Am.* **80**, 1008–1012 (1983).

43. Danowski, B. A., Imanaka-Yoshida, K., Sanger, J. M. & Sanger, J. W. Costameres Are Sites of Force Transmission to the Substratum in Adult Rat Cardiomyocytes . *The Journal of Cell Biology* **118**, 1411–1420 (1992).

44. Goldspink, G. Changes in muscle mass and phenotype and the expression of autocrine and systemic growth factors by muscle in response to stretch and overload. *J. Anat.* **194**, 323–334 (1999).

45. Deconinck, N. Pathophysiology of Duchenne muscular dystrophy: Current hypotheses. *Pediatr. Neruology* **36**, 1–7 (2007).

46. Straub, V., Rafael, J. A., Chamberlain, J. S. & Campbell, K. P. Animal Models for Muscular Dystrophy Show Different Patterns of Sarcolemmal Disruption . *The Journal of Cell Biology* **139**, 375–385 (1997).

47. Lapidos, K., Kakkar, R. & McNally, E. The dystrophin glycoprotein complex: signaling strength and integrity for the sarcolemma. *Circ. Res.* **94**, 1023–1031 (2004).

48. Mizuno, Y. Prevention of myonecrosis in mdx mice: Effect of immobilization by the local tetanus method. *Brain Dev.* **14**, 319–322 (1992).

49. Carafoli, E. & Molinari, M. Calpain: A protease in search of a function? *Biochem. Biophys. Res. Commun.* **247**, 193–203 (1998).

50. Brenman, J. E., Chaos, D. S., Xia, H., Aldape, K. & Bredt, D. S. Nitric oxide synthase complexed with dystrophin and absent from skeletal muscle sarcolemma in Duchenne muscular dystrophy. *Cell* **82**, 743–752 (1995).

51. Crosbie, R. H. *et al.* mdx muscle pathology is independent of nNOS perturbation . *Human molecular genetics* **7**, 823–829 (1998).

52. Huang, P. L., Dawson, T. M., Bredt, D. S., Snyder, S. H. & Fishman, M. C. Targeted disruption of the neuronal nitric oxide synthase gene . *Cell* **75**, 1273–1286 (1993).

53. Thomas, G. D. Functional muscle ischemia in Duchenne and Becker muscular dystrophy. *Frontiers in physiology* **4**, 381 (2013).

54. Wynn, T. A. Cellular and molecular mechanisms of fibrosis. *J. Pathol.* **214**, 199–210 (2008).

55. Rockey, D., Bell, P. & Hill, J. Fibrosis - A Common Pathway to Organ Injury and Failure. *N. Engl. J. Med.* **372**, 1138–1149 (2015).

56. Remuzzi, G. & Bertani, T. Pathophysiology of Progressive Nephropathies . *The New England Journal of Medicine* **339**, 1448–1456 (1998).

57. King Prof, T. E., Pardo Prof, A. & Selman MD, M. Idiopathic pulmonary fibrosis. *Lancet* **378**, 1949–1961 (2011).

58. Bataller, R. & Gao, B. Liver Fibrosis in Alcoholic Liver Disease . *Seminars in Liver Disease* **35**, 146–156 (2015).

59. Kharraz, Y., Guerra, J., Pessina, P., Serrano, A. L. & Muñoz-Cánoves, P. Understanding the process of fibrosis in Duchenne muscular dystrophy. *Biomed Res. Int.* **2014**, 965611–965631 (2014).

60. Chronic Kidney Disease Fact Sheet. *US Department of Health and Human Services, Centers for Disease Control and Prevention* 1–4 (2017).

61. Wynn, T. Fibrotic disease and the T(H)1/T(H)2 paradigm. *Nat. Rev. Immunol.* **4**, 583–594 (2004).

62. Meng, X., Nikolic-Paterson, D. & Lan, H. Inflammatory processes in renal fibrosis. *Nat. Rev. Nephrol.* **10**, 493–503 (2014).

63. Mann, C. J. *et al.* Aberrant repair and fibrosis development in skeletal muscle. *Skelet. Muscle* **1**, 21 (2011).

64. Mantovani, A. *et al.* The chemokine system in diverse forms of macrophage activation and polarization. *Trends Immunol.* **25**, 677–686 (2004).

65. Murakami, S. & Okada, H. Lymphocyte-fibroblast interactions. *Crit. Rev. Oral Biol. Med.* **8**, 40–50 (1997).

66. Donlin, L. T., Jayatilleke, A., Giannopoulou, E. G., Kalliolias, G. D. & Ivashkiv, L. B. Modulation of TNF-induced macrophage polarization by synovial fibroblasts. *J. Immunol.* **193**, 2373–2383 (2014).

67. Maurer, D. H., Hanke, J. H., Mickelson, E., Rich, R. R. & Pollack, M. S. Differential presentation of HLA-DR, DQ, and DP restriction elements by interferon-gamma-treated dermal fibroblasts. *J. Immunol.* **139**, 715 (1987).

68. Arnold, L. *et al.* Inflammatory monocytes recruited after skeletal muscle injury switch into antiinflammatory macrophages to support myogenesis. *J. Exp. Med.* **204**, 1057–1069 (2007).

69. Hinz, B. *et al.* The myofibroblast: One function, multiple origins. *Am. J. Pathol.* **170**, 1807–1816 (2007).

70. Lieber, R. L. & Ward, S. R. Cellular mechanisms of tissue fibrosis. 4. Structural and functional consequences of skeletal muscle fibrosis. *Am. J. Physiol. Physiol.* **305**, C241–C252 (2013).

71. Vidal, B. *et al.* Fibrinogen drives dystrophic muscle fibrosis via a TGFbeta/alternative macrophage activation pathway. *Genes Dev.* **22**, 1747 (2008).

72. Brandan, E. & Gutierrez, J. Role of proteoglycans in the regulation of the skeletal muscle fibrotic response. *FEBS J.* **280**, 4109–4117 (2013).

73. Smith, L. R. & Barton, E. R. Regulation of fibrosis in muscular dystrophy. *Matrix Biol.* **68**–**69**, 602–615 (2018).

74. Flanders, K. C. Smad3 as a mediator of the fibrotic response. *Int. J. Exp. Pathol.* **85**, 47–64 (2004).

75. Leask, A. & Abraham, D. TGF-β signaling and the fibrotic response. *FASEB J.* **18**, 816–

827 (2004).

76. Le Grand, F. & Rudnicki, M. A. Skeletal muscle satellite cells and adult myogenesis. *Curr. Opin. Cell Biol.* **19**, 628–633 (2007).

77. Porter, J. D. *et al.* A chronic inflammatory response dominates the skeletal muscle molecular signature in dystrophin-deficient mdx mice. *Hum. Mol. Genet.* **11**, 263–272 (2002).

78. Bell, C. D. & Conen, P. E. Histopathological changes in Duchenne muscular dystrophy. *J. Neurol. Sci.* **7**, 529–544 (1968).

79. Duance, V. C., Dunn, M., Stephens, H. R., Bailey, A. J. & Dubowitz, V. A role for collagen in the pathogenesis of muscular dystrophy? *Nature* **284**, 470–472 (1980).

80. Desguerre, I. *et al.* Endomysial Fibrosis in Duchenne Muscular Dystrophy: A Marker of Poor Outcome Associated With Macrophage Alternative Activation. *J. Neuropathol. Exp. Neurol.* **68**, 762–773 (2009).

81. Klingler, W., Jurkat-Rott, K., Lehmann-Horn, F. & Schleip, R. The role of fibrosis in Duchenne muscular dystrophy. *Acta Myol.* **31**, 184 (2012).

82. Schabort, E. J., van der Merwe, M., Loos, B., Moore, F. P. & Niesler, C. U. TGF-beta's delay skeletal muscle progenitor cell differentiation in an isoform-independent manner. *Exp. Cell Res.* **315**, 373 (2009).

83. Cencetti, F. *et al.* TGFβ1 evokes myoblast apoptotic response via a novel signaling pathway involving S1P4 transactivation upstream of Rho-kinase-2 activation. *FASEB J.* **27**, 4532–4546 (2013).

84. Cencetti, F., Bernacchioni, C., Nincheri, P., Donati, C. & Bruni, P. Transforming Growth Factor- 1 Induces Transdifferentiation of Myoblasts into Myofibroblasts via Up-Regulation of Sphingosine Kinase-1/S1P3 Axis. *Mol. Biol. Cell* **21**, 1111–1124 (2010).

85. Zhu, J. *et al.* Relationships between transforming growth factor-beta1, myostatin, and decorin: implications for skeletal muscle fibrosis. *J. Biol. Chem.* **282**, 25852 (2007).

86. Yang, X., Yang, S., Wang, C. & Kuang, S. The hypoxia-inducible factors HIF1α and HIF2α are dispensable for embryonic muscle development but essential for postnatal muscle regeneration. *J. Biol. Chem.* **292**, 5981–5991 (2017).

87. Ono, Y., Sensui, H., Sakamoto, Y. & Nagatomi, R. Knockdown of hypoxia-inducible factor-1α by siRNA inhibits C2C12 myoblast differentiation. *J. Cell. Biochem.* **98**, 642–649 (2006).

88. Majmundar, A. J. *et al.* HIF modulation of Wnt signaling regulates skeletal myogenesis in vivo. *Development* **142**, 2405–2412 (2015).

89. Villalta, S. A., Nguyen, H. X., Deng, B., Gotoh, T. & Tidball, J. G. Shifts in macrophage phenotypes and macrophage competition for arginine metabolism affect the severity of muscle pathology in muscular dystrophy . *Human Molecular Genetics* **18**, 482–496

90. Wynn, T. A. & Vannella, K. M. Macrophages in Tissue Repair, Regeneration, and Fibrosis. *Immunity* **44**, 450–462 (2016).

91. Farini, A. *et al.* T and B lymphocyte depletion has a marked effect on the fibrosis of dystrophic skeletal muscles in the scid/mdx mouse. *J. Pathol.* **213**, 229 (2007).

92. Chapman, M. A., Mukund, K., Subramaniam, S., Brenner, D. & Lieber, R. L. Three distinct cell populations express extracellular matrix proteins and increase in number during skeletal muscle fibrosis. *Am. J. Physiol. Physiol.* **312**, C131–C143 (2017).

93. Joe, A. W. B. *et al.* Muscle injury activates resident fibro/adipogenic progenitors that facilitate myogenesis. *Nat. Cell Biol.* **12**, 153–163 (2010).

94. Heredia, J. E. *et al.* Type 2 Innate Signals Stimulate Fibro/Adipogenic Progenitors to Facilitate Muscle Regeneration. *Cell* **153**, 376–388 (2013).

95. Contreras, O., Rebolledo, D. L., Oyarzún, J. E., Olguín, H. C. & Brandan, E. Connective tissue cells expressing fibro/adipogenic progenitor markers increase under chronic damage: relevance in fibroblast-myofibroblast differentiation and skeletal muscle fibrosis. *Cell Tissue Res.* **364**, 647–660 (2016).

96. Lemos, D. R. *et al.* Nilotinib reduces muscle fibrosis in chronic muscle injury by promoting TNF-mediated apoptosis of fibro/adipogenic progenitors. *Nat. Med.* **21**, 786–794 (2015).

97. Micallef, L. *et al.* The myofibroblast, multiple origins for major roles in normal and pathological tissue repair. *Fibrogenesis & tissue repair* **5**, S5–S5 (2012).

98. Mack, M. & Yanagita, M. Origin of myofibroblasts and cellular events triggering fibrosis. *Kidney International* **87**, 297–307 (2015).

99. Buehler, M. J. Nature Designs Tough Collagen: Explaining the Nanostructure of Collagen Fibrils. *Proc. Natl. Acad. Sci. U. S. A.* **103**, 12285–12290 (2006).

100. Smith, L. R., Hammers, D. W., Sweeney, H. L. & Barton, E. R. Increased collagen cross-linking is a signature of dystrophin-deficient muscle: Collagen X-Linking in DMD. *Muscle and Nerve* **54**, 71–78 (2016).

101. Fadic, R. *et al.* Increase in decorin and biglycan in Duchenne Muscular Dystrophy: role of fibroblasts as cell source of these proteoglycans in the disease. *J. Cell. Mol. Med.* **10**, 758–769 (2006).

102. Cynthia Martin, F. *et al.* Fibronectin is a serum biomarker for Duchenne muscular dystrophy. *PROTEOMICS – Clin. Appl.* **8**, 269–278 (2014).

103. Chen, X. & Li, Y. Role of matrix metalloproteinases in skeletal muscle: Migration, differentiation, regeneration and fibrosis. *Cell Adh. Migr.* **3**, 337–341 (2009).

104. Li, H., Mittal, A., Makonchuk, D. Y., Bhatnagar, S. & Kumar, A. Matrix metalloproteinase-9 inhibition ameliorates pathogenesis and improves skeletal muscle regeneration in muscular dystrophy. *Hum. Mol. Genet.* **18**, 2584–2598 (2009).

105. Blakney, A. K., Swartzlander, M. D. & Bryant, S. J. The effects of substrate stiffness on the in vitro activation of macrophages and in vivo host response to poly(ethylene glycol)-based hydrogels. *J. Biomed. Mater. Res.* **100**, 1375 (2012).

106. Friedemann, M. *et al.* Instructing Human Macrophage Polarization by Stiffness and Glycosaminoglycan Functionalization in 3D Collagen Networks. *Adv. Healthc. Mater.* **6**, 1600967-n/a (2017).

107. Engler, A. J. *et al.* Myotubes Differentiate Optimally on Substrates with Tissue-Like Stiffness: Pathological Implications for Soft or Stiff Microenvironments. *J. Cell Biol.* **166**, 877–887 (2004).

108. Patel, K. & Shackel, N. A. Current status of fibrosis markers. *Curr. Opin. Gastroenterol.* **30**, 253–259 (2014).

109. Joyce DO, N. C., Oskarsson MD, B. & Jin MD, PhD, L.-W. Muscle Biopsy Evaluation in Neuromuscular Disorders. *Phys. Med. Rehabil. Clin. N. Am.* **23**, 609–631 (2012).

110. Muntoni, F. Is a muscle biopsy in Duchenne dystrophy really necessary? *Neurology* **57**, 574–575 (2001).

111. Olsen, D. B., Gideon, P., Jeppesen, T. D. & Vissing, J. Leg muscle involvement in facioscapulohumeral muscular dystrophy assessed by MRI. *J. Neurol.* **253**, 1437–1441 (2006).

112. Weber, M.-A., Nagel, A. M., Jurkat-Rott, K. & Lehmann-Horn, F. Sodium (23Na) MRI detects elevated muscular sodium concentration in Duchenne muscular dystrophy. *Neurology* **77**, 2017–2024 (2011).

113. Vappou, J. Magnetic resonance- and ultrasound imaging-based elasticity imaging methods: a review. *Crit. Rev. Biomed. Eng.* **40**, 121–134 (2012).

114. Jaffrin, M. Y. & Morel, H. Body fluid volumes measurements by impedance: A review of bioimpedance spectroscopy (BIS) and bioimpedance analysis (BIA) methods. *Med. Eng. Phys.* **30**, 1257–1269 (2008).

115. Kim, C. T., Findley, T. W. & Reisman, S. R. Bioelectrical impedance changes in regional extracellular fluid alterations. *Electromyogr. Clin. Neurophysiol.* **37**, 297 (1997).

116. Ditroilo, M., Hunter, A. M., Haslam, S. & De Vito, G. The effectiveness of two novel techniques in establishing the mechanical and contractile responses of biceps femoris. *Physiol. Meas.* **32**, 1315–1326 (2011).

117. Moroni, G. *et al.* The value of 18F-FDG PET/CT in the assessment of active idiopathic retroperitoneal fibrosis. *Eur. J. Nucl. Med. Mol. Imaging* **39**, 1635–1642 (2012).

118. Guiraud, S. *et al.* Identification of serum protein biomarkers for utrophin based DMD therapy. *Sci. Rep.* **7**, 43697 (2017).

119. Nadarajah, V. D. *et al.* Serum matrix metalloproteinase-9 (MMP-9) as a biomarker for monitoring disease progression in Duchenne muscular dystrophy (DMD). *Neuromuscul. Disord.* **21**, 569–578 (2011).

120. Ayoglu, B. *et al.* Affinity proteomics within rare diseases: a BIO-NMD study for blood biomarkers of muscular dystrophies. *EMBO Molecular Medicine* **6**, 918–936 (2014).

121. Rodino-Klapac, L. R., Chicoine, L. G., Kaspar, B. K. & Mendell, J. R. Gene therapy for Duchenne muscular dystrophy: Expectations and challenges. *Arch. Neurol.* **64**, 1236–1241 (2007).

122. Zhang, Y. & Duan, D. Novel Mini–Dystrophin gene dual adeno-associated virus vectors restore neuronal nitric oxide synthase expression at the sarcolemma. *Hum. Gene Ther.* **23**, 98–103 (2012).

123. Duan, D. Systemic AAV Micro-dystrophin Gene Therapy for Duchenne Muscular Dystrophy. *Mol. Ther.* **26**, 2337–2356 (2018).

124. Mendell, J. R. & Rodino-Klapac, L. R. Duchenne muscular dystrophy CRISPR/Cas9 treatment. *Cell Res.* **26**, 513–514 (2016).

125. Long, C. *et al.* Postnatal genome editing partially restores dystrophin expression in a mouse model of muscular dystrophy. *Science* **351**, 400–403 (2016).

126. Nelson, C. E. *et al.* In vivo genome editing improves muscle function in a mouse model of Duchenne muscular dystrophy. *Science* **351**, 403–407 (2016).

127. Aartsma-Rus, A. *et al.* Development of Exon Skipping Therapies for Duchenne Muscular Dystrophy: A Critical Review and a Perspective on the Outstanding Issues. *Nucleic Acid Ther.* **27**, 251 (2017).

128. Wilschut, K. J., Ling, V. B. & Bernstein, H. S. Concise Review: Stem Cell Therapy for Muscular Dystrophies. *Stem Cells Transl. Med.* **1**, 833–842 (2012).

129. Boldrin, L., Neal, A., Zammit, P. S., Muntoni, F. & Morgan, J. E. Donor satellite cell engraftment is significantly augmented when the host niche is preserved and endogenous satellite cells are incapacitated. *Stem Cells* **30**, 1971 (2012).

130. Kapsa, R. *et al.* In vivo and in vitro correction of the mdx dystrophin gene nonsense mutation by short-fragment homologous replacement. *Hum. Gene Ther.* **12**, 629–642

(2001).

131. Cossu, G. & Mavilio, F. Myogenic stem cells for the therapy of primary myopathies: Wishful thinking or therapeutic perspective? *J. Clin. Invest.* **105**, 1669–1674 (2000).

132. Bertoni, C. & Rando, T. A. Dystrophin gene repair in mdx muscle precursor cells in vitro and in vivo mediated by RNA-DNA chimeric oligonucleotides. *Human gene therapy* **13**, 707–718 (2002).

133. Wong, S. H. A. *et al.* Evaluation of Sca-1 and c-Kit as selective markers for muscle remodelling by nonhemopoietic bone marrow cells. *Stem cells* **25**, 1364–1374 (2007).

134. Morales, M. G. *et al.* Reducing CTGF/CCN2 slows down mdx muscle dystrophy and improves cell therapy. *Human Molecular Genetics* **22**, 4938–4951 (2013).

135. De Luca, A. Pre-clinical drug tests in the mdx mouse as a model of dystrophinopathies: an overview. *Acta Myol.* **31**, 40 (2012).

136. Simões e Silva, A. C., Silveira, K. D., Ferreira, A. J. & Teixeira, M. M. ACE2, angiotensin-(1-7) and Mas receptor axis in inflammation and fibrosis. *Br. J. Pharmacol.* **169**, 477–492 (2013).

137. Israili, Z. H. Clinical pharmacokinetics of angiotensin II (AT1) receptor blockers in hypertension. *J. Hum. Hypertens.* **14**, S73–S86 (2000).

138. Tyralla, K. *et al.* High-dose enalapril treatment reverses myocardial fibrosis in experimental uremic cardiomyopathy. *PLoS One* **6**, e15287 (2011).

139. Brilla, C. G., Funck, R. C. & Rupp, H. Lisinopril-mediated regression of myocardial fibrosis in patients with hypertensive heart disease. *Circulation* **102**, 1388–1393 (2000).

140. Adamo, C. M. *et al.* Sildenafil reverses cardiac dysfunction in the mdx mouse model of Duchenne muscular dystrophy. *Proc. Natl. Acad. Sci. U. S. A.* **107**, 19079–19083 (2010).

141. Buyse, G. M. *et al.* Efficacy of idebenone on respiratory function in patients with Duchenne muscular dystrophy not using glucocorticoids (DELOS): a double-blind randomised placebo-controlled phase 3 trial. *Lancet* **385**, 1748–1757 (2015).

142. Hori, Y. S. *et al.* Resveratrol ameliorates muscular pathology in the dystrophic mdx mouse, a model for Duchenne muscular dystrophy. *J. Pharmacol. Exp. Ther.* **338**, 784–794 (2011).

143. Lehmann-Horn, F. *et al.* Rationale for treating oedema in Duchenne muscular dystrophy with eplerenone. *Acta Myol.* **31**, 31 (2012).

144. Hastie, N. D. Wilms' tumour 1 (WT1) in development, homeostasis and disease. *Development* **144**, 2862–2872 (2017).

145. Thibaud, E. *et al.* Donor splice-site mutations in WT1 are responsible for Frasier syndrome. *Nat. Genet.* **17**, 467–470 (1997).

146. Pelletier, J. *et al.* Germline mutations in the Wilms' tumor suppressor gene are associated with abnormal urogenital development in Denys-Drash syndrome. *Cell* **67**, 437–447 (1991).

147. Scharnhorst, V., Van der Eb, A. J. & Jochemsen, A. G. WT1 proteins: Functions in growth and differentiation. *Gene* **273**, 141–161 (2001).

148. Wagner, K., Wagner, N. & Schedl, A. The complex life of WT1. *J. Cell Sci.* **116**, 1653–1658 (2003).

149. Sharma, P. M., Bowman, M., Madden, S. L., Rauscher, F. J. & Sukumar, S. RNA editing in the Wilms' tumor susceptibility gene, WT1. *Genes Dev.* **8**, 720–731 (1994).

150. Moore, A. W., McInnes, L., Kreidberg, J., Hastie, N. D. & Schedl, A. YAC complementation shows a requirement for Wt1 in the development of epicardium, adrenal

gland and throughout nephrogenesis. *Development* **126**, 1845 (1999).

151. Herzer, U., Crocoll, A., Barton, D., Howells, N. & Englert, C. The Wilms tumor suppressor gene wt1 is required for development of the spleen. *Curr. Biol.* **9**, 837,S1-840,S1 (1999).

152. Kreidberg, J. A. *et al.* WT-1 is required for early kidney development. *Cell* **74**, 679–691 (1993).

153. Miyamoto, Y., Taniguchi, H., Hamel, F., Silversides, D. W. & Viger, R. S. A GATA4/WT1 cooperation regulates transcription of genes required for mammalian sex determination and differentiation. *BMC Mol. Biol.* **9**, 44 (2008).

154. Wilhelm, D. & Englert, C. The Wilms tumor suppressor WT1 regulates early gonad development by activation of Sf1. *Genes Dev.* **16**, 1839–1851 (2002).

155. Motamedi, F. J. *et al.* WT1 controls antagonistic FGF and BMP-pSMAD pathways in early renal progenitors. *Nat. Commun.* **5**, 4444 (2014).

156. Hartwig, S. *et al.* Genomic characterization of Wilms' tumor suppressor 1 targets in nephron progenitor cells during kidney development. *Development* **137**, 1189–1203 (2010).

157. Martinez-Estrada, O. M. *et al.* Wt1 is required for cardiovascular progenitor cell formation through transcriptional control of snail and E-cadherin. *Nat. Genet.* **42**, 89–93 (2010).

158. Cano, E., Carmona, R. & Muñoz-Chápuli, R. Wt1-expressing progenitors contribute to multiple tissues in the developing lung. *Am. J. Physiol. Cell. Mol. Physiol.* **305**, L322–L332 (2013).

159. Chau, Y.-Y. *et al.* Acute multiple organ failure in adult mice deleted for the developmental regulator Wt1. *PLoS Genet.* **7**, e1002404 (2011).

160. Bandiera, R. *et al.* WT1 Maintains Adrenal-Gonadal Primordium Identity and Marks a Population of AGP-like Progenitors within the Adrenal Gland. *Dev. Cell* **27**, 5–18 (2013).

161. Palmer, R. E. *et al.* WT1 regulates the expression of the major glomerular podocyte membrane protein podocalyxin. *Curr. Biol.* **11**, 1805–1809 (2001).

162. Wagner, N., Wagner, K.-D., Xing, Y., Scholz, H. & Schedl, A. The major podocyte protein nephrin is transcriptionally activated by the Wilms' tumor suppressor WT1. *J. Am. Soc. Nephrol.* **15**, 3044–3051 (2004).

163. Smart, N. *et al.* De novo cardiomyocytes from within the activated adult heart after injury. *Nature* **474**, 640–644 (2011).

164. Wagner, K.-D. *et al.* Oxygen-regulated expression of the Wilms' tumor suppressor Wt1 involves hypoxia-inducible factor-1 (HIF-1). *FASEB Journal* **17**, 1364–1366 (2003).

165. Caricasole, A. *et al.* RNA Binding by the Wilms Tumor Suppressor Zinc Finger Proteins. *Proc. Natl. Acad. Sci. U. S. A.* **93**, 7562–7566 (1996).

166. Richard, D. J., Schumacher, V., Royer-Pokora, B. & Roberts, S. G. E. Par4 is a coactivator for a splice isoform-specific transcriptional activation domain in WT1. *Genes Dev.* **15**, 328–339 (2001).

167. Silberstein, G. B., Horn, K. Van, Strickland, P., Roberts, C. T. & Daniel, C. W. Altered Expression of the WT1 Wilms Tumor Suppressor Gene in Human Breast Cancer. *Proc. Natl. Acad. Sci. U. S. A.* **94**, 8132–8137 (1997).

168. Natoli, T. A. *et al.* A mutant form of the wilms' tumor suppressor gene WT1 observed in denys-drash syndrome interferes with glomerular capillary development. *J. Am. Soc. Nephrol.* **13**, 2058–2067 (2002).

169. Davies, R. C. *et al.* WT1 interacts with the splicing factor U2AF65 in an isoform-

dependent manner and can be incorporated into spliceosomes. *Genes Dev.* **12**, 3217–3225 (1998).

170. Maheswaran, S., Englert, C., Bennett, P., Heinrich, G. & Haber, D. A. The WT1 gene product stabilizes p53 and inhibits p53-mediated apoptosis. *Genes Dev.* **9**, 2143–2156 (1995).

171. Maheswaran, S. *et al.* Physical and Functional Interaction Between WT1 and p53 Proteins . *Proceedings of the National Academy of Sciences of the United States of America* **90**, 5100–5104 (1993).

172. Rupprecht, H. D., Drummond, I. A., Madden, S. L., Rauscher, F. J. & Sukhatme, V. P. The wilms' tumor suppressor gene WT1 is negatively autoregulated. *J. Biol. Chem.* **269**, 6198 (1994).

173. Drummond, L. *et al.* Repression of the Insulin-Like Growth Factor II Gene by the Wilms Tumor Suppressor WT1. *Science (80-.).* **257**, 674–678 (1992).

174. Duarte, A., Caricasole, A., Graham, C. F. & Ward, A. Wilms' tumour-suppressor protein isoforms have opposite effects on Igf2 expression in primary embryonic cells, independently of p53 genotype. *Br. J. Cancer* **77**, 253–259 (1998).

175. Ryan, G., Steele-Perkins, V., Morris, J. F., Rauscher, F. J. & Dressler, G. R. Repression of Pax-2 by WT1 during normal kidney development. *Development* **121**, 867–75 (1995).

176. Wang, Z. Y., Madden, S. L., Deuel, T. F. & F J Rauscher, 3rd. The Wilms' tumor gene product, WT1, represses transcription of the platelet-derived growth factor A-chain gene. *Journal of Biological Chemistry* **267**, 21999 (1992).

177. Parenti, R. *et al.* Immunohistochemical expression of wilms' tumor protein (WT1) in developing human epithelial and mesenchymal tissues. *Acta Histochem.* **115**, 70–75 (2013).

178. Niksic, M., Slight, J., Sanford, J. R., Caceres, J. F. & Hastie, N. D. The Wilms' tumour protein (WT1) shuttles between nucleus and cytoplasm and is present in functional polysomes . *Human molecular genetics* **13**, 463–471

179. Sontake, V. *et al.* Fibrocytes Regulate Wilms Tumor 1-Positive Cell Accumulation in Severe Fibrotic Lung Disease. *J. Immunol.* **195**, 3978–3991 (2015).

180. Sontake, V. *et al.* Wilms' tumor 1 drives fibroproliferation and myofibroblast transformation in severe fibrotic lung disease. *JCI Insight* **3**, (2018).

181. Karki, S. *et al.* Wilms' tumor 1 (Wt1) regulates pleural mesothelial cell plasticity and transition into myofibroblasts in idiopathic pulmonary fibrosis. *FASEB J.* **28**, 1122–1131 (2014).

182. Crawford, J., Raykha, C., Charles, D., Gan, B. & O'Gorman, D. WT1 expression is increased in primary fibroblasts derived from Dupuytren's disease tissues. *J. Cell Commun. Signal.* **9**, 347–352 (2015).

183. McGreevy, J. W., Hakim, C. H., McIntosh, M. A. & Duan, D. Animal models of Duchenne muscular dystrophy: from basic mechanisms to gene therapy. *Dis. Model. Mech.* **8**, 195–213 (2015).

184. Sicinski, P. *et al.* The Molecular Basis of Muscular Dystrophy in the mdx Mouse: A Point Mutation . *Science* **244**, 1578–1580 (1989).

185. Bulfield, G., Siller, W. G., Wight, P. A. L. & Moore, K. J. X chromosome-linked muscular dystrophy (mdx) in the mouse. *Proc. Natl. Acad. Sci. U. S. A.* **81**, 1189–1192 (1984).

186. Zhou, L. *et al.* Haploinsufficiency of utrophin gene worsens skeletal muscle inflammation

and fibrosis in mdx mice. *J. Neurol. Sci.* **264**, 106–111 (2007).

187. Huang, P. *et al.* Impaired Respiratory Function in mdx and mdx/utrn+/- Mice. *Muscle and Nerve* **43**, 263–267 (2011).

188. Grady, R. M. *et al.* Skeletal and Cardiac Myopathies in Mice Lacking Utrophin and Dystrophin: A Model for Duchenne Muscular Dystrophy. *Cell* **90**, 729–738 (1997).

189. McDonald, A. A., Hebert, S. L., Kunz, M. D., Ralles, S. J. & McLoon, L. K. Disease course in mdx:utrophin+/− mice: comparison of three mouse models of Duchenne muscular dystrophy. *Physiol. Rep.* **3**, e12391 (2015).

190. Quinlan, J. G. *et al.* Evolution of the mdx mouse cardiomyopathy: Physiological and morphological findings. *Neuromuscul. Disord.* **14**, 491–496 (2004).

191. Matsumura, K. & Campbell, K. P. Dystrophin-glycoprotein complex: Its role in the molecular pathogenesis of muscular dystrophies. *Muscle Nerve* **17**, 2–15 (1994).

192. Fisher, R. *et al.* Amelioration of the dystrophic phenotype of mdx mice using a truncated utrophin transgene. *Nature* **384**, 349–353 (1996).

193. Campbell, K. P., Ervasti, J. M., Ohlendieck, K., Matsumura, K. & Kahl, S. D. Association of dystrophin-related protein with dystrophin-associated proteins in mdx mouse muscle. *Nature* **360**, 588–591 (1992).

194. Gutpell, K. M., Hrinivich, W. T. & Hoffman, L. M. Skeletal muscle fibrosis in the mdx/utrn+/- mouse validates its suitability as a murine model of Duchenne muscular dystrophy. *PLoS One* **10**, (2015).

195. van Putten, M. *et al.* Comparison of skeletal muscle pathology and motor function of dystrophin and utrophin deficient mouse strains. *Neuromuscular Disorders* **22**, 406–417

196. Schindelin, J. *et al.* Fiji: An open-source platform for biological-image analysis. *Nat. Methods* **9**, 676–682 (2012).

197. Rueden, C. T. *et al.* ImageJ2: ImageJ for the next generation of scientific image data. *BMC Bioinformatics* **18**, 529–26 (2017).

198. Bankhead, P. *et al.* QuPath: Open source software for digital pathology image analysis. *Sci. Rep.* **7**, 16878–7 (2017).

199. Kramarzova, K. *et al.* Real-time PCR quantification of major wilms' tumor gene 1 (WT1) isoforms in acute myeloid leukemia, their characteristic expression patterns and possible functional consequences. *Leukemia* **26**, 2086–2095 (2012).

200. Magro, G. *et al.* Oncofetal expression of wilms' tumor 1 (WT1) protein in human fetal, adult and neoplastic skeletal muscle tissues. *Acta Histochem.* **117**, 492–504 (2015).

201. Ramani, P. & Cowell, J. K. The expression pattern of Wilms' tumour gene (WT1) product in normal tissues and paediatric renal tumours. *J. Pathol.* **179**, 162–168 (1996).

202. Murphy, A. P. *et al.* Noninvasive quantification of fibrosis in skeletal and cardiac muscle in mdx mice using EP3533 enhanced magnetic resonance imaging. *Magn. Reson. Med.* (2018).

203. Verhaart, I. E. C. *et al.* Assessment of cardiac function in three mouse dystrophinopathies by magnetic resonance imaging. *Neuromuscular Disorders* **22**, 418–426 (2011).

204. Bondoc, A. B. *et al.* Application of 3-D echocardiography and gated micro-computed tomography to assess cardiomyopathy in a mouse model of Duchenne muscular dystrophy. *Ultrasound Med. Biol.* **40**, 2857–2867 (2014).

205. Wagner, K.-D. *et al.* The Wilms' tumor suppressor Wt1 is expressed in the coronary vasculature after myocardial infarction. *FASEB J.* **16**, 1117–1119 (2002).

206. Yang, W. & Hu, P. Skeletal muscle regeneration is modulated by inflammation. *Journal*

of Orthopaedic Translation **13**, 25–32 (2018).

207. Marcet-Palacios, M., Davoine, F., Adamko, D. J., Moqbel, R. & Befus, A. D. Human lymphocytes express the transcriptional regulator, Wilms tumor 1: The role of WT1 in mediating nitric oxide-dependent repression of lymphocyte proliferation. *Biochemical and Biophysical Research Communications* **363**, 283–287 (2007).

208. Scharnhorst, V., Dekker, P., Eb, A. J. van der & Jochemsen, A. G. Internal Translation Initiation Generates Novel WT1 Protein Isoforms with Distinct Biological Properties. *J. Biol. Chem.* **274**, 23456–23462 (1999).

209. Dohi, S. *et al.* WT1 peptide vaccine stabilized intractable ovarian cancer patient for one year: A case report. *Anticancer Res.* **31**, 2441–2446 (2011).

210. Dubrovsky, L. *et al.* A TCR-mimic antibody to WT1 bypasses tyrosine kinase inhibitor resistance in human BCR-ABL(+) leukemias. *Blood* **123**, 3296–3304 (2014).

APPENDICIES

Appendix A: Approval of Animal Protocol

Western

AUP Number: 2017-038
PI Name: Hoffman, Lisa M
AUP Title: Hoffman Breeding Protocol
Approval Date: 05/30/2017
Official Notice of Animal Use Subcommittee (AUS) Approval: Your new Animal Use Protocol (AUP) entitled "Hoffman Breeding Protocol" has been APPROVED by the Animal Use Subcommittee of the University Council on Animal Care. This approval, although valid for four years, and is subject to annual Protocol Renewal.2017-038::1

1. This AUP number must be indicated when ordering animals for this project.
2. Animals for other projects may not be ordered under this AUP number.
3. Purchases of animals other than through this system must be cleared through the ACVS office. Health certificates will be required.

The holder of this Animal Use Protocol is responsible to ensure that all associated safety components (biosafety, radiation safety, general laboratory safety) comply with institutional safety standards and have received all necessary approvals. Please consult directly with your institutional safety officers.
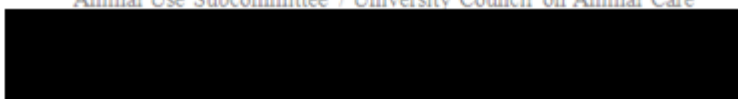Submitted by: Copeman, Laura
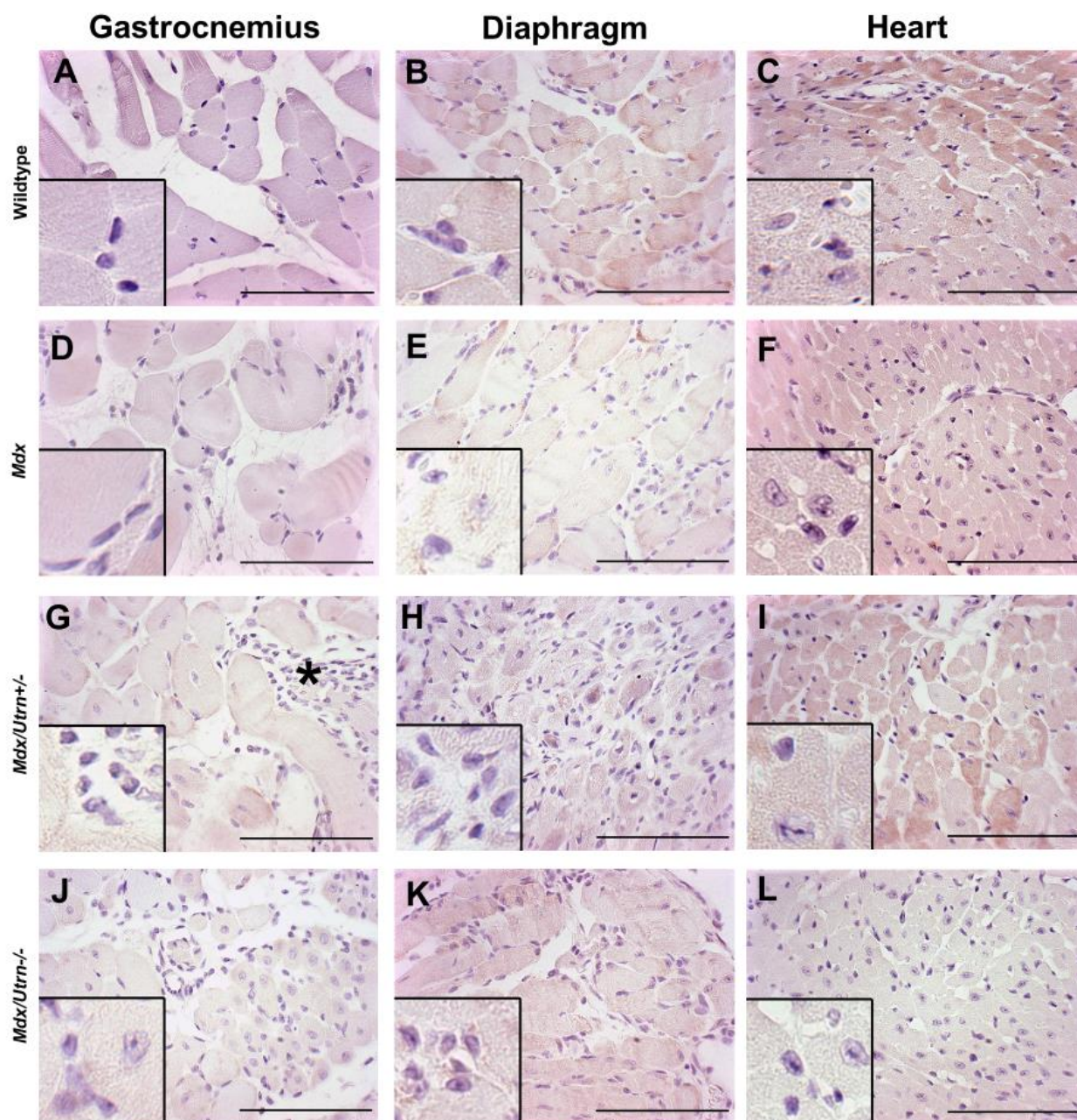on behalf of the Animal Use Subcommittee
University Council on Animal Care
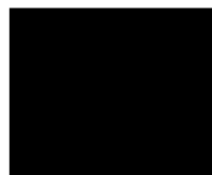
The University *of* Western Ontario
Animal Use Subcommittee / University Council on Animal Care

Appendix B: Representative images of negative control muscle in 4-5 week old wildtype, *Mdx*, *Mdx/Utrn+/-*, and *Mdx/Utrn-/-* mice.

Gastrocnemius, diaphragm, and heart muscle was acquired from 4-5 week old mice of several genotypes, and immunohistochemically stained without an antibody. Representative images of IHC analysis of muscle are shown for wildtype (A-C), *Mdx* (D-F), *Mdx/Utrn+/-* (G-I), and *Mdx/Utrn-/-* (J-L) mice. In the bottom left corner, a section of magnified nuclei are provided for examination. Asterisks indicate large example regions of cells resembling inflammatory infiltrate (scale bar = 100μm).

Appendix C: Representative images of negative control muscle in 8-10 week old wildtype, *Mdx*, *Mdx/Utrn+/-*, and *Mdx/Utrn-/-* mice.
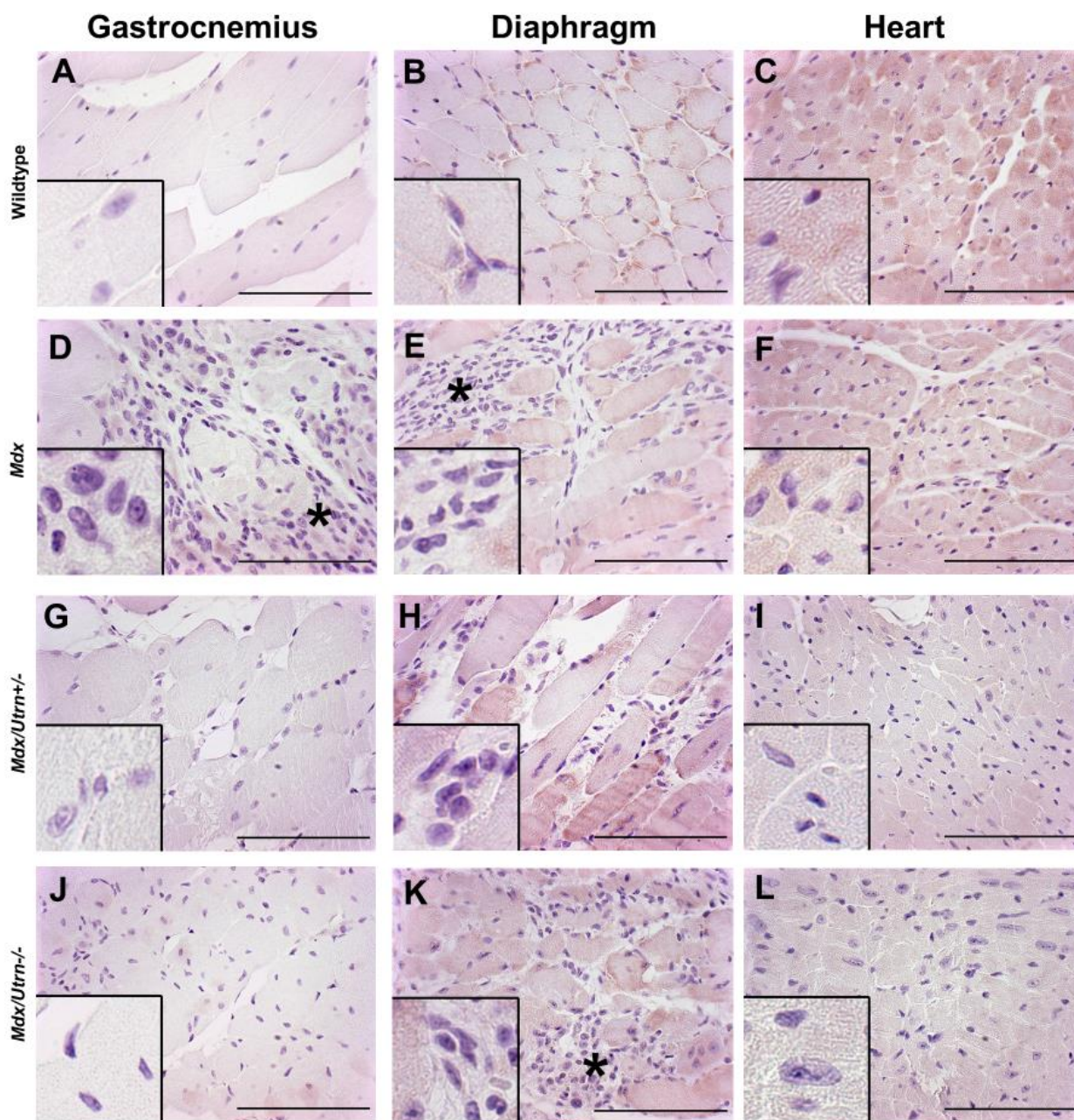
Gastrocnemius, diaphragm, and heart muscle was acquired from 8-10 week old mice of several genotypes, and immunohistochemically stained without an antibody. Representative images of IHC analysis of muscle are shown for wildtype (A-C), *Mdx* (D-F), *Mdx/Utrn+/-* (G-I), and *Mdx/Utrn-/-* (J-L) mice. In the bottom left corner, a section of magnified nuclei are provided for examination. Asterisks indicate large example regions of cells resembling inflammatory infiltrate (scale bar = 100μm).

Appendix D: Representative images of negative control muscle in 10-14 month old wildtype, *Mdx*, and *Mdx/Utrn+/-* mice.
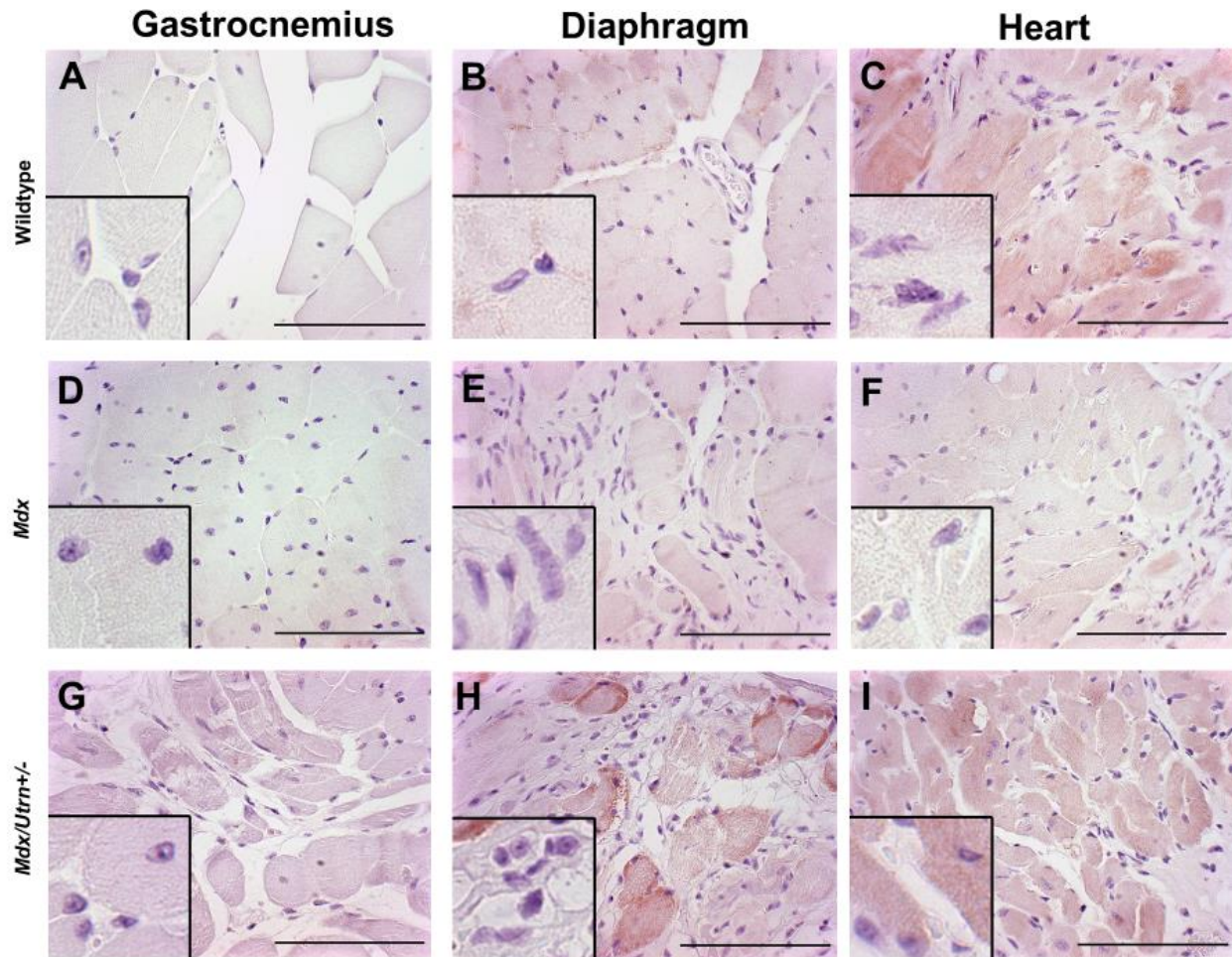

Gastrocnemius, diaphragm, and heart muscle was acquired from 10-14 month old mice of several genotypes, and immunohistochemically stained without an antibody. Representative images of IHC analysis of muscle are shown for wildtype (A-C), *Mdx* (D-F), and *Mdx/Utrn+/-* (G-I) mice. In the bottom left corner, a section of magnified nuclei are provided for examination. Asterisks indicate large example regions of cells resembling inflammatory infiltrate (scale bar = 100μm).

Appendix E: Example division of image into muscle cytoplasm and non-muscle tissue components.
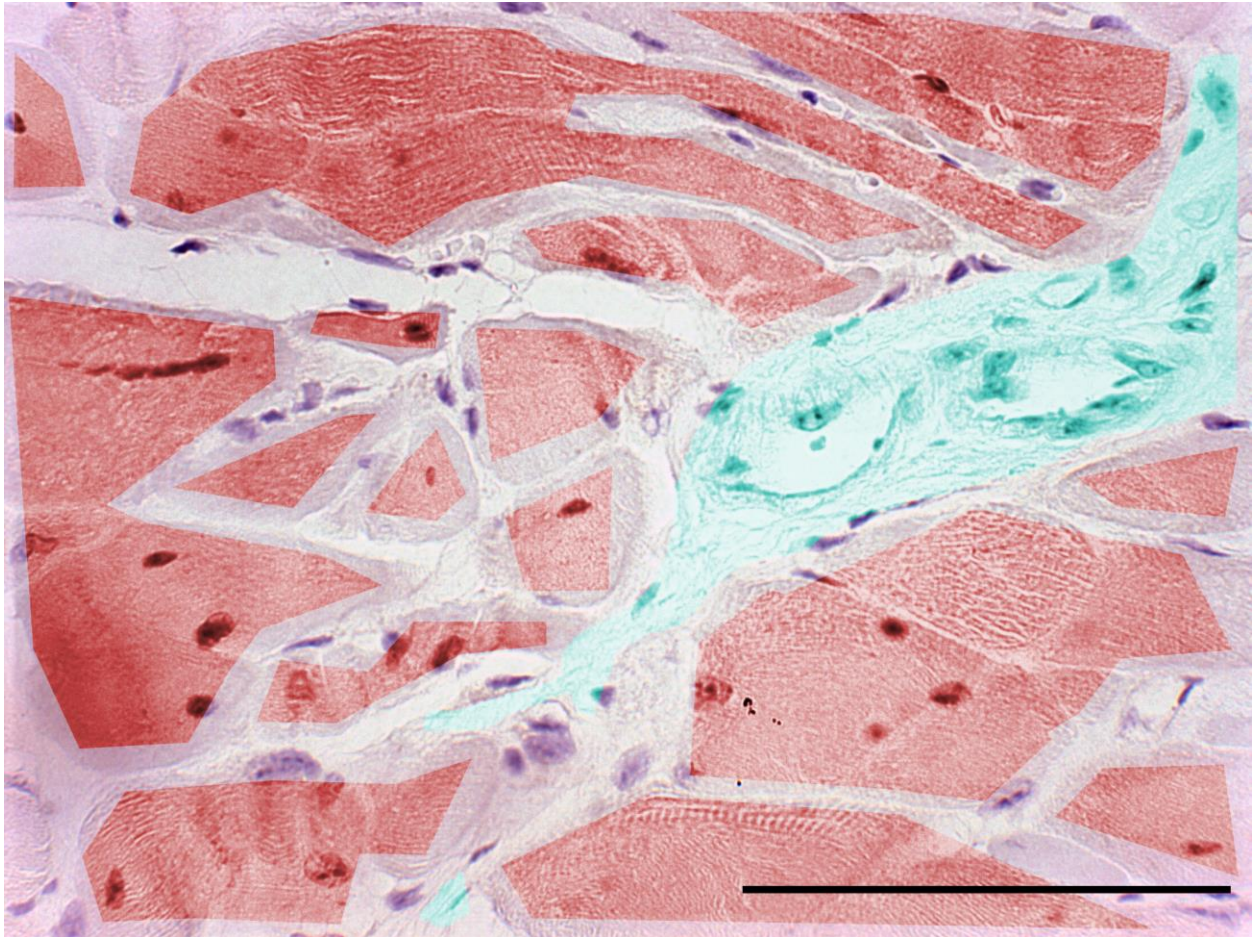
An example section of 10-14 month old *Mdx/Utrn+/-* gastrocnemius evaluated immunohistochemically for Wt1, with nuclei counterstained using hematoxylin. The region of muscle cytoplasm has been identified with red coloring, while the region of non-muscle tissue has been identified with teal coloring. In the case where the border of the image is present, a prominent edge is present between tissue structures, or where there is uncertainty over whether the region is muscle or non-muscle tissue, no coloring has been conducted (scale bar = 100μm).

Appendix F: Representative images of immunohistochemically stained, hematoxylin negative, muscle in 4-5 week old wildtype, *Mdx*, *Mdx/Utrn+/-*, and *Mdx/Utrn-/-* mice.


Gastrocnemius, diaphragm, and heart muscle was acquired from 4-5 week old mice of several genotypes, and immunohistochemically stained for Wt1, in the absence of hematoxylin. Representative images of Wt1 IHC analysis of muscle are shown for wildtype (A-C), *Mdx* (D-F), *Mdx/Utrn+/-* (G-I), and *Mdx/Utrn-/-* (J-L) mice. In the bottom left corner, a section of magnified nuclei are provided for examination. Asterisks indicate large example regions of cells resembling inflammatory infiltrate (scale bar = 100μm).

Appendix G: Representative images of immunohistochemically stained, hematoxylin negative, muscle in 8-10 week old wildtype, *Mdx*, *Mdx/Utrn+/-*, and *Mdx/Utrn-/-* mice.
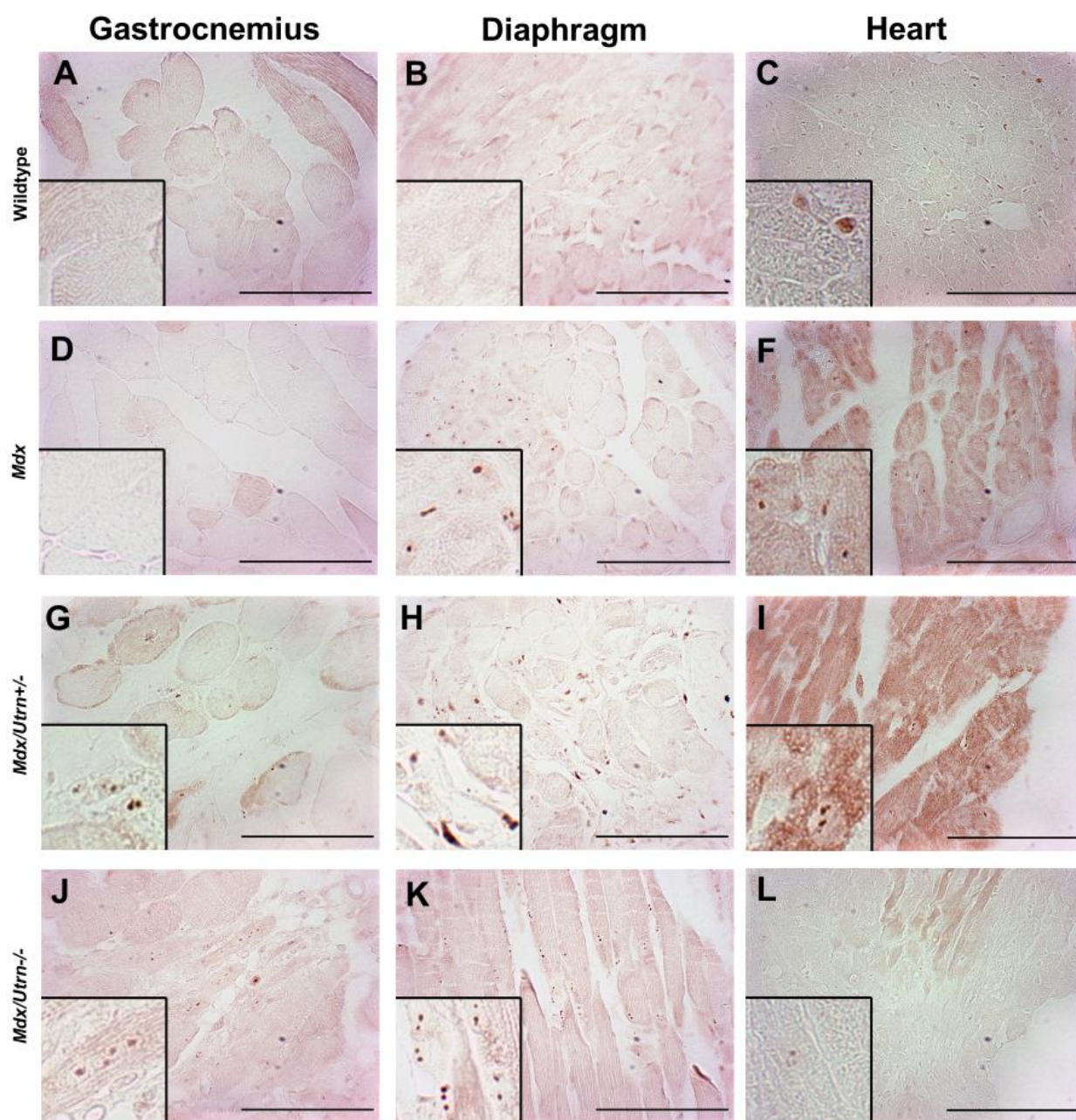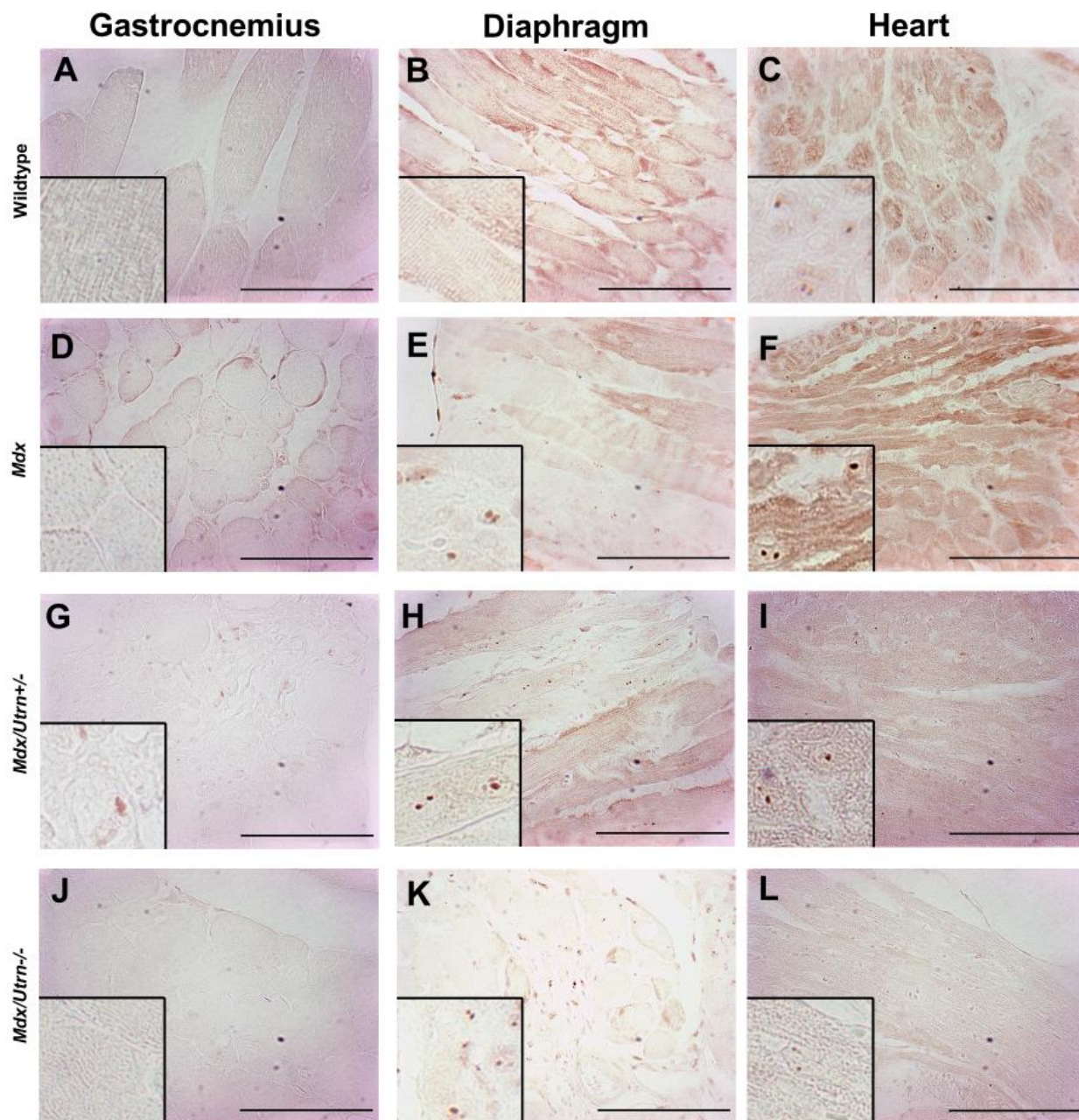

Gastrocnemius, diaphragm, and heart muscle was acquired from 8-10 week old mice of several genotypes, and immunohistochemically stained for Wt1, in the absence of hematoxylin. Representative images of Wt1 IHC analysis of muscle are shown for wildtype (A-C), *Mdx* (D-F), *Mdx/Utrn+/-* (G-I), and *Mdx/Utrn-/-* (J-L) mice. In the bottom left corner, a section of magnified nuclei are provided for examination. Asterisks indicate large example regions of cells resembling inflammatory infiltrate (scale bar = 100μm).

Appendix H: Representative images of immunohistochemically stained, hematoxylin negative, muscle in 10-14 month old wildtype, *Mdx*, and *Mdx/Utrn+/-* mice.
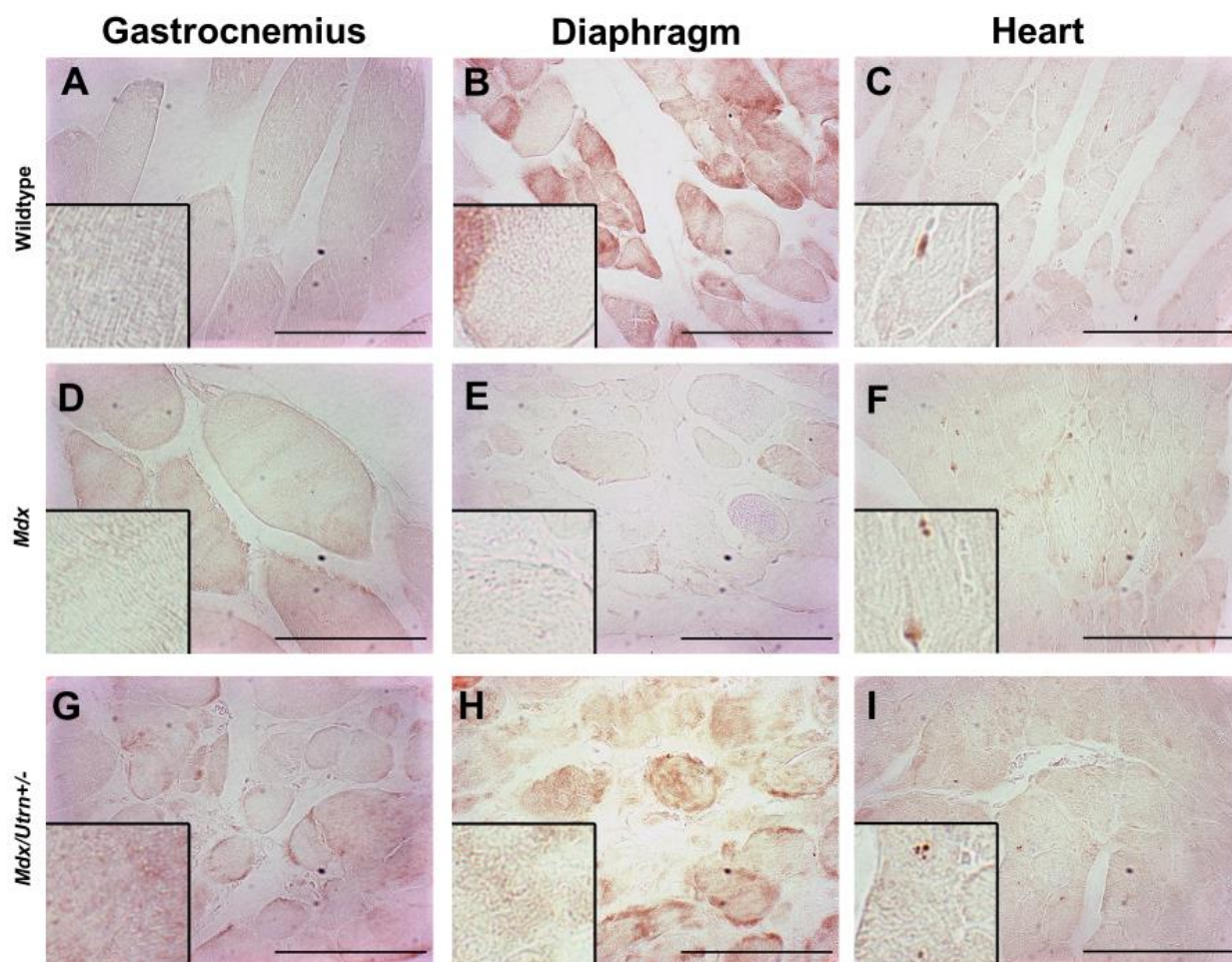
Gastrocnemius, diaphragm, and heart muscle was acquired from 10-14 month old mice of several genotypes, and immunohistochemically stained for Wt1, in the absence of hematoxylin. Representative images of Wt1 IHC analysis of muscle are shown for wildtype (A-C), *Mdx* (D-F), and *Mdx/Utrn+/-* (G-I) mice. In the bottom left corner, a section of magnified nuclei are provided for examination. Asterisks indicate large example regions of cells resembling inflammatory infiltrate (scale bar = 100µm).

Appendix I: Primer efficiency validation for total Wt1 and Wt1 isoform controls.
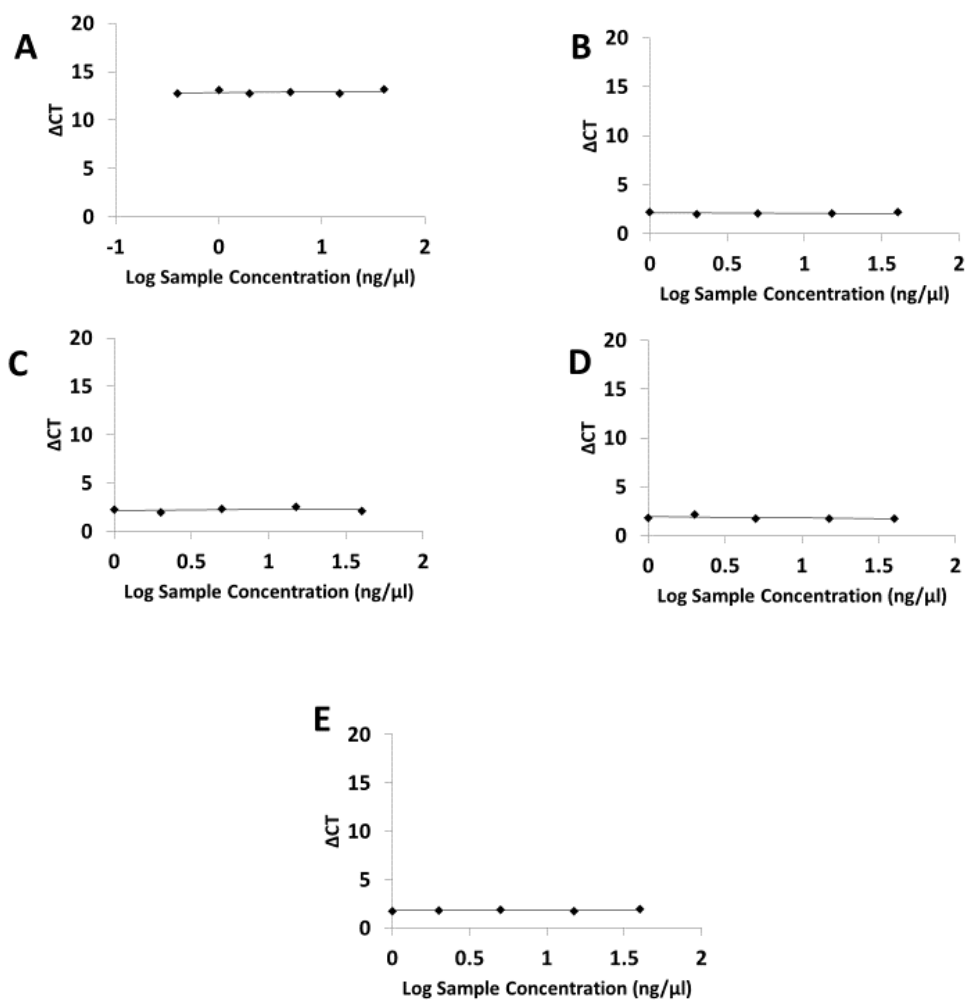
Graphs depicting primer validation for qPCR experiments, where the absolute value of the slope of the graph is ≤0.1. For whole *Wt1*, validation was conducted against the geometric mean of *Gapdh*, *Actb*, and *Ppia* (A). For each major *Wt1* isoform, A (B), B (C), C (D), and D (E) validation was conducted against the sum of all isoforms together.

Appendix J: Two-Way ANOVA with Tukey's Multiple Comparisons Tests for all groups

A

Nuclear Positivity Gastrocnemius

Time x Genotype	Time	Genotype
0.081	0.061	<0.001***

	4-5 Week vs. 8-10 Week	4-5 Week vs. 10-14 Month	8-10 Week vs. 10-14 Month
Wildtype	0.911	0.320	0.541
Mdx	0.976	0.936	0.999
Mdx/Utrn+/-	0.006**	0.031*	0.726

Muscle Cytoplasm Positivity Gastrocnemius

Time x Genotype	Time	Genotype
0.585	0.099	0.841

	4-5 Week vs. 8-10 Week	4-5 Week vs. 10-14 Month	8-10 Week vs. 10-14 Month
Wildtype	0.301	0.443	0.956
Mdx	0.624	0.785	0.269
Mdx/Utrn+/-	0.714	0.637	0.230

Collagen Content Gastrocnemius

Time x Genotype	Time	Genotype
<0.001***	<0.001***	<0.001***

	4-5 Week vs. 8-10 Week	4-5 Week vs. 10-14 Month	8-10 Week vs. 10-14 Month
Wildtype	0.986	0.762	0.850
Mdx	0.606	0.933	0.816
Mdx/Utrn+/-	0.055	<0.001***	<0.001***

Non-muscle Positivity Gastrocnemius

Time x Genotype	Time	Genotype
0.341	0.537	0.758

	4-5 Week vs. 8-10 Week	4-5 Week vs. 10-14 Month	8-10 Week vs. 10-14 Month
Wildtype	0.298	0.223	0.981
Mdx	0.981	0.405	0.509
Mdx/Utrn+/-	0.814	0.808	>0.999

B

Nuclear Positivity Diaphragm

Time x Genotype	Time	Genotype
<0.001***	<0.001***	<0.001***

	4-5 Week vs. 8-10 Week	4-5 Week vs. 10-14 Month	8-10 Week vs. 10-14 Month
Wildtype	0.999	0.282	0.301
Mdx	0.048*	<0.001***	<0.001***
Mdx/Utrn+/-	0.911	0.022*	0.051

Muscle Cytoplasm Positivity Diaphragm

Time x Genotype	Time	Genotype
0.229	0.285	0.109

	4-5 Week vs. 8-10 Week	4-5 Week vs. 10-14 Month	8-10 Week vs. 10-14 Month
Wildtype	0.979	0.999	0.970
Mdx	0.103	0.030*	0.808
Mdx/Utrn+/-	0.914	>0.999	0.914

Collagen Content Diaphragm

Time x Genotype	Time	Genotype
<0.001***	<0.001***	<0.001***

	4-5 Week vs. 8-10 Week	4-5 Week vs. 10-14 Month	8-10 Week vs. 10-14 Month
Wildtype	>0.999	0.822	0.826
Mdx	0.983	<0.001***	<0.001***
Mdx/Utrn+/-	0.215	<0.001***	<0.001***

Non-muscle Positivity Diaphragm

Time x Genotype	Time	Genotype
0.517	0.823	0.002**

	4-5 Week vs. 8-10 Week	4-5 Week vs. 10-14 Month	8-10 Week vs. 10-14 Month
Wildtype	0.915	0.388	0.215
Mdx	>0.999	0.991	0.993
Mdx/Utrn+/-	0.994	0.887	0.834

C

Nuclear Positivity Heart

Time x Genotype	Time	Genotype
0.386	0.607	0.479

	4-5 Week vs. 8-10 Week	4-5 Week vs. 10-14 Month	8-10 Week vs. 10-14 Month
Wildtype	0.769	0.584	0.233
Mdx	0.575	0.983	0.471
Mdx/Utrn+/-	0.939	0.640	0.835

Muscle Cytoplasm Positivity Heart

Time x Genotype	Time	Genotype
0.805	0.817*	0.022*

	4-5 Week vs. 8-10 Week	4-5 Week vs. 10-14 Month	8-10 Week vs. 10-14 Month
Wildtype	>0.999	0.890	0.890
Mdx	0.989	0.985	0.950
Mdx/Utrn+/-	0.605	0.464	0.969

Collagen Content Heart

Time x Genotype	Time	Genotype
0.117	<0.001***	0.017*

	4-5 Week vs. 8-10 Week	4-5 Week vs. 10-14 Month	8-10 Week vs. 10-14 Month
Wildtype	0.969	0.561	0.423
Mdx	0.850	0.002**	<0.001***
Mdx/Utrn+/-	0.995	0.341	0.390

Non-muscle Positivity Heart

Time x Genotype	Time	Genotype
0.312	0.184	0.165

	4-5 Week vs. 8-10 Week	4-5 Week vs. 10-14 Month	8-10 Week vs. 10-14 Month
Wildtype	0.044*	0.993	0.055
Mdx	0.974	0.997	0.989
Mdx/Utrn+/-	0.970	0.978	0.999

P-values for two-way ANOVA on gastrocnemius (A), diaphragm (B), and heart (C), with Tukey's multiple comparisons test, conducted for collagen content, proportion of Wt1 immunoreactive nuclei, muscle cytoplasm immunoreactivity, and non-muscle immunoreactivity, for age point. Asterisks indicate significant differences between groups (* < 0.050, ** < 0.010, *** < 0.001). Three biological and three technical replicates were used.

Appendix K: Wt1 immunoreactivity does not change in muscle cytoplasm or non-muscle tissue compared to the age-matched wildtype.
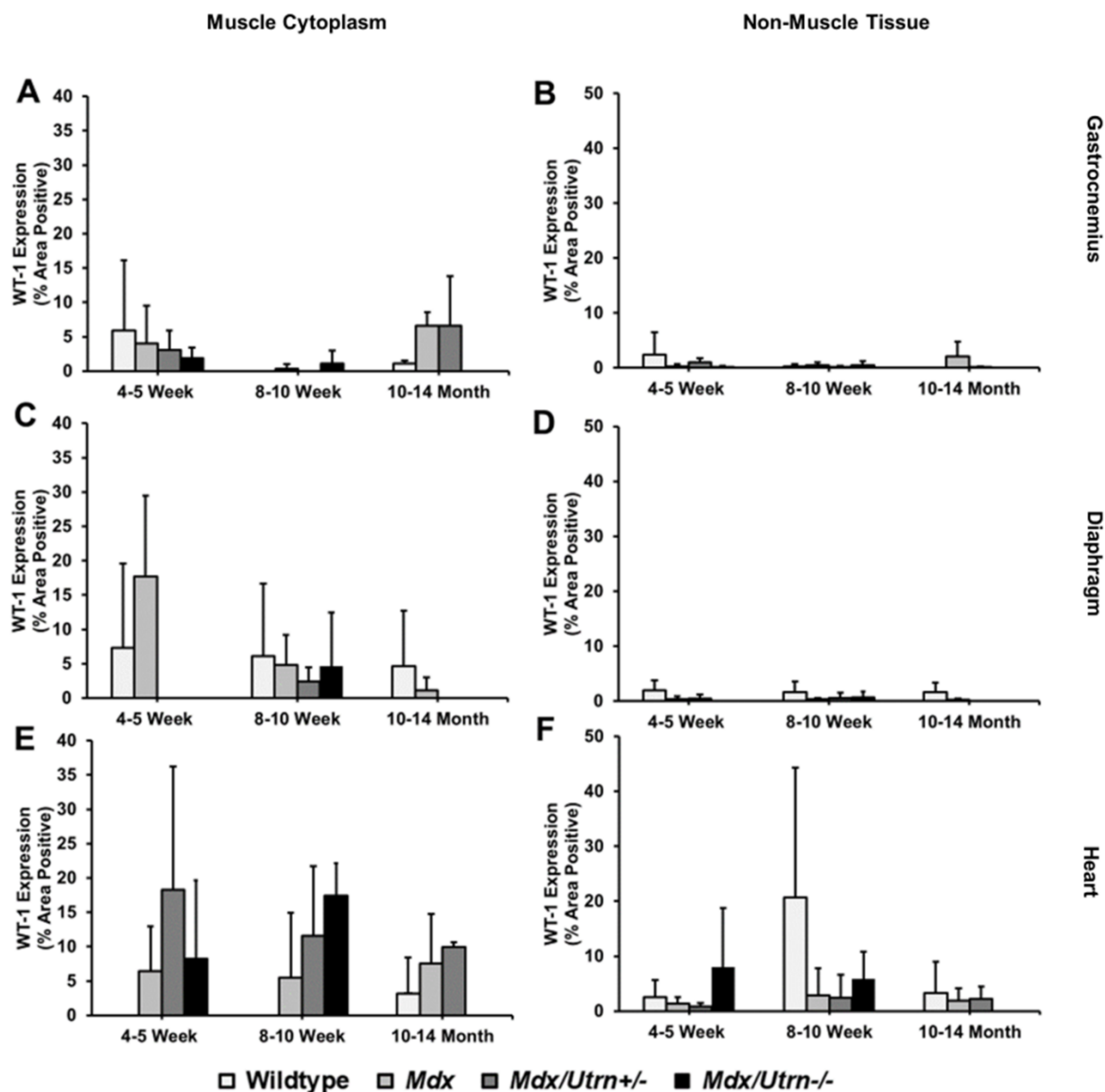
Graphs depicting Wt1 immunoreactivity as a fraction of the muscle cytoplasm, for the gastrocnemius (A), diaphragm (C), and heart (E), or as a fraction of the non-muscle tissue, for the gastrocnemius (D), diaphragm (E), and heart (F). Percent of positive tissue area is expressed as mean +SD. Asterisks indicate significant differences with age-matched wildtype (* < 0.050, ** < 0.010, *** < 0.001). Three biological and three technical replicates were used.

Appendix L: Wt1 immunoreactivity does not change in muscle cytoplasm or non-muscle tissue over time.
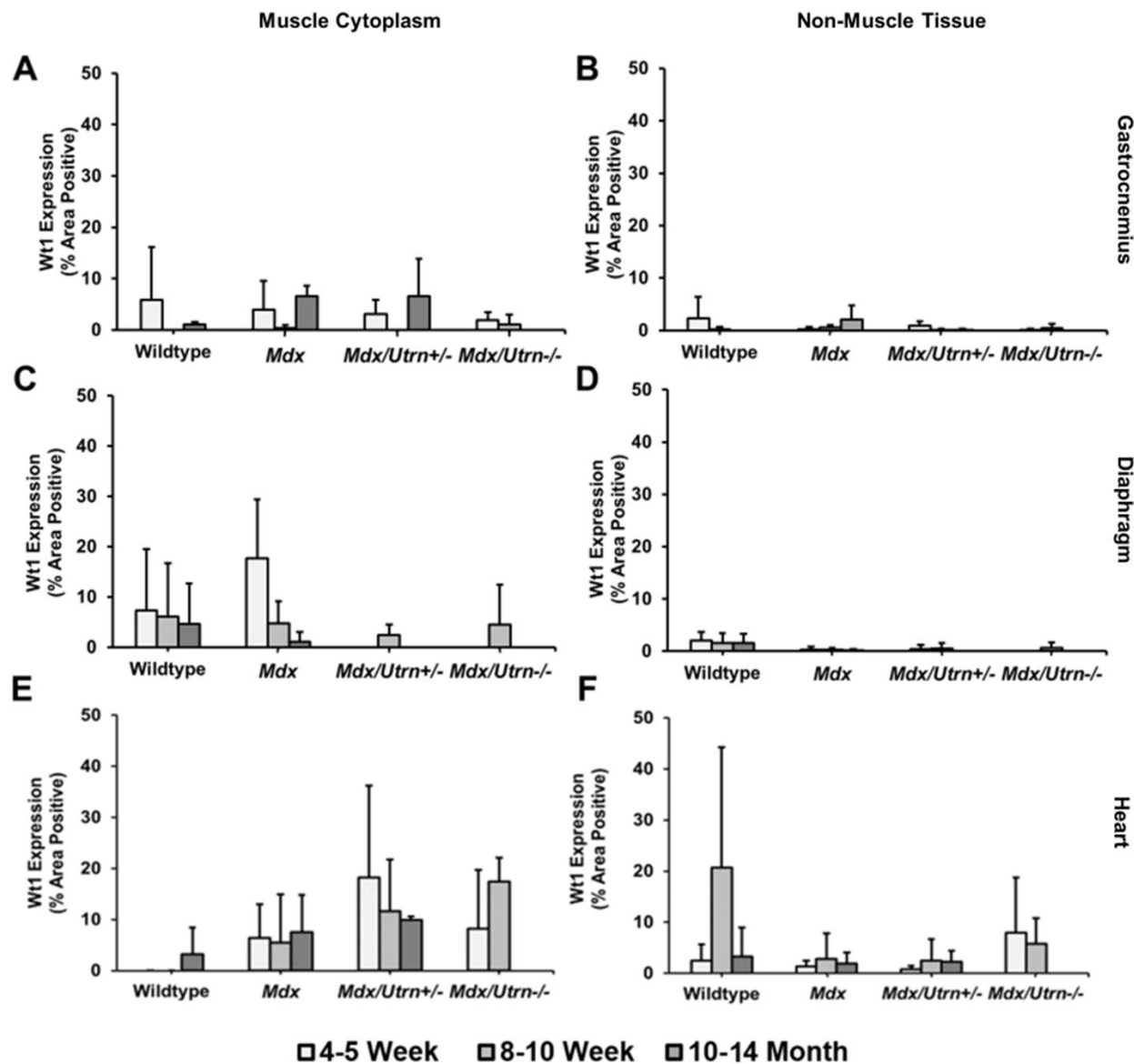
Graphs depicting Wt1 immunoreactivity as a fraction of the muscle cytoplasm, for the gastrocnemius (A), diaphragm (C), and heart (E), or as a fraction of the non-muscle tissue, for the gastrocnemius (D), diaphragm (E), and heart (F). Percent of positive tissue area is expressed as mean +SD. Asterisks indicate significant differences with age-matched wildtype (* < 0.050, ** < 0.010, *** < 0.001). Three biological and three technical replicates were used.

Appendix M: There is significantly greater collagen deposition in 8-10 week old diaphragm compared to 8-10 week old heart.
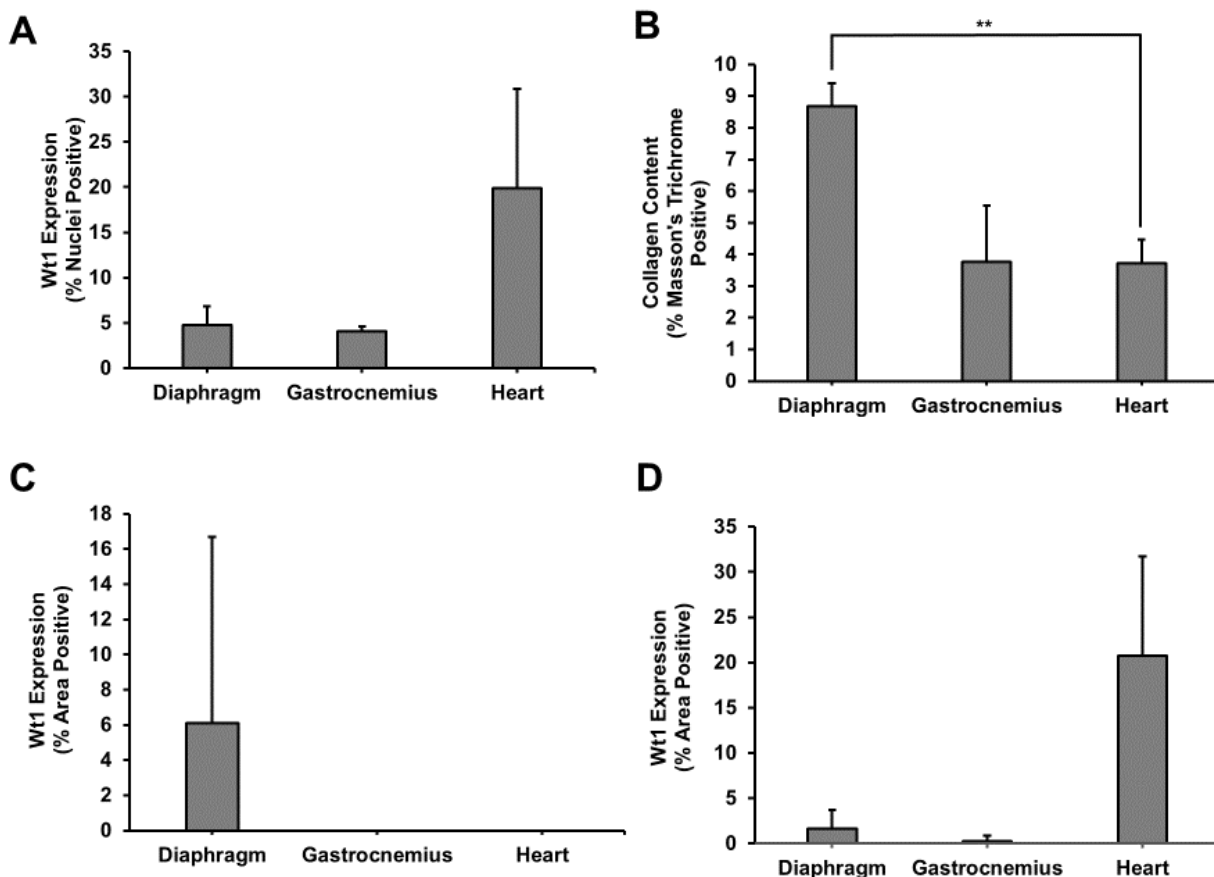
Graphs depicting Wt1 immunoreactivity as a fraction of nuclei positive (A), area of the muscle cytoplasm positive (C), and area of the non-muscle tissue positive (D), as well as the collagen content of the tissue (B), for 8-10 week old wildtype mouse diaphragm, gastrocnemius, and heart. Percent of positive nuclei or tissue area is expressed as mean +SD. Asterisks indicate significant differences. (* < 0.050, ** < 0.010, *** < 0.001). Three biological and three technical replicates were used.

PATRICK MURPHY

Education & Awards

HONORS SPECIALIZATION IN MEDICAL CELL BIOLOGY 2013-2017

LONDON, ONTARIO **UNIVERSITY OF WESTERN ONTARIO**

· Western Scholarship of Excellence

· Dean's Honors List 2013-2017

· Western Gold Medal 2017

· NSERC Undergraduate Student Research Award 2017

· Graduated with Distinction 2017

MSC IN ANATOMY AND CELL BIOLOGY RESEARCH 2017-ONGOING

LONDON, ONTARIO **UNIVERSITY OF WESTERN ONTARIO**

· Western Graduate Research Scholarship 2017

· Collaborative Training Program in Musculoskeletal Health Research Trainee

· Frederick Banting and Charles Best Canada Graduate Scholarship – Master's Program 2018

Job Experience

TEACHING ASSISTANT 2017-2018

LONDON, ONTARIO **UNIVERSITY OF WESTERN ONTARIO**

· Aided in overseeing groups of up to 100 students enrolled in Anatomy & Cell Biology 3309: Mammalian Histology. This involved acting as part of a teaching assistant team, including answering student questions and providing instruction to students as they completed laboratory activities, as well as marking assignments and exams.

Research Experience

RESEARCH LAB ASSISTANT – PHYSICS 2013-2014

LONDON, ONTARIO **UNIVERSITY OF WESTERN ONTARIO**

· Invited to perform research at the lab of Dr. Giovanni Fanchini. Conducted sample preparation, sonication, and electron spin resonance (ESR) testing for a number of substances, most notably finding evidence for strontium aluminate taking on multiple forms at subzero temperatures. Summer research focused on graphene thin films and their thermodynamic properties, and involved extensive work with photothermal deflection spectroscopy, atomic force microscopy, ultraviolet spectroscopy, and radiofrequency sputtering.

RESEARCH LAB ASSISTANT – BIOCHEMISTRY 2015

LONDON, ONTARIO **UNIVERSITY OF WESTERN ONTARIO**

· Invited to perform research at the lab of Dr. Ilka Heinemann. Research was directed to produce T7 RNA polymerase mutants which would be capable of initiating reliably without GTP. Conducted extensive laboratory research, gaining experience in maintaining cell lines, affinity chromatography, site-directed mutagenesis, and a number of other techniques.

RESEARCH LAB ASSISTANT – CELL BIOLOGY 2016-ONGOING

LONDON, ONTARIO **UNIVERSITY OF WESTERN ONTARIO**

· Invited to perform research at the lab of Dr. Lisa Hoffman as part of Honors Thesis course, continuing over the following year as a graduate student. Research was directed to identify WT1 as a candidate biomarker for fibrosis in Duchenne's Muscular Dystrophy. Conducted extensive laboratory research, gaining experience in maintaining cell lines, immunohistochemistry, image quantification, and a number of other techniques.

Volunteering History

SCINAPSE AWARD WINNER   **2014-2015**

LONDON, ONTARIO   **UNIVERSITY OF WESTERN ONTARIO**

· Co-authored and presented an award-winning project on the application of radio-frequency magnetic fields to combat focal neocortical epilepsy. Notably, one of only two projects to come away with two awards: those being both the People's Choice Award and the Physics Award.

ACB SOCIAL COMMITTEE MEMBER   **2017-ONGOING**

LONDON, ONTARIO   **UNIVERSITY OF WESTERN ONTARIO**

· Aided in planning, recruiting, and running of a number of events intended to promote intra-departmental collaboration, raise money for departmental activities, and to bring awareness to graduate opportunities for undergraduate students. These events include, but are not limited to, the running of a fundraising bakesale and a pumpkin carving competition.

Course History

COMPLETED

· MSK 9000

· MSK 9100

· ACB 9520

Publication and Presentation History

ELECTRON SPIN RESONANCE SPECTRA OF STRONTIUM ALUMINATE AT HIGH MICROWAVE FIELDS AND STRONG ILLUMINATION

OTTAWA, ONTARIO, CANADA

CAP CONGRESS   **JUNE 13, 2016**

· Poster was presented on research conducted over the fall and winter semesters of 2013-2014, from the lab of Dr. Giovanni Fanchini.

INVESTIGATING CCN1 AND WT1 AS POTENTIAL BIOMARKERS OF FIBROSIS IN DUCHENNE MUSCULAR DYSTROPHY

NEW LONDON, NEWHAMPSHIRE, UNITED STATES OF AMERICA

TISSUE REPAIR & REGENERATION GORDON RESEARCH CONFERENCE   **JUNE 4, 2017**

· Poster was presented on research conducted over the fall and winter semesters of 2016-2017, from the lab of Dr. Lisa Hoffman.

INVESTIGATING WT1 AS A FIBROTIC BIOMARKER IN DUCHENNE MUSCULAR DYSTROPHY

LONDON, ONTARIO, CANADA

ACB RESEARCH DAY   **OCTOBER 27, 2017**

· Poster was presented on research conducted studying WT1 expression, from the lab of Dr. Lisa Hoffman.

INVESTIGATING WT1 AS A FIBROTIC BIOMARKER IN DUCHENNE MUSCULAR DYSTROPHY

LONDON, ONTARIO, CANADA

LONDON HEALTH RESEARCH DAY   **MAY 10, 2018**

· Poster was presented on research conducted studying WT1 expression, from the lab of Dr. Lisa Hoffman.

INVESTIGATING WT1 AS A FIBROTIC BIOMARKER IN DUCHENNE MUSCULAR DYSTROPHY

LONDON, ONTARIO, CANADA

CANADIAN BONE AND JOINT CONFERENCE   **MAY 11, 2018**

· Poster was presented on research conducted studying WT1 expression, from the lab of Dr. Lisa Hoffman.

INVESTIGATING WT1 AS A FIBROTIC BIOMARKER IN DUCHENNE MUSCULAR DYSTROPHY

TORONTO, ONTARIO, CANADA

CANADIAN CONNECTIVE TISSUE CONFERENCE   **MAY 23, 2018**

· Poster was presented on research conducted studying WT1 expression, from the lab of Dr. Lisa Hoffman.

INVESTIGATING WT1 AS A FIBROTIC BIOMARKER IN DUCHENNE MUSCULAR DYSTROPHY

LONDON, ONTARIO, CANADA

ACB RESEARCH DAY   **OCTOBER 5, 2018**

· Poster was presented on research conducted studying WT1 expression, from the lab of Dr. Lisa Hoffman.

INVESTIGATING WT1 AS A FIBROTIC BIOMARKER IN DUCHENNE MUSCULAR DYSTROPHY

LONDON, ONTARIO, CANADA

LONDON HEALTH RESEARCH DAY   **APRIL 30, 2019**

· Poster was presented on research conducted studying WT1 expression, from the lab of Dr. Lisa Hoffman.

INVESTIGATING WT1 AS A FIBROTIC BIOMARKER IN DUCHENNE MUSCULAR DYSTROPHY

LONDON, ONTARIO, CANADA

CHILD HEALTH RESEACH DAY   **MAY 24, 2019**

· A talk was given on research conducted studying WT1 expression, from the lab of Dr. Lisa Hoffman. This talk was recognized with the second place award for basic science talks at this conference.

INVESTIGATING WT1 AS A FIBROTIC BIOMARKER IN DUCHENNE MUSCULAR DYSTROPHY

MONTREAL, QUEBEC, CANADA

CANADIAN CONNECTIVE TISSUE CONFERENCE   **MAY 29, 2019**

· Poster was presented, and a talk was also given, on research conducted studying WT1 expression, from the lab of Dr. Lisa Hoffman. This research was recognized with a Travel Award at this conference.